TAMPEREEN TEKNILLINEN YLIOPISTO
TAMPERE UNIVERSITY OF TECHNOLOGY

VIIVI JOKINEN

RELIABILITY AND LIMITATIONS OF COMPRESSION TESTING OF VARIOUS BIOMATERIALS

Master of Science Thesis

Examiner: Minna Kellomäki and Jonathan Massera
Examiner and topic approved on 29th March 2017

ABSTRACT

VIIVI JOKINEN: Reliability and Limitations of Compression Testing of Various Biomaterials
Tampere University of Technology
Master of Science Thesis, 106 pages, 3 Appendix pages
August 2017
Master's Degree Programme in Bioengineering
Major: Tissue Engineering
Examiner: Professor Minna Kellomäki and Academy Research Fellow Jonathan Massera

Keywords: static compression test, compressive behavior, biomaterials, reliability, limitations

Tissue engineering (TE) uses biomaterials, cells, and bioactive molecules to create 3D structures called scaffolds. Scaffolds are temporary structures that provide a template and support for cells, and tissue regeneration. It should mimic, as closely as possible, the one of the tissues to be replaced. Hence, mechanical tests are of paramount importance. However, there are various biomaterials, with distinct mechanical properties for different applications. Consequently, performing a conventional compression test is complicated. The accuracy and reproducibility of the testing machine as well as the impact of sample's geometry, microstructure and machinability should be evaluated for safe TE applications.

The objective of this thesis was to study the reliability and limitations of static conventional compression test and compression testing device (Instron Electropuls E 1000). Two reference materials and various biomaterials, with various properties, were compression tested to attain a better understanding of the performance and limitations of the testing device. Also, reproducibility between devices was evaluated. The stress-strain behavior was determined for the materials and evaluated by comparing the results with other similar studies in the literature. Accuracy and reproducibility of the compression tests were considered.

The results showed that the compressive properties are dependent on many factors such as compressive rate, sample size, cell structure and material density. The viscoelasticity of a hydrogel, the non-homogeneous structure of a joint scaffold and the brittleness of a bioactive glass scaffold complicated and hampered the reliability of the compression test. Fixed uniaxial compressive platen led to uneven load distribution on hard biomaterial's cross-section area. Careful sample preparation, surface finish or self-aligning platen could improve the reliability. The testing device showed good reproducibility, and accuracy for compressive strength. However, compressive modulus underestimated the results by > 34 %. The strain was measured from the platen displacement and the quality and integrity of the sample surface may have caused error in strain measurements. With an optical extensometer, strain could be measured precisely from the center part without touching the sample. This method could exclude the surface artifacts and improve accuracy. In conclusion, the accuracy and reproducibility of conventional compression test are questionable. The compression test should be performed with caution. However, the limitations and reliability of the compression test can be enhanced with additional equipment, careful preparation and report of the used methods.

TIIVISTELMÄ

VIIVI JOKINEN: Puristuskokeen luotettavuus ja haasteet monenlaisia biomateriaaleja testattaessa
Tampereen teknillinen yliopisto
Diplomityö, 106 sivua, 3 liitesivua
Elokuu 2017
Biotekniikan diplomi-insinöörin tutkinto-ohjelma
Pääaine: Kudosteknologia
Tarkastaja: professori Minna Kellomäki ja akatemiatutkija Jonathan Massera

Avainsanat: staattinen kompressiotesti, kompressiokäyttäytyminen, biomateriaalit, luotettavuus, haasteet

Kudosteknologia hyödyntää biomateriaaleja, soluja ja bioaktiivisia molekyylejä kehittääkseen kolmiulotteisia kudossiirteitä. Näitä kudosteknologisia kudossiirteitä voidaan käyttää väliaikaisena alustana ja tukirakenteena soluille sekä kudosten rekonstruktioon. Olennaista on, että kudossiirre käyttäytyisi mahdollisimman samalla lailla kuin kohdekudos. Tämän vuoksi mekaanisten ominaisuuksien karakterisointi on tärkeää. Uusien biomateriaalien ja niiden erityislaatuisten mekaanisten ominaisuuksien lisääntyessä perinteisten mekaanisten testien suorittamisesta on tullut hankalampaa. Testilaitteen tarkkuus ja toistettavuus sekä näytteiden muodon, mikrorakenteen ja eheyden vaikutus mekaanisten testien tuloksiin on tärkeää arvioida kudosteknologisten sovellusten turvallisuuden vuoksi.

Työn tavoite oli selvittää tavanomaisen puristuskokeen ja -laitteen (Instron Electropuls E 1000) luotettavuus sekä haasteet. Työssä testattiin kahta vertailumateriaalia sekä useaa eritavoin käyttäytyvää biomateriaalia. Usean materiaalien testaaminen antoi paremman käsityksen laitteen suorituskyvystä ja rajoitteista. Testien toistettavuutta tutkittiin eri laitteiden tuloksia vertailemalla. Lisäksi testien tarkkuutta ja toistettavuutta arvioitiin vertaamalla biomateriaalien jännitys-myötymä -käyttäytymistä samankaltaisten testien tuloksiin.

Työssä havaittiin, että materiaalien kompressio-ominaisuudet ovat riippuvaisia useasta tekijästä, kuten puristusnopeudesta, näytekappaleen koosta, materiaalin tiheydestä ja huokosten rakenteesta. Bioaktiivisen lasin hauraus, hydrogeelin viskoelastisuus ja nivelimplantin epähomogeeninen rakenne vaikeuttivat testiä ja heikensivät tulosten luotettavuutta. Yksiakselinen puristuslevy ja näytteiden vino pinta aiheuttivat puristusvoimien jakautumisen epätasaisesti näytteen pintaan testin aikana. Näytteiden huolellinen valmistus ja pinnan viimeistely tai itseasettuvan puristuslevyn käyttö voisivat parantaa testin luotettavuutta. Materiaalien puristuslujuuden tarkkuus ja testien toistettavuus olivat hyviä. Laite kuitenkin aliarvioi testinäytteiden jäykkyyden > 34 %. Myötymä mitattiin kompressiolevyn siirtymänä näytteen pinnalta. Tällöin näytteiden laatu ja pinnan eheys voivat aiheuttaa epätarkkuutta myötymään. Optinen myötymämittari mittaa myötymän näytteen keskeltä, jolloin pinnan artefaktit voitaisiin jättää huomioimatta. Tämä keino voisi parantaa tuloksien tarkkuutta. Yhteenvetona, biomateriaalien kompressio tulokset ovat harvoin tarkkoja ja toistettavia. Perinteinen puristuskoe tulisi suorittaa huolellisesti sekä harkitsevaisesti. Puristuskokeen luotettavuutta voidaan parantaa lisälaitteilla, huolellisella näytteiden valmistelulla ja tutkimuksen raportoinnilla.

PREFACE

This study was performed in Biomaterials and Tissue Engineering Group in BioMediTech Institute and Faculty of Biomedical Science and Engineering at the Tampere University of Technology.

First, I would like to express my sincere gratitude to Dean, Professor Minna Kellomäki and Academy Research Fellow Jonathan Massera for the guidance and support throughout the project and for the great opportunity to work in such an interesting project. I enjoyed the process from start to finish.

Thank you so much PhD. Amy Nommetots-Nomm and MSc. Sanna Karjalainen for your support and for sharing your wisdom with me. Thank you Janne Koivisto, Lasse Söderlund, Raimo Peurakoski, Markus Hannula, Aleksi Hänninen, Elina Talvitie and Laura Johansson for helping me. Thanks to all the colleagues for the positive working environment. Thank you PhD. Tony M. Keaveny, Dr. Mark S. Thompson, Instron®, AIREX® and Sawbones® for the cooperation.

Finally, thank you for everything my dear friends and family. I am so lucky to have you by my side.

Tampere, 2.8.2017

Viivi Jokinen

CONTENTS

LIST OF FIGURES

LIST OF SYMBOLS AND ABBREVIATIONS

B50	Specific bioactive glass composition
B_4C	Boron carbide
CNS	Central nervous system
ECM	Extracellular matrix
e.g.	For example
etc.	Latin et cetera, and so on
et al.	Latin et alii or et alieae, and others
GG	Gellan gum
ISO	International Organization for Standardization
i.e.	Latin id est, in other words
n	Number of the samples
PEG	Polyethylene glycol
PET	Polyethylene terephthalate
PGA	Polyglycolic acid
PLA	Polylactide
PNS	Peripheral nervous system
PU	Polyurethane
R^2	Correlation coefficient
SI	International System of Units
SiC	Silicon carbide
UV	ultraviolet
wt-%	Mass percentage
µCT	Micro computed tomography
3D	Three-dimensional
©	The copyright sign
®	The registered trademark
&	And

A_0	Cross-sectional area
C_i	Constant where i={0, 1, 2, 3, 4, 5}
E	Compressive modulus
F	Force
i	The rank of a value in population
k	Spring
L_F	Loading factor
l_i	Instantaneous length
l_0	Initial length
m	Weibull modulus
N	Total number of the strength values
P	Failure probability
P_{fi}	Failure probability of each i^{th} ranked strength value
SG	Specific gravity
t	Time
T_c	Crystallization temperature
T_g	Glass transition temperature
TGA	Thermogravimetric analysis
T_p	Crystallization peak
U_y	Energy Absorbed to Yield

V	Volume
x_i	The i^{th} ranked data point for x-axis
y_i	The i^{th} ranked data point for y-axis
ε	Engineering strain
ε_y	Yield strain
ε_0	Initial strain
$\varepsilon_{\mathbf{80N}}$	Strain at 80 N
$\varepsilon_{\mathbf{220N}}$	Strain at 220 N
$\varepsilon_{\mathbf{440N}}$	Strain at 440 N
$\varepsilon_{\mathbf{900N}}$	Strain at 900 N
η	Dashpot
ρ	Density
ρ_s	Density of solid material
ρ_v	Density of void
ρ_{H2O}	Density of water
σ	Engineering stress
σ_{fi}	Strength value of the i^{th} ranked test sample
σ_{max}	Maximum stress
σ_{min}	Minimum stress
σ_{y}	Yield point
σ_0	Initial stress
σ_{10}	Compressive strength at 10 % strain
σ_0^*	Characteristic strength
τ	Relaxation time
ϕ	Porosity
Δl	Change in length
$\Delta\varepsilon$	Change in strain
$\Delta\sigma$	Change in stress

1. INTRODUCTION

Tissue engineering (TE) is a field that aims to heal, repair or replace damaged structure that needs medical treatment. The function of tissue may suffer due to trauma, injury, disease or ageing. TE creates three-dimensional (3D) structures called scaffolds that activate tissue regeneration and healing of the tissue. A functional scaffold can be built by combining biomaterials, cells and signaling molecules. Inside the human body scaffolds should mimic the original tissue. Thus, an important property of the biomaterial is to provide sufficient mechanical support during the healing process. The mechanical properties of the biomaterial can be tested by a compression test, which provides fundamental behavior and properties of biomaterials. [1, 2] In the case of unsuccessful testing or interpretation, the engineered outcome of the biomaterial might have unwanted side effect, such as inflammation or early failure. The crucial factors in the mechanical testing of biomaterials are reproducibility and reliability. [3]

Biomaterials range from strong to soft depending on the targeted application. Bone tissue are stronger and stiffer than for example nerve tissue or elastic cartilage. [2, 4] Here the challenge lies in assessing the mechanical properties of such a wide range of biomaterials. There are no clear guidelines for testing new biomaterials used as scaffolds. Viscoelasticity, porosity, brittleness are a few properties among others that make the conventional compression test complicated to perform and analyze. The variation in the compressive results of biomaterial batches or between different sized specimens have raised questions about the reliability. The equipment, sample design, testing methods, equipment etc. have shown to have influence on the results. [5-7] Thus, there are many limitations and challenges in compression testing, but to achieve reliable results the limitations and challenges need to be first detected.

The aim of this thesis was to study the reliability and limitations of conventional compression tests and our mechanical testing device (Instron Electropuls E 1000). Two porous reference materials, viscoelastic hydrogel scaffolds, a solid polymer rod, knitted polymer scaffolds, brittle bioactive glass scaffolds, and a strong cancellous bone were compression tested to get better understanding of the compression test and performance of the mechanical testing device. Aside from the understanding of the mechanical properties of the various types of biomaterials, in this study 3D prototyping of bioactive glass scaffold as well as Gellan Gum (GG) hydrogel processing were emphasized.

2. THERORETICAL BACKGROUND

2.1 Axial and Static Compression Test

Conventionally a mechanical test aims to determine the mechanical properties of a material by loading a specimen uniaxially. During the test, the given load and corresponding deformation of the specimen are measured. The most common axial loading modes are tensile and compression. During the tensile test, the specimen is stretched. On the contrary, during the compression test, the specimen is compressed. Additionally, there are other mechanical test modes. For example, the torsion and shear tests are perpendicular to the tensile and compression test. The loading condition can be static or dynamic, which means that the specimen is loaded once or cyclically. [3, 8] This thesis focuses only on static compression test.

2.1.1 Stress-Strain

During a mechanical test, an external force is applied on the surface of the tested specimen. This force is measured and called load. The external force causes material deformation. This deformation, in the case of a compression test, is seen as contraction of the tested specimen and is measured as displacement. The relationship between load and displacement can be used to characterize the mechanical properties of the specimen. However, load and displacement are sample size dependent. Therefore, to minimize the effect of the sample size, load and displacement are normalized to the materials surface and length to give stress and strain. They usually give broader understanding of the material's properties and the results are more comparable between studies. The normalized parameters are also called engineering stress and engineering strain. [3, 8] Engineering stress can be expressed as:

$$\sigma = \frac{F}{A_0} \tag{1}$$

in which F is the applied force normal to the specimen surface and A_0 is the cross-section area of the specimen. According to the international system of units (SI) engineering stress is expressed in megapascals (MPa) which equals 10^6 newtons per square meter. Engineering strain, referred as strain, is calculated using the following equation

$$\varepsilon = \frac{l_i - l_0}{l_0} = \frac{\Delta l}{l_0} \tag{2}$$

in which l_0 is the initial length and l_i is the instantaneous length of the specimen after load is applied. The change in length can be expressed as Δl and due to the same unit in the denominator and numerator, engineering strain is unitless. However, the unit of the strain can be expressed as millimeter per millimeter or as a percentage after multiplying it by 100. Compression test leads to a decrease in the initial length, which turns Δl negative. For the tensile test, Δl is positive. [8] This is a way to describe the direction of the load and separate compression and tensile test. However, generally the strain is changed to positive if there is no need to describe the direction of the test.

The relationship between engineering stress and engineering strain is used to characterize the stiffness and strength of the material. The representative stress-strain curve can be seen in Figure 1 (a). In the linear part of the curve, stress and strain are proportional to each other. Hooke's law can be used,

$$\sigma = E\epsilon \tag{3}$$

where the constant E is the Young's modulus or in case of the compressive test, compressive modulus. Young's modulus describes the ability of the material to resist elastic deformation, hence the stiffness. The highest point of the stress-strain curve before the decrease in stress, can be called failure point, fracture strength or ultimate strength (σ_{max}). The decrease in stress is a sign of a fracture. As there might be a case when no fracture appears, the strength of the material is determined at a specific strain point. The point where the linear part of the curve starts to bow is called yield point (σ_y). Before the yield point the deformation is elastic, hence material deformation is reversible. On the contrary, after the yield point, material deformation is plastic making deformation permanent. The plastic deformation is different for crystalline and amorphous materials, but the deformation results in a breakage of old atomic bonds and reformation of new bonds. The resilience of the material is the energy absorbed at the point of yield. The absorbed energy until yield can be determined by the following equation

$$U_y = \int_0^{\epsilon_y} \sigma d\varepsilon \tag{4}$$

in which U_y is the absorbed energy until yield and ε_y is the yield strain. The coloured part of the stress-strain curve in Figure 1 (a) illustrates where absorbed energy is taken. It characterizes the capacity of the material to absorb energy under deformation and then recover the energy upon unloading. [3, 8, 9]

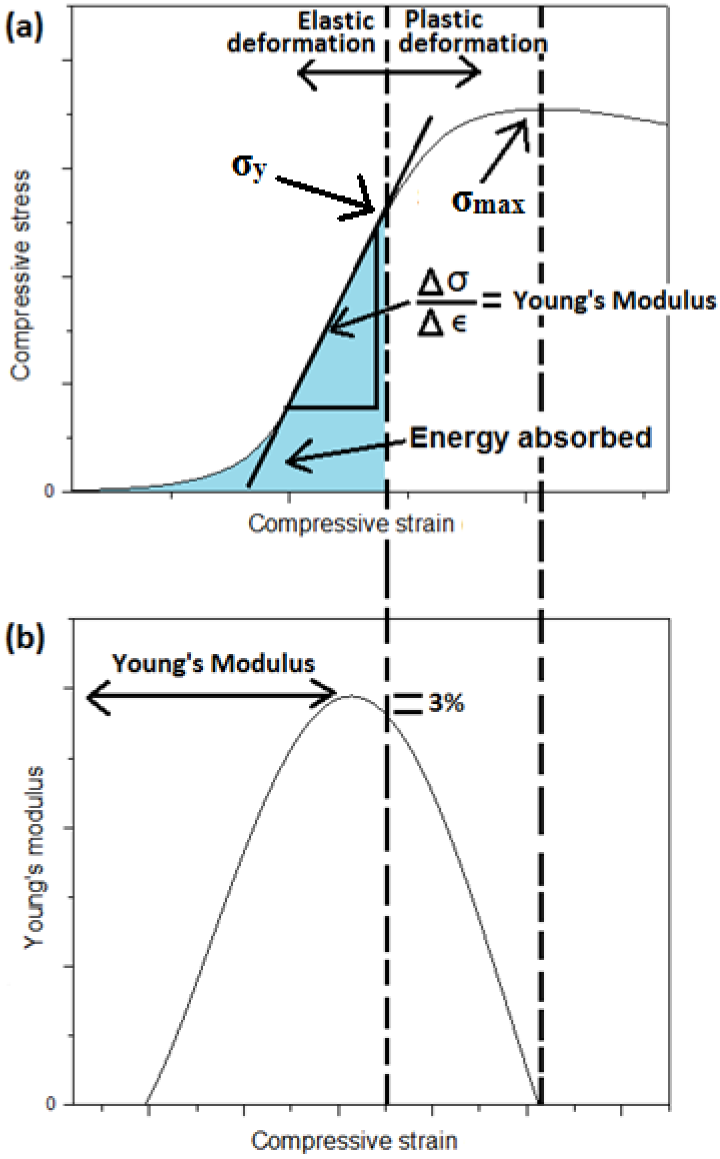

Figure 1. Schematic stress-strain curve (a) and gradient of the curve (b) used to determine the Young's modulus, yield point and the absorbed energy [10].

As there are different kind of stress-strain curves depending on material behavior, sometimes other methods can be used to facilitate the evaluation process. In this thesis, one method is represented. The gradient of the stress-train curve (Figure 1(b)) can be obtained by fitting the fifth degree polynomial to the stress-strain curve and then taking the first derivate. The equation of the fifth degree polynomial is

$$\sigma(x) = C_5x^5 \pm C_4x^4 \pm C_3x^3 \pm C_2x^2 \pm C_1\mathrm{x} \pm C_0 \tag{5}$$

in which $\sigma(x)$ is the displacement of the compressive platen (in mm) and C_i is coefficient for every degree term. The fifth degree polynomial appears similar to the original curve but may have local maximum and minimum. Taking the derivate of the fifth polynomial fit, from zero to the highest stress point, gives the gradient of the curve. The derivate of the curve can be used to obtain Young's modulus, detect the yield point and ultimately the material's strength (Figure 1 (b)). The Young's modulus is the maximum point of the derivative curve. The yield point can be found on the right side of the Young's modulus from the derivative curve at point where the maximum is decreased by 3 %. The ultimate strength is the point where the derivative curve crosses the x-axis. [10, 11]

2.1.2 Deformation

The two basic behaviors observed under compression are the elastic solid and the viscous fluid [8]. However, the behavior of a biological tissue is more complicated. Almost all tissues have both, elastic and viscous behavior [4, 12]. As biomaterials aim to mimic human tissues, it is expected that various biomaterials can exhibit similar behavior. This behavior is called viscoelasticity [2, 4, 7].

Hysteresis, stress relaxation and creep are viscoelastic responses to stress. A sign of hysteresis is the change in the stress-strain curve when the material is loaded cyclically. Stress relaxation and creep may appear during the compression test and will be discussed in this study. [7, 8]

The viscoelastic behavior of the material depends on the stress, time and temperature. Figure 2 illustrates the response of various materials in relation to time and stress. The applied load causes elastic material to deform immediately. When the load is released, the elastic material recovers from the deformation instantaneously like a string. On the contrary, the viscous material has time dependent deformation and cannot completely return to the initial formation. The viscoelastic material has both properties. It may first have instantaneous deformation like an elastic material, but then the deformation becomes time-dependent similarly as in viscous material. The viscoelastic deformation can also be explained via mechanical energy that is stored or dissipated. Viscoelastic materials have the ability of store mechanical energy during deformation but then dissipating at a varying rate upon unloading of the material. [4, 8, 13] Thus, viscoelastic materials are good impact absorbers. This property is very important for supportive tissues like cartilage [14].

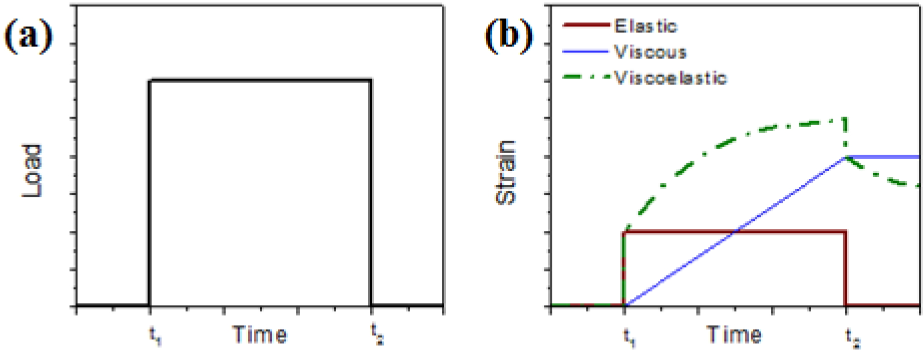

Figure 2. Elastic, viscoelastic and viscous behavior under load (a) and their time-deformation relationship (b) [8].

The viscoelastic behavior and time-dependency can be tested by loading the material. The temperature should be kept constant during the test. If the material is rapidly deformed to a particular strain that then remains constant for a specific time and thereafter a change in stress can be seen, it is called stress relaxation (Figure 3 (a)) [7]. Usually during the stress relaxation, the stress first decreases fast but then slowly stabilizes in time. If the material is loaded with a constant stress for a specific time and a change in strain can be seen, it is called creep (Figure 3 (b)). [8] Hence, the tests are complementary, the stress relaxation test uses constant strain and the creep test uses constant stress. [15]

The time- dependency of viscoelastic behavior may be represented with mathematical models. Hooke's law models the elastic deformation as a spring and Newton's law the viscous deformation as a dashpot. These two laws are used to model linear viscoelasticity at a small level of deformation. When the material's viscoelastic property is characterized via electric analog, capacitors and resistors are used. [13, 15] A schematic illustration of time-dependency, spring and dashpot models and equations for stress relaxation and creep can be seen in Figure 3.

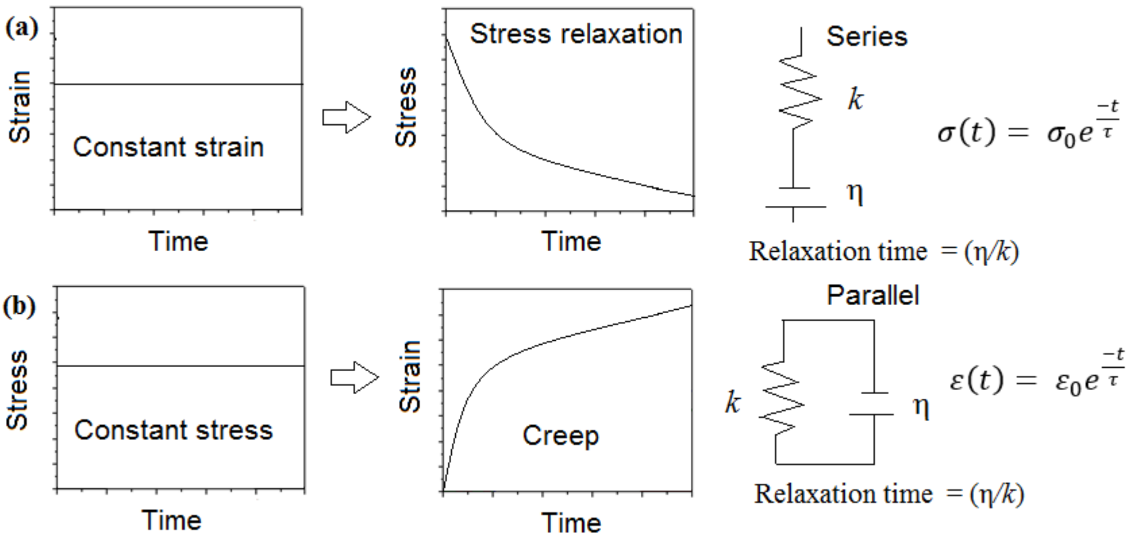

Figure 3. Stress relaxation (a) and creep (b) as a function of time along with their, spring and dash point models and equations. In the equation σ_0 and ε_0 are constant applied stress and strain, t is time and τ is relaxation time that can be modeled with spring (k) and dashpot (η) [15].

Due to the complexity of viscoelastic behavior, many models combine dashpots and springs to understand material responses. Maxwell model combines dashpot and spring elements in series and is applicable for basic stress relaxation phenomena. However, it is not taking into account that the deformation in creep may not be reversible. Kelvin or Voigt model uses elements in parallel and is more realistic for modeling creep than Maxwell model. Nevertheless, it cannot model instantaneous deformation. A good approximation for viscoelastic behavior for polymeric materials provides a linear solid model, which combines the two, Maxwell model and Kelvin-Voigt model. The linear solid model may be used for both creep and stress relaxation. [3] However, some tissues and biomaterials may exhibit non-linear viscoelastic behavior, which cannot be modeled with linear solid models [2, 16, 17].

2.1.3 Failure

The stress-strain curve can be divided into regions depending on the type of deformation the material exhibits. Figure 4 illustrates an example of a stress-strain curve of a compressed cancellous bone. The stress-strain curve is divided into a toe region, elastic region and plastic region. The toe region is the non-linear region where the deformation of the specimen is high in comparison with the applied load. During that period, alignment or settling of the specimen happens. For some materials, such as elastic metal alloys, there is no toe region. The elastic region is a linear part of the curve where the Young's modulus can be determined. The plastic region starts when the specimen yields and deformation becomes irreversible. In the stress-strain curve, it can be seen as the linear region changing to non-linear. The highest point of the curve represents the highest stress the material can withstand. After that point, the material deformation may propagate differently. A final fracture might be sudden or imminent, depending on the material and structure. [3, 4]

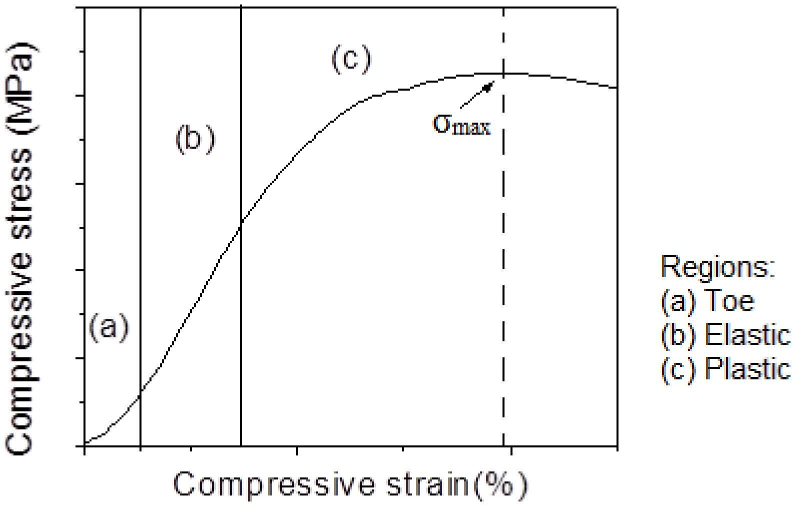

Figure 4. Stress-strain curve and representative regions [3].

The process and possibility of the material failure can be evaluated from the stress-strain curve. Hence, it is used to ensure safety or to understand the material's behavior. Biomaterials may have more complicated failure modes, but the two basic failure modes for solid materials are a ductile fracture and a brittle fracture. [4, 18] The fracture typically has two steps, which are crack formation and propagation. During ductile fracture, the material experiences plastic deformation. The fracture process is slow as the size of the crack becomes wider while the material is resisting the deformation by buckling or bending. The crack is described as stable. The brittle fracture on the contrary is hard to predict and propagates rapidly. Hence, the brittle fracture is mostly an undesired fracture mode. Depending on the microstructure of the brittle material, the fracture can be transgranular or intergranular. The transgranular fracture occurs by crack propagation along crystal structure breaking atomic bonds. The fracture is called cleavage and may look grainy or smooth as the fracture ignores the grain structure. The crack propagation of intergranular fracture follows the path that the grain boundaries form, hence the cross-section of the fracture shows 3D structure of the grains. [8, 19]

The fracture strength or compressive strength describes the ability of the material to withstand stresses before a critical crack that causes the total structure failure. As discussed before, for brittle materials the fracture strength is complicated due to its unexpected mode. The fracture depends highly on the structure, hence resulting in scatter of fracture strengths. In 1951, Weibull proposed a function that describes the probability of the failure. This approach is a statistical method that describes the variability of material strength. The idea of the Weibull modulus is based on the "weakest link" approach. The approach uses the strength of the weakest structural unit to describe material properties. A high value for Weibull modulus indicates consistent material strength and good reliability. In contrast, a low value describes the scattered material strength and the uncertainty of material strength. Failure probability, P can be defined with three-parameter distribution

$$P = 1 - exp\left[\int_{V_0}^{V} \left(\frac{\sigma - \sigma_{min}}{\sigma_0}\right)^m dV\right], \tag{6}$$

in which σ_0 is characteristic strength, σ_{min} minimum strength and *m* is Weibull modulus. The characteristic strength, σ_0, can be used to present the uniaxial strength of body with P=0.632. This equation can be simplified by using two-parameter distribution that assumes σ_{min} is zero by following equation:

$$\ln\left(ln\left(\frac{1}{1-P}\right)\right) = mln(\sigma_{max}) - mln(\sigma_0^*), \tag{7}$$

and

$$\sigma_0^* = \sigma_0 (L_F V)^{1/m} \tag{8}$$

where σ_{max} is the maximum stress, L_F loading factor and σ_0^* is the characteristic strength of a body at the same failure probability (0.632) as with three-parameter distribution. By using regression analysis for the equation of two-parameter distribution, the Weibull modulus can be detected as a slope of ln(ln(1/(1-P))) against ln(σ_{max}). The approach needs a high number of tested specimens to ensure reliability. [20, 21]

In case the stress-strain curve is analyzed from the region of large plastic deformation, engineering stress and engineering strain cannot be used to obtain reliable values. During large plastic deformation, the original cross-section area starts changing as the material tries to resist the load. Thus, the true stress and strain curve needs to be used. The true stress and strain scheme uses actual load, cross-section area, and gauge length. In case of compression, true stress gives lower value and the true strain gives higher value when compared with engineering stress and engineering strain. [8, 22, 23]

2.2 Considerations of Compression Test

Many factors influence the quality of a compression test results. This chapter provides an overview on how equipment, methods and procedures may be tailored for reliable compression testing.

2.2.1 Equipment

Universal testing systems have typically specialized fixtures in the static compression and tensile test. Systems that are more sophisticated may have other additional loading modes, such as dynamic testing modes. The actuator is a part of the testing system that sends feedback regarding the loads to control the platen displacement. Two basic types of actuation of universal testing machines are electromechanical screw driven electric motor and servohydraulic load frame. The screw driven machines are more economic and generally suited for small biomaterial specimens due to the high precision. The high cost servohydraulic machines are more suitable for cyclic loading or high load magnitudes. [3, 24]

The displacement of the test specimen under compression is measured by a transducer. The most common transducers are strain gauge, extensometer and linear variable differential transformer (LVDT). The accuracy of the extensometer and strain gauge is the same for both, as the basic technology of measuring the displacement is the same. In case there is possibility of damaged specimen surface, optical methods, such as optical extensometer, are recommended. Optical methods can exclude damaged area and measure the displacement of the specimen from the center of the specimen. [3, 24]

The basic testing machines are able to give uniaxial compressive load but there are other properties that may vary. The size, load capacity, software, cross-head adjusting system as well as other accessories for the device may change the ease of use and the reliability of the results. For example, it is preferable to use a small load cell for delicate viscoelastic hydrogels and bigger one for strong and stiff metals. On another hand, the load cell capacity may also limit the force the machine can distribute. [6, 24, 25]

Generally, device instructions (e.g. Bose) give guidelines for optimizing the device performance. Before testing it is important to calibrate the load cells and to adjust channel filters to minimize the inaccuracies and noises. The malfunction of compression testing instruments may be due to different electrical noises (e.g. area close to power line) or temperature fluctuations. Additionally, the place of the load frame may cause unwanted resonance, such as base vibration or excessive load vibration. Other considerations like humidity, temperature, ventilation and dust should be considered. [6, 25]

2.2.2 Environment and Methods

The specimen storage is important for biomaterials as the material may be sensitive for example to heat and humidity. The standard ambient laboratory environment is 23 ˚C and 50 % relative humidity [24, p. 80]. Especially viscoelastic materials are sensitive to the temperature and compressive rate changes. Generally, decreasing temperature or increasing the compressive rate results in higher stiffness [3]. During very low strain rates there is a possibility of creep behavior. Sterilization and biocompatibility tests *in vitro* and *in vivo* are needed for safety of biomaterial applications [4, 26]. Sterilization can be also performed using high or low temperatures, pressure or irradiation. Sterilization may change the material structure significantly by inducing for example chain scission in polymeric materials during irradiation [27]. The compression test can be performed in wet conditions to simulate physiological conditions *in vitro*. For example, saline solutions, such as phosphate-buffered saline (PBS), could be used for immersing test specimen. All these factors require special considerations prior compressive characterization. [3, 4, 15, 27]

There are also other compressive experimental methods. The indentation test is specifically used with brittle ceramic materials to measure the hardness of the material. The indentation test needs two parallel and uniform surfaces but is not as dependent on the other specimen features as the compression test. Indentation techniques have been developed for measurement at the micro- and nanoscale. Additionally, there are different shapes of indenters used such as a spherical and a square based diamond pyramid. [20, 28] If the specimen is rod or beam, or has a non-homogenous design, the appropriate compressive method is three point loading or four point loading. The three point loading is the most used, but in the four point loading the stress is distributed more evenly. [29] Both methods remove the problem of cutting shorter specimens. The used compressive methods should be optimized to characterize the mechanical properties of the test material. International Organization for Standardization (ISO) provides methodologies for mechanical testing and result interpretation for various biomaterials that are published and accessible to everyone [3]. The importance of standards ISO lies in that it provides the possibility of repeatable and reliable testing methods.

2.2.3 Specimen

A uniform stress distribution throughout the specimen is difficult to obtain, but it is crucial for reliable test results. The most common problems are buckling and barreling (see Figure 5). [23, 30] Buckling is the deflection of the specimen which occurs when the relationship between specimen length and diameter is too high. A ratio of 2:1 between length and diameter is used as a standard to prevent buckling [9, p. 151].

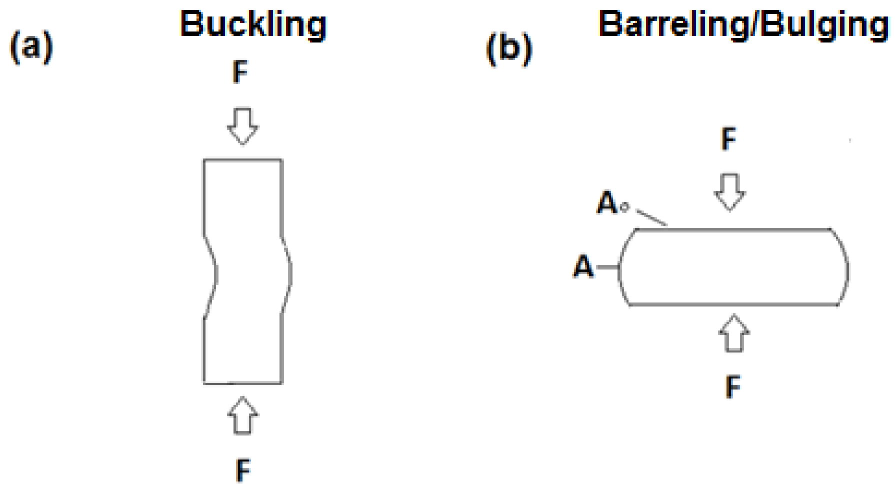

Figure 5. Buckling (a) and bulging (b) of test specimen. F is compressive force applied on the specimen, A_0 is the initial cross-section area of the specimen and A is the cross-section area of the specimen in the middle part [23].

Barreling or bulging happens when the specimen's length decreases under compression and, therefore, the friction between the surface of the compressed specimen and the platen increases. The specimen tries to maintain its volume constant. As the middle part of the specimen becomes less restrained, the structure becomes a barrel like shape. The barreling can be minimized by decreasing friction with lubricants and using machined concentric rings to keep lubricant from squeezing out during the compression test. [3, 23, 30]

Compressive platen is a solid flat compressive surface. Hence, the specimen's cross-sectional surface should be flat and parallel to ensure uniform axial loading. A slight misalignment may cause initial non-uniform stress distribution, which causes error in the specimen strain. Figure 6 (a) illustrates the problem during a compression test if the specimen has non-paralleled surfaces. The compressive platen is unaligned and the load is directed first to the highest part of the specimen causing uneven load distribution on the specimen. A self-aligning platen, or in other words, spherical seating is an additional accessory for compressive devices that is designed to center the loading axis perpendicular to the specimen surface (Figure 6 (b)). [10, 31] It facilitates the compressive test and allows some tilt in specimens still achieving uniform axial loading. The surface parallelism is especially a problem for stiff materials. Ductile materials are able to adapt to the surface unevenness. [30, 32] Additionally, the unevenness of the specimen can be minimized by polishing or grinding stiff specimen surfaces [9, 33].

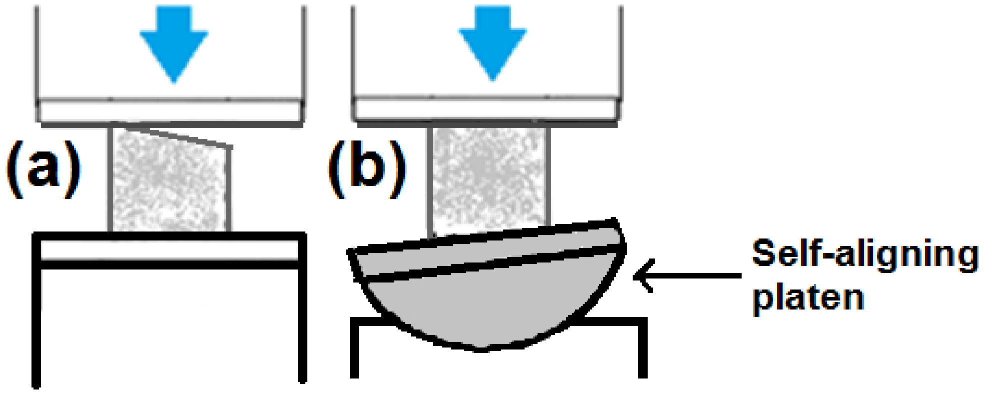

Figure 6. Uniaxial compression test conducted on tilted specimen causes unaligned stress distribution along the specimen (a). Self-aligning compression platen adjust the compressive platen position (b) [31].

Another important consideration to keep in mind, from the specimen's perspective, is its microstructure. The way a material acts under forces depends on many aspects, however structural integrity prior testing is important. Specimen surface can be damaged for example due to scratching, cutting and punching [24]. Fractured surfaces are weaker compared to the intact middle part (Figure 7). This causes inaccuracies, if compressive strain is measured from the interface of compressive platen and specimen surface. [5] This problem can be avoided by using an optical extensometer as discussed earlier. Additionally, other methods, such as glued surfaces, alumina platens and piled specimens have been used for conventional compression test. However, these methods are not always suitable for biomaterials. For example, glues would run through a porous biomaterial structure and the test would not represent the material's inherent properties. As the accuracy is necessary for the biomaterial applications, extensometers are recommended [7].

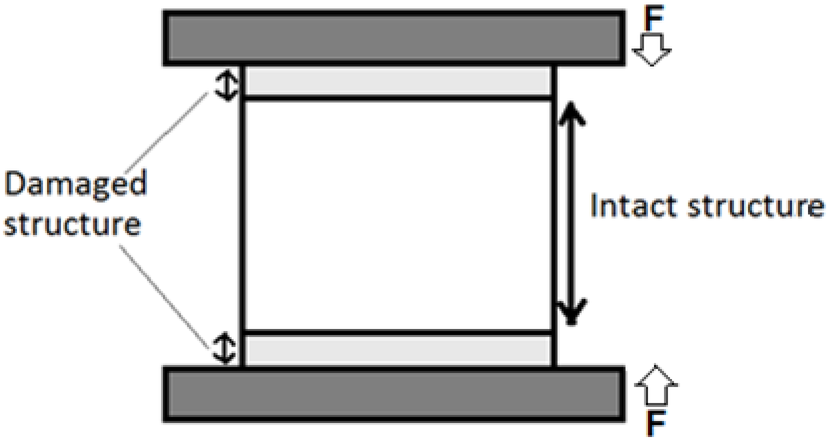

Figure 7. Damaged surface influences on strain during compression test [5].

To highlight some considerations, well controlled processing, sample size, geometry, structure and surface finish are crucial specimen aspects [3]. Table 1 gathers the general limiting factors, problems and solutions. The biomaterial's properties and compression tests on such particular materials are discussed in detail in the following section.

Table 1. Summarized limitations of compression testing specimens and solutions to enhance the reliability of compressive test results [3, 9, 24].

Specimen property	Problem	Ways to minimize error
Barreling effect	Friction between the surface of a compressed specimen and compressive platen, which causes the middle part of the specimen to barrel.	• Use a lubricant or/and • Use a concentric ring • Polish loading platens
Buckling effect	The relationship between the specimen length and diameter is too high and the specimen deflects.	• Use 2:1 ratio between specimen length and diameter
Damaged surface	Inaccuracy on the compressive strain.	• Use equipment that measures the strain from the midpoint of the test specimen without touching (e.g. optical extensometer)
Slipping of the specimen	Contact between grip and specimen does not hold still the specimen and the specimen moves during testing.	• Use an additional layer between the platen and specimen to enhance the contact [34, 35]
Surface adhesion	Strain gauge reading may be effected.	• Use a protective coating material for the strain gauge [36]
Tilted or uneven surface	Slight misalignment causes initial non-uniform stress distribution and inaccuracy in strain.	• Prepare specimen carefully • Use appropriate tools to prepare specimens • Surface finish (e.g. polish or grind) to adjust unevenness • Use a self-aligning platen for tilted surface [10, 31]

Preparing of the specimens is sometimes complicated depending on the material. It demands caution as the cutting material or other preparation tool may damage the specimen and reduce the material's mechanical properties. The cutting rate or type of the cutting tool can be adjusted to minimize the damage. Finished specimens should be carefully examined, before compression test, to evaluate the surface damage and its effect on mechanical properties. Evaluation can be done visually but more precise knowledge of the structure can be achieved by other techniques such as optical microscope or X-ray. [9, 19, 24]

2.3 Biomaterials under Compression

Various biomaterials are used in TE to mimic tissue-like structures. During the years, the amount, function and properties of biomaterials have increased. The first generation biomaterials were easily available. They were not interacting with the host tissue, hence termed as inert. The next generation biomaterials were designed to interact with the host tissue and active biological responses. Synthetic biomaterials, which could degrade inside the body, came in the 1960's [37]. It was a big step for biomaterials and led to new discoveries. However, the rate of degradation introduced a new challenge as too fast or low degradation rate could impair safety and limit functionality [38]. Bioactive glasses, that have the ability to form interfacial bonding with the living tissue, were discovered by Larry Hench in 1972 and later reached clinical use [39-41]. The third generation biomaterials combine both properties, resorbability and bioactivity, in one and focuses on activating the tissue regeneration at molecular level [42]. Nowadays the desired properties of biomaterials are biocompatibility, sufficient mechanical properties, resorbability and bioactivity. [1, 43] However, the main requirement is biocompatibility, which means that the biomaterial is safe and does not cause any toxic or harmful effect inside the body [44].

Biomaterials can be classified in many ways that describe their properties. Different kind of classifications can be seen in Figure 8. Typically, chemical structure and bonding are used to classify three major groups: ceramics, polymers, and metal. The fourth important group is composites, which are made by combining two or more of these three materials. [1, 4]

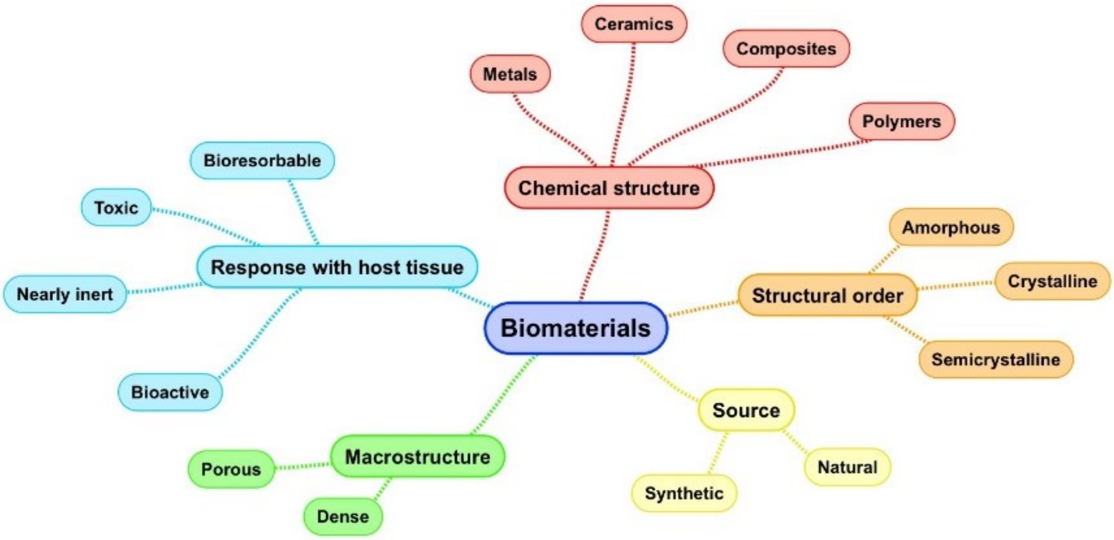

Figure 8. Various classifications of biomaterials that describe biomaterial's properties [1].

The difference in mechanical properties can be explained through atomic or molecular bonding and their packing. Figure 9 illustrates different bonding mechanisms. Pure metals have seas of electrons that can move freely, which make pure metal more ductile. Metal alloys are mixed of metallic elements or metallic and non-metallic elements. Metal alloys are stronger than pure metals as they have other elements blocking the atomic movement. [3, 8] Ceramic materials create strong bonds, such as ionic or covalent, between atoms that have difference in electronegativity [20]. This makes ceramics strong, but there is no space for plastic deformation. Polymers have strong covalent and weak Van der Waals bonds that make polymers weaker than metals [45]. By cross-linking the weak bonds, the amount of weak bonds can be decreased making structure stronger but irreversible, termed thermoset polymer. Thermoplastic polymers on the contrary have a structure that can be reversible changed by introducing energy. Composite materials are combinations of different materials and hence the properties can be widely modified. [3, 8]

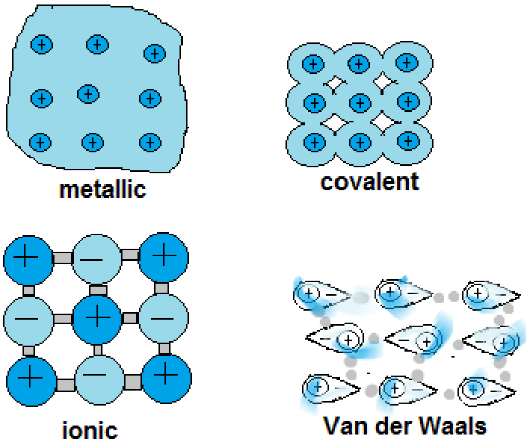

Figure 9. Bonding mechanism drives the physical properties of various material types [4, p. 16].

Biomaterials can be synthetic or natural. Natural materials have generally advantage of the bioactivity, but the limitations are that there are variations from batch to batch, cost and the availability might be limited. Synthetic biomaterials are a potential alternative to natural sources, as synthetic biomaterials are artificially produced and can be designed to meet the desired properties and function. [1, 46, 47]

The atomic order of biomaterial can be used to characterize the structural properties. If the atoms in the structure are arranged in periodic order, the material is crystalline. Contrary if there is no long range order material is amorphous. Material can also be semicrystalline, which means that it has both, arranged and random units. If the crystalline material has several different crystals, it is called polycrystalline. The structural order and property of the material may be different depending on the direction. For example, wood consists of fibers that grow vertically and make wood strong along the fibers, but perpendicularly to its fibers wood is not as strong. This is termed anisotropy. [8, 20, 27]

Biomaterials are used in medical applications. Thus, there is always some amount of interaction with the human body. Even inert alumina hip prosthesis activates response in the body that leads to the encapsulation of nearly inert material. Nowadays biomaterials in TE application should interact with the human body, hence degradation and bioactivity are important properties of the biomaterials. However, the degradation process is complicated from its mechanical aspects. [3, 38, 48, 49] The interaction of the biomaterial with tissue should be optimized so that degradation and tissue healing process would occur at the same rate. Additionally, the damaged side should have enough support throughout the healing process. Bioactivity can be used to active specific biological responses and enhance the material’s biocompatibility inside the human body by means of adhesive factors, growth factors or other cell signaling molecules [50].

The macrostructure of the biomaterial can be divided into porous or dense. High porosity is generally a desired property in TE as it enhances the biocompatibility of the material by ensuring the penetration of essentials, such as cells and nutrients. Important considerations are the size, shape, interconnectivity and location of pores. However, high porosity typically leads to weak mechanical properties [8, 51]. The stress concentration on the porous materials might be more complex than is thought [19, 51]. The selection of biomaterial is challenging when at the same time sufficient mechanical properties, suitable degradation rate and high porosity are desired [52].

2.3.1 Considerations in Compression Testing Biomaterials

This chapter provides basic overview of important considerations when the compression test is used for the mechanical characterization of biomaterials. As previously discussed the biomaterials can be classified into metals, ceramics, polymers, and composites. [3, 7] Some general differences in compressive properties and challenges in compression testing are discussed on different biomaterials.

Under compression metal and metal alloys exhibit a wide range of elastic modulus and compressive strength. Typically, metal alloys exhibit higher compressive modulus and compressive strength than pure metals and pure metals are more ductile compared with metal alloys. [3] Neither metal nor metal alloys exhibit a toe region. The stress-strain curve has a linear elastic region that ends to brittle or ductile fracture. Hence, the length of plastic region varies depending on the metal ductility. [8] Usually the compressive results are reported in GPa or MPa. The high strength of metals or metal may cause practical difficulties for mechanical tests. As the change in displacement becomes short, the displacement of a gauge becomes harder to measure. According to ISO 4506 [53] the clamp on extensometer should be avoided and recommends the use of a resistive strain gauge. Thus, with strong materials the quality of test machine and deformation measurement device becomes more critical. Metals have been used in medical implants for long time in different kind of load bearing applications. For example, Young’s modulus for titanium alloy dental implant has been reported at 110-116 GPa [4, p. 61].

Ceramics are typically stiff and strong, but brittle. Brittleness can be seen in the stress-strain curve as an almost unexisting plastic region during the compression test. The elastic region may be complex, but typically for solid ceramics it is described as a linear slope ending unexpectedly [8]. Highly porous ceramics may act differently having after the elastic region a plateau in which pores collapse progressively and lead to the failure of the structure [19]. Ceramics are sensitive to small imperfections. The flaws may be cracks, pores or other impurities in structure. Processing methods, such as cutting, thermal processing or mechanical stresses may cause defects that make a potential reason for an unexpected fracture. The compressive properties of brittle ceramic materials typically range from MPa to GPa. For example, ultimate strength and Young’s Modulus for solid hydroxyapatite have been reported 120-900 MPa and 35-120 GPa, respectively [54, p. 23]. For safe and reliable compressive results, several samples need to be tested to track the boundary conditions. The statistical method, Weibull Modulus, can be used to characterize reliability of the tested fracture strength. The ceramics, especially bioactive glasses [41, 55], have shown to be potential in orthopedics and dental scaffolds [20, 54].

Polymers are used in many different TE applications as their properties can be tailored widely. The atomic composition of the repeating structure can be modified. The stiffness can be customized by tailoring the amount of branching side chains, changing side chain lengths and polarities. The crystallinity of polymers can be modified by controlling the polymer chain orientation, by copolymerizing or blending with other polymers. Polymer behavior can be classified in brittle, plastic and highly elastic [8]. Polymers are not as strong as metals, but can be designed to be suitable for bone tissue applications [56]. Desired function of the polymers is the biodegradability, which should be tuned to match to the target tissue. The degradation mechanism can be enzymatic or hydrolytic [56]. Thermoset and thermoplastic polymers have different structures and properties. Thermosets have a cross-linked structure that makes the structure more rigid, but also irreversible [27]. Thermoplastics are sensitive to change in temperature, hence the temperature and compressive rate during the mechanical test are important. Compressive properties and failure modes of polymers depend on many factors. The failure may be sudden in elastic range if the material is brittle. Then again, more ductile polymer starts yielding before fracture occurs. [15]

Hydrogels are a type of polymeric material. The hydrogels have a polymeric network that contains of large amount of water. Inside the structure, polymers are connected covalently, trapping inside the water molecules. The structure is gel-like and has similarities with the extracellular matrix (ECM). The stress-strain curves may vary as the response to compression may vary from elastic to viscoelastic. [57] The compressive results of hydrogels are generally reported in kPa. For example, strength for collagen hydrogel with aldehyde modified dextran was reported at 32.5±1.6 kPa [58]. Hydrogel scaffolds are considered as a promising biomaterial due to their good biocompatibility. Synthetic and natural hydrogel scaffolds have been studied for nervous tissue [59], tendon [60], ligament, cartilage [61], skin [62], blood vessels and heart valves. [57, 63] Table 2 summarizes some of the biomaterials’ properties and problems that need to be considered during the compression test. It also gives methods to improve accuracy or precision.

Table 2. Problems and ways to minimize the measurement error for various material properties [3, 6, 7].

Material property	Problem	Ways to minimize error
Anisotropic	The properties of the specimen vary depending on the compressive direction.	• Test two groups of test specimen with axes parallel and perpendicular • Coordinate axes should be considered depending on the specimen structure
Brittle	Deformation is unstable.	• The equipment quality is important • Use high number of samples and evaluate the strength reliability using the Weibull modulus
Strong	Change in displacement is small. Displacement of the gauge becomes hard to measure (high noise to signal ratio).	• The equipment quality is important
Viscoelastic	Stress relaxation and creep of the specimen may occur.	• The compressive rate and testing environment need to be considered

2.4 Structure of Biological Tissue

Tissue physiology and biomechanics are important for TE. There are many kinds of tissues and functions in the human body. The function and location determine the structure of the tissue. For example, the bones in the spine are strong providing the main support for standing. On another hand, bones inside the ear are sensitive and transmit sound waves to the inner ear, enabling us to hear. [2, 64] This chapter focuses on the biomechanics of bone and cartilage. Both of them are connective tissue but have different properties and functions.

2.4.1 Bone

The most important roles of the bone are to form the skeleton that gives form to the body, enable body movement, store minerals, and create the armor around the internal organs. Bone has also a part in homeostatic regulation of blood calcium levels. The function of the skeleton may be compromised due to any disease, trauma, or biological process like ageing. Important research has been made on bone structure, growth, regeneration, adaptation and aging to develop mechanical testing of bone and bone-implant systems. [2, 65-67]

Bone tissue is a specialized form of connective tissue with hard and mineralized ECM. The composition of ECM varies depending on the tissue type as it consists of macromolecules secreted by resident cells. ECM is a very important structure for tissue reconstruction, as it gives tissue specific support, conducts cell signals, and dynamically reacts on environmental changes [68]. A closer look at nanostructure shows that bone's ECM consists of organic and inorganic components. The organic matrix mainly consists of type I collagen fibrils (>90 %) and the rest of the organic materials are non-collagenous proteins, proteoglycans and phospholipids. The organic part of the bone creates some fracture resistance, as it is capable to absorb shock. The inorganic part provides the rigidity of the bone tissue. The mineralized component is calcium phosphate as crystalline hydroxyapatite. The mineral content of the bone can vary a lot between species, age, the location of the bone etc. About one percent of the bone are cells. [69, 70]

Bone does not only consist of bone tissue, but has hematopoietic cells, adipose cells, blood vessels and nerves. In the microstructure (see Figure 10 (b)) there are Harvesian canal, Volkmann's canal, canaliculi, and lamellae. Haversian canal is surrounded with nested lamellae that creates circle-shaped osteon. Osteocytes are situated in lacuna. Haversian and Volkmann's canals contain the vascular and nerve supply of the bone. Bone is typically covered with a fibrous tissue capsule called periosteum, apart from the area where a bone is connected to another bone. In the bone connecting area the surface is covered with articular cartilage. [65, 71] Figure 10 shows the cross-section of a typical long bone divided in macro-, micro-, and nanostructure [71].

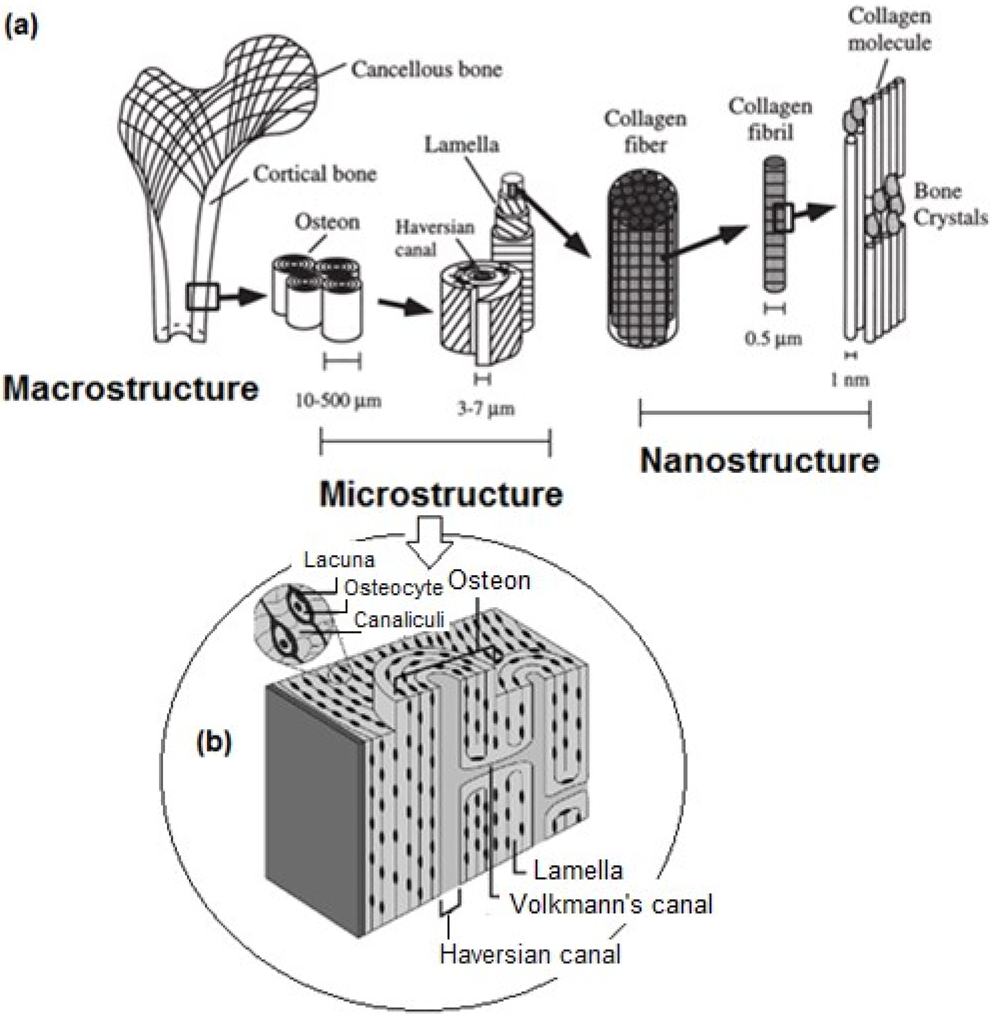

Figure 10. Hierarchical structure of the bone divided into macrostructural, micro-structural and nanostructural parts (a), adapted from [71]. Haversian canal and Volkmann's canal travelling inside the bone (b), modified from [4, p. 142].

The bone tissue can be classified according to its macroscopic structure to cortical bone or cancellous bone. The cortical bone or compact bone is dense and strong bone tissue that is located in the outer layer of the bone. The trabecular bone or spongy bone, resembles a spongy like structure that has strut like trabeculae oriented depending on the stresses on bone. These structural differences are related to their main function. The cortical bone gives support and structure when again cancellous bone has metabolic functions. Significant difference can be seen in porosity and in mechanical properties. [70, 71]

The structural part is not the only important aspect to understand, but the bone growth and regeneration processes are of particular interest when studying bone treatment options. The bone is a living tissue with several types of cells. Osteoprogenitor cells are derived from mesenchymal stem cells and are located in the outer layer of bone. Osteoprogenitor cells are actively involved in bone regeneration, which is called osteogenesis. Osteoprogenitor cells differentiate to osteoblasts that secrete the ECM of the bone. Eventually, osteoblasts get entrapped in the mineralized matrix and are called osteocytes. Some of the osteoblast may remain inactive and are called bone-lining cells. Those cells create the non-remodeling surface of the bone. Osteoclasts are multinucleated and phagocytic cells, that rise from hematopoietic lineage. The role of osteoclasts is to resorb bone, especially damaged bone. The bone structure is dynamic and a new bone is created as the old bone is degraded. [65, 72]

The maturation state of bone has influence on the bone structure. The bone has high regeneration potential and is able to remodel itself. Various signals and chemical enzymes controls the resorption and formation cycles. Immature bone or woven bone has randomized and non-lamellar structure. It can be found in a newborn, fracture calluses or in the metaphyseal region of a growing bone. Lamellar bone is mature. Lamellar has less cells than the woven but it has an organized structure leading to stronger bone. [66, 67]

The mechanical properties of bone may differ depending on many factors such as bone tissue type, location, porosity, apparent density and mineral content [73-76]. Thus, a significant difference in mechanical properties can be seen between different species [70]. Even the same species have individual bone structure that depends on age, gender, diseases etc. In general, the mineral content of the bone increases until maturity [9]. Table 3 gathers some results of bone mechanical properties for varying species, location and bone tissue type.

Table 3. Ultimate strength and Young's modulus for cancellous bone and cortical bone from different locations and species.

Reference		σ_{max}	**E**
	Cancellous Bone		
	Human		
Martens et al. [75]	Femoral head	9.3±4.5 MPa	900±710 MPa
Martens et al. [75]	Proximal femur	6.6±6.3 MPa	616±707 MPa
Ciarelli et al. [76] see Kuhn et al. [77]	Distal femur	5.6±3.8 MPa	298±224 MPa
	Canine		
Kuhn et al. [77]	Distal femur	7.12±4.6 MPa	209±140 MPa
	Cortical bone		
	Human		
Reilly et al. [78] see An et al. [9]	Femur	~167-215 MPa	~14.7-19.7 GPa
	Cattle		
Pal [6, p. 30]	Femur	147±1.1 MPa	8.7 GPa
	Bovine		
Li et al. [79]	Femur, longitudinal	214±28 MPa	19.1±2.8 GPa
	Femur, transverse	131±22 MPa	11.6±2.4 GPa

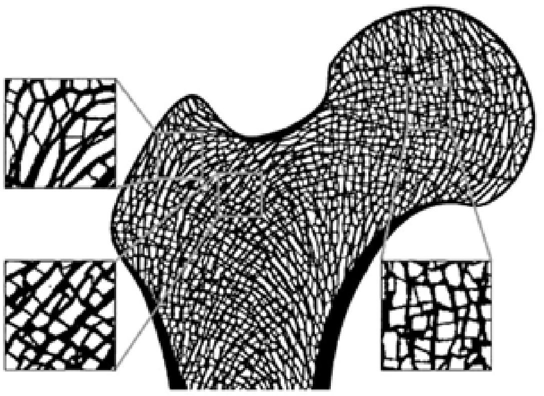

Figure 11. Anisotropy of proximal femur, adapted from [80].

There is variation in the mechanical properties of cancellous or cortical bone when samples of different species, anatomical location, bone tissue type or orientation are compared (Table 3). The cortical part has less heterogeneity than cancellous bone, which is related to its primary functions. The cancellous bone is highly anisotropic (Figure 11), non-homogeneous, porous and viscoelastic, which makes mechanical testing more challenging [80]. Sample preparation, test method and equipment need to be well planned. As the bone is living tissue, it needs to be handled with care. The bone can be kept moist by leaving some soft tissue around the bone during harvesting and then storing the bone in a freezer. Freezing is used to preserve cells and maintain the ECM of the bone. However, it does not completely stop bone deformation. [9] Hence, the freezing period and thawing-freezing times should be considered [9, 81]. Due to viscoelastic behavior, the temperature and compressive rate have effect on mechanical properties [82]. Additionally, whether one performs mechanical tests on wet or dry bone specimens is notable [9]. For example, saline can be used if the bone should be maintained moist during preparation and testing [83].

2.4.2 Cartilage

Cartilage gives elasticity and support for the body. Three different types of cartilage can be found in the body. Hyaline cartilage can be found for example in joints, trachea and nose. Elastic cartilage is highly elastic and can be found in the outer ear, larynx and epiglottis. The third cartilage is fibrous cartilage, that gives strength and resiliency in intervertebral discs. [66, 84, 85] The amount of movement cartilage permits varies depending on location and function. For example, cranial bones are connected tightly to each other without movement, cartilage in intervertebral disc moves slightly and joints that connect bones together allow a wide range of movement [65].

The hyaline cartilage is also called articular cartilage. The articular cartilage consists of a low amount of cartilage cells (~2-10 %) called chondrocytes. Chondrocytes mature from mesenchymal stem cells. After skeletal growth, chondrocytes are adult and have limited ability to divide. Chondrocytes depends on the diffusion of nutrients as there are no nerves, blood vessels or lymphatic tissue in the cartilage. Chondrocytes take care of cartilage by producing ECM. [6, 85]

The main component is water (65-80 %). Most of the solid part is collagen that gives structure and tensile strength. Collagen type II is dominant in the cartilage but there are also other collagen types as V, VI, IX, X and XI. Proteoglycans, such as glycosaminoglycans and hyaluronic acid, are shock absorbers in the articular cartilage. Minor solid components are for example fibronectin, lipids and decorin. The cartilage composition varies depending on location, age, injury or disease. For example, the number of cells decreases after fetal phase. [67, 85, 86] Table 4 summarizes different properties of bovine cartilage.

Table 4. Bovine cartilage properties and age differences, adapted from [86, p. 494].

Property	**Fetal**	**Adolescent**	**Adult**
Chondrocyte density (cells/ml, middle zone)	240 000	170 000	80 000
Collagen content (%)	4-5	6-8	10-14
Glycosaminoglycan content (%)	2.1-2.2	2.1-2.2	1.8-2.2
Water content (%)	88	82	80
Bulk E (MPa)	0.15	0.28	0.30
Middle/deep zone E (MPa)	0.13	0.65	-
Superficial E (MPa)	0.03	0.15	-

The structure of the articular cartilage depends on the location in the body. As the structure is heterogenous it is generally divided into four zones: superficial, middle, deep and calcified zone (Figure 12). These zones have characteristic properties and hence the compressive properties depend on the zone. Figure 12 illustrates structural differences between the zones. [84, 86]

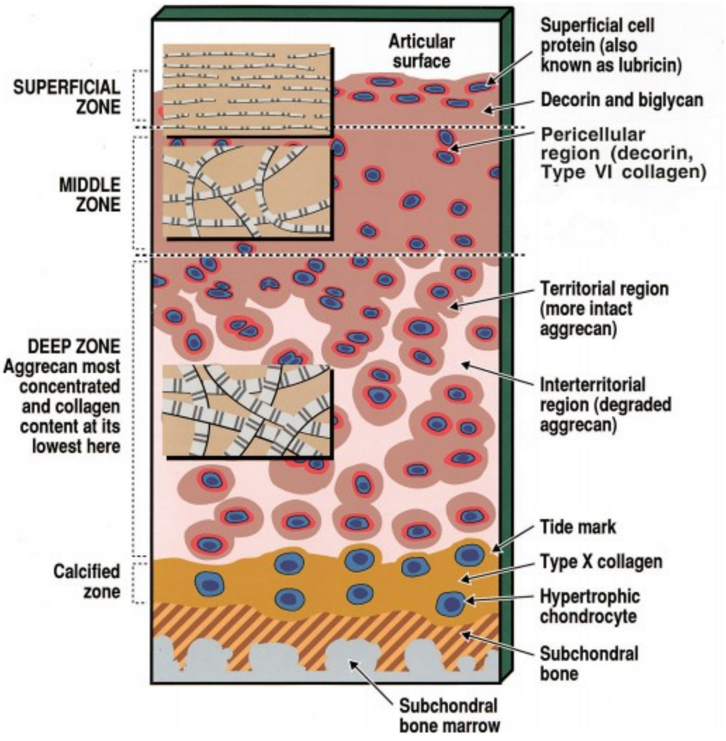

Figure 12. Articular cartilage divided in functional zones depending on structural components [84, p. 28].

Due to these structural factors, the cartilage is anisotropic. It has also pores for fluids to move and proteoglycans to absorb shock. The amount of water inside the cartilage effects the viscoelastic response, which is notable when characterizing the mechanical properties from a stress-strain curves. The compressive stiffness is related to the amount of proteoglycans, but mechanical tests are challenging to perform. For example, in addition to the heterogenous and viscoelastic properties, synovial cartilage is thin. Thus, there are many difficulties in order to explore the mechanical properties of cartilages. [84, 87, 88]

2.5 Scaffolds for Tissue Engineering

Scaffolds have an important role in TE. Scaffolds are biomaterial based 3D structures and are used as a temporary platform for cells to adhere, migrate, grow, and differentiate. The desired properties of scaffolds are biocompatibility, suitable mechanical properties, high porosity, biodegradability and bioactivity. Scaffolds are placed on damaged or dysfunctional tissue to promote repair or/and tissue regeneration. [2, 52, 64] Mechanical properties are one of the many important properties of scaffolds, but it has great influence on the function. Scaffolds should be designed to transmit the forces that the native tissue exhibits but also to degrade at a specific rate. The scaffold should support the tissue but also promote cell adhesion, growth and blood vessel formation. Due to the variety of tissues and their mechanical properties, there are various needs of scaffolds. For example, dentine needs to bear great forces during eating. Joints on another hand need to absorb different loads and bear stretch. Thus, mechanical tests are critical to characterize scaffold properties. [3, 4, 43] A wide range or biomaterials and properties have been produced for different tissue types. This chapter provides an overview for bone scaffolds and soft tissue scaffolds.

2.5.1 Bone Scaffolds

Ideal bone scaffolds give temporary support for bone regeneration by resorbing and eventually leaving behind new healed tissue [89]. The choice of material has great influence on the properties. There are a variety of biomaterials used in bone grafts. Metals, such as titanium and iron alloys, are strong enough but do not interact with bone and some of them have corrosive properties. Wide variety of degradable polymers have been used in TE. For example, polyglycolic acid (PGA) and polylactide (PLA) have been used commercially in bone scaffolds. [90] The degradation process is important for polymers. PGA degrades faster than PLA as it is more hydrophilic, but PGA has disadvantages. Degradation of PGA may cause a decrease in pH and result in necrosis [47]. Lately, attention has been brought to ceramic biomaterials, due to their similarity to bone composition. However, also ceramics have disadvantages in degradation, as it is difficult to control. Additionally, ceramics have a brittle property, that is challenging as any impurities or defects may cause unexpected failure and lower material’s strength [47, 91, 92].

The bone regeneration and materials resorption should be balanced. Too fast material degradation would leave the bone without support. On the other hand, a too slow degradation process could impede the bone regeneration. [44, 89] Additionally, the healing rates need to be considered as it varies depending on age. Younger individuals have faster healing rate than elderly people. [47] Bone regeneration can be induced by using growth factors or cells. More recently, specially designed bioceramics have been developed to induce bone regeneration. Those materials are called bioactive. [39, 54, 91]. Bioactive materials can be divided into class A and B. Osteoconductive biomaterials, such as calcium phosphates, some titania-based and glass ceramics, are in class B. These materials activate an extracellular response at the bone-implant interface, which supports the migration of capillaries, fibrovascular tissues and osteoprogenitor cells into the scaffold. This mechanism later triggers the new bone formation along the surface. Class A biomaterials, such as bioactive glasses and some glass ceramics, have intra- and extracellular response with surrounding osseous tissue. Osteoinductive materials activate surrounding mesenchymal stem cells to differentiate into osteoblasts. Generally, bone-bonding biomaterials form an interface with the bone through an apatite or calcium phosphate layer. [20, 93]

The architecture of the scaffold is important for osteogenesis, but it also influences to mechanical properties. The high porosity (>60 %) and interconnected pores with a diameter of at least 100 μm provides cell migration, vascularization, diffusion of essentials nutrients and bioresorbability. Vascularization is crucial for the survival of the cells in the inner parts of the scaffolds, thus the pore sizes 300-500 μm are usually preferred. [94, 95] The increase in pore size enhances the bone regeneration, but makes the scaffold structure weaker [19, 96].

A variety of preparation methods have been used for porous ceramics. Macroporous ceramic scaffolds can be prepared by partial sintering and direct foaming, or by using sacrificial fugitive or replica templates [97]. The challenges for porous scaffolds are the combination of mechanical properties and interconnected pores [97-100]. The 3D-printing techniques are used to enhance the control of the scaffold's architecture. Stereolithography is based on ultraviolet (UV) laser that moves over a bath of photopolymerizable liquid which begins to polymerize when exposed to the laser. This results in a solid layer after which the second layer is started and then the following one until desired scaffold structure is created. Selective laser sintering uses a laser to bind powders locally. Robocasting or direct ink writing is an extrusion based method, that plots struts through a nozzle and creates layers into 3D structures. [52] 3D-printing is generally considered as a potential method to customize the architecture of scaffolds and hence maximize mechanical properties [19, 52, 101]. Table 5 gathers some 3D-printed scaffolds' compositions and their respective mechanical properties.

Table 5. Compressive properties summarized for 3D-printed bone scaffolds.

Reference	Material	σ_{max}	m	E
Miranda et al. [102]	Hydroxyapatite	~50±10 MPa	3.2±0.2	7±2 GPa
	β-tricalcium phosphate	~15±5 MPa	-	2±1 GPa
Roohani-Esfahani et al. [33]	Strontium- hardystonite -gahnite	122±12 MPa	12-17	~2.4 GPa
Serra et al. [103]	PLA/PEG(a)	-	-	92±2 MPa
	PLA/PEG/G5(b)			100±4 MPa
Zhang et al. [104]	20Sr-MBG(c)	8.5±2.0 MPa	-	-
Zocca et al. [105]	Lithium alumino-silicate glass	3-15	-	-

(a) Poly(95L/5DL) lactic and polyethylene glycol
(b) Poly(95L/5DL) lactic, polyethylene glycol and bioactive calcium phosphate glass
(c) 20 % Strontium and bioactive glass scaffold

Generally, bone scaffolds that contain ceramic have limited mechanical properties due to variation in the compressive values. [52, 95] However, the compressive properties are similar to bone tissue [9].

2.5.2 Soft Tissue Scaffolds

Tissues can be divided into hard and soft tissue depending on their mechanical properties. Soft tissue is not as stiff as hard tissue. The structure and function of these tissues vary; hence the desired properties and structural needs of the scaffolds depend greatly on soft tissue type. [4, 6, 64] Some compressive strengths of different soft tissue scaffolds are gathered in Table 6.

Table 6. Compressive properties of soft tissue scaffolds.

Reference	Tissue	Material	Compressive strength
Bhardwaj et al. [106]	Skin (dermis)	Fibroin-keratin	~43 kPa (dry) ~21 kPa (hydrated)
Ellä et al. [107]	Joint	Knitted poly(L/D) lactide 96/4	~160-250 MPa
Zhu et al. [108]	Articular cartilage	Collagen/CH–PCL/CS composite(a)	~0.15 MPa (dry) ~39 kPa (hydrated)

(a) Collagen, chitosan–polycaprolactone and chondroitin sulfate composite

General challenges in soft tissue scaffolds such as blood vessels, skeletal muscle, and myocardium, are that they are mechanically active and have high volume and cell density [109]. Various materials, synthetic and natural have been used for soft tissue scaffolds. Both have disadvantages and advantages. However, the composition of synthetic materials can be controlled more easily to match mechanical properties and degradation rate of the substitute tissue. Also the surface properties can be tuned to be favorable to cells, but the degradation may cause unwanted reaction such as inflammation. [109] Synthetic biodegradable polymers, such as PLA, PGA and their copolymers have been studied widely. These materials have potential as porous scaffolds. For example, knitted poly(L/D)lactide 96/4 scaffolds have shown to be suitable for joint reconstruction [107]. Skin tissue, nervous tissue and cartilage tissue scaffolds are discussed more closely.

Skin burns or wounds can be healed or treated with skin implants. Especially important for skin scaffolds is that the scaffold attaches to the damaged skin and supports growth of blood vessels. Currently, vascularization can be introduced to about 0.4 mm thick material, which limits skin scaffold usage. Skin has various cells but the most common are keratinocytes, melanocytes and fibroblasts. Fibroblasts produce ECM giving the strength and resilience for the skin. [4, 68, 110] There are two important skin layers, thin barrier layer called epidermis and well vascularized layer called dermis. The skin engineered products can heal epidermis or dermis, but only few of them can heal both layers. There are many commercial products. Dermagraft® and Trancyte® use donor cells combined in synthetic scaffold to replace and heal dermis. Trancyte® also uses silicone membrane that temporarily mimics epidermal barrier. [110]

The nervous system is a network that controls and regulates movement, perception, behavior, memory, language and learning through neural circuits. It can be divided in central nervous system (CNS) and peripheral nervous system (PNS). The brain and the spinal cord belongs to CNS. PNS consist of nerves and ganglia that connects to all over the body outside of CNS. Neurons transmit signals through electrical and chemical signals. Neurons consist of axons that send signals and dendrites that receive signals. [66, 111] CNS have limited regeneration ability but PNS is more capable to regenerate. Neural scaffolds are used as a substrate to support and guide axonal regeneration. Generally, scaffolds have an oriented structure with fibers or channels that have properties to guide axons. For example, Neuragen^{TM} is a commercial nerve guide scaffold made of collagen-glycosaminoglycan. Also a polylactide-based mesh has shown its potentiality [112]. The elasticity of the scaffold has been found to be important for glial cells that are crucial for neural homeostasis [113]. The reported compressive modulus of polyethylene glycol (PEG) hydrogel for neural regeneration was about 260-280 kPa [114]. However, the effect of scaffolds on neural implantation is not yet well understood. [115, 116]

The aim of cartilage scaffolds is to give immediate support to cells and promote chondrocyte attachment, proliferation and maintenance. Interaction between cells and ECM is important, as cartilage has no blood vessels or nerves. Chondrocytes receive nutrition by diffusion, which makes cartilage a unique tissue. The regeneration process of cartilage is very limited. Due to limited regenerative properties, cartilage scaffolds can be pre-seeded by cultured cells, but the relationship between biosynthetic activity and seeding density is under exploration [85]. Cell types used in scaffolds are chondrocytes and mesenchymal stem cells harvested from various tissues. Also, signaling molecules, such as growth factors, can be used to control cell signaling. The three different cartilages, hyaline, fibrous and elastic cartilage, have different mechanical properties such as previously discussed. The engineered cartilage scaffolds should be optimized for age differences and tissue types. [14, 84, 85] Various scaffold materials, such as collage, fibrin gel, hyaluronic acid, polyglycolic acids and ceramics have been used for cartilage repair [85, p. 548].

3. MATERIAL AND METHODS

3.1 Materials and Sample Preparation

Materials with various properties, i.e. porous, solid, viscoelastic, hard, soft, brittle and anisotropic, were used in this study. Samples were prepared with a cylindrical form. Prior to mechanical tests, the length and diameter (ϕ) of the samples were measured using a Vernier caliper. All the measured values are reported using mean and standard deviation.

3.1.1 PET Foam

Three different densities (100 kg/m^3, 135 kg/m^3 and 210 kg/m^3) of thermoplastic and closed cell polyethylene terephthalate (PET) foams were prepared for compression tests. PET foams were provided by AIREX®, Switzerland. The mechanical properties are available from the website [117] and can be seen in Appendix 1. The distributor of the AIREX® T92 PET foam sheets (1220x610x5 mm) was Velox Oy, Finland.

Cylindrical PET foam samples were prepared in various ways. The sheets of PET foam included a welding line, which was included or excluded in the center of the samples (Figure 13). The samples were prepared in different sizes using a hollow punch tool. Additionally, five samples were hand prepared using a scalpel. The gathered information of the sample design can be seen in Table 7.

Figure 13. PET foam sample with welding line (a). PET foam without welding line having different densities (210 kg/m^3, 135 kg/m^3 and 100 kg/m^3) (b).

Table 7. Gathered information of prepared PET foam samples. PET foams are divided according to the density manufacturer reported.

Density (kg/m^3)	Surface preparation	Welding line (Yes/No/Both)	Diameter (mm)	Preparation method
210±10	-	Both	10, 14	Punched
210±10	-	Yes	6	Punched
210±10	-	Yes	10.2±0.2	Handmade
210±10	Epoxy	Yes	10	Punched
210±10	Silicon	No	10	Punched
135±8	-	Both	10	Punched
100±10	-	Both	10	Punched

The core structure of the foams was closed cells, hence a thin layer of epoxy based glue or silicone glue were added to fill the cut open cells at the surface. The sheet of PET foam was 5 mm thick, which gave the thickness of the samples. The only exception was epoxy glued samples that had some unevenness on the surface. The length of two batches of epoxy glued samples was measured from three different points and the average was calculated. The length of the samples with the epoxy glued layer was 5.2±0.1 mm (tested with Instron E 1000) and 5.5±0.2 mm (tested with Instron 4411). Three diameters of the punched samples were 6 mm, 10 mm, and 14 mm. The diameter of hand-carved samples was 10.2±0.2 mm, which was the average of three measured points. The apparent density was measured for the densest PET foam with and without welding line using the following equation:

$$\rho = \frac{m}{V} \tag{9}$$

where ρ is the density, *m* the mass and *V* the volume of the sample. Measured mass for densest PET foam with welding line was 94.0±26.1 mg (n=5) and without welding line was 75.7±1.0 mg (n=5). The volume of both samples was 392.7 mm^3. Calculated apparent densities with and without a welding line were 239.5±66.5 kg/m^3 and 192.8±2.5 kg/m^3 respectively. The porosities of PET foams were estimated using equation

$$\phi = \frac{\rho_v}{\rho_s} * 100\ \% = \left(\frac{\rho_s - \rho}{\rho_s}\right) * 100\ \% \tag{10}$$

where ϕ is the porosity, ρ_v is the void density, ρ_s is the density of the solid material and ρ is the density of the material. The used density was the value received from the manufacturer. The density of the solid material was calculated by following equation

$$SG = \frac{\rho_s}{\rho_{H2O}} \tag{11}$$

where *SG* is the specific gravity and ρ_{H2O} is the density of water. The used specific gravity for the PET foam was 1.37 [118] and the water density at 23 °C was 997.539 kg/m^3 [119].

Estimated porosities were about 93±5 %, 90±5 % and 85±5 % from the lowest to the highest density.

3.1.2 PU Foam

PU foam is used as an alternative material for the different properties of the cancellous bone to test orthopaedical devices [120]. In this study, three densities (80 kg/m^3, 160 kg/m^3, 320 kg/m^3) of polyurethane (PU) foam samples were prepared (Figure 14) and used as a second reference material. The PU foams were received in 13x18x4 cm sheets from Sawbones® Europe AB, Malmö, Sweden. The mechanical properties are available from the website [120] and can be seen in Appendix 1. The samples were drilled and cut into smaller size. The core structure of the PU foams was closed cells. The measured parameters of apparent density, diameter, length, mass, and porosity can be seen in Table 8.

Figure 14. PU foam samples of densities 320 kg/m^3, 160 kg/m^3 and 80 kg/m^3.

Table 8. Measured parameters of PU foam samples.

Apparent density (kg/m^3)	Diameter (mm)	Length (mm)	Mass (mg)	Porosity (%)	n
82.2±1.5	9.77±0.02	5.0±0.1	30.5±0.5	93±5	20
160.5±2.3	9.77±0.02	5.2±0.1	62.0±0.9	86±5	20
319.4±3.2	9.77±0.02	5.1±0.2	121.4±2.3	71±5	20

The diameter was measured three times on five samples. The average of fifteen measured diameters was used for all of the samples. The length and mass were measured for every one of the samples. The length was measured first by taking three different points of the length and then using the average. The apparent density and porosities were measured using the same method than for PET foam samples. The apparent density was calculated by using the equation (9). Porosities were calculated by using equations (10) and (11) The used densities were the values received from the manufacturer. The used specific gravity for PU foam was 1.11 [118] and water density at 23 ˚C was 997.539 kg/m^3 [119].

3.1.3 Hydrogel Scaffold

Hydrogel samples were made of GG, spermine tetrahydrochloride (SPM) and sucrose by the method described by Koivisto et al. and Salonen [34, 35]. A sucrose solvent was prepared dissolving 10.0 g of sucrose (Sucrose, BioXtra ≥ 99.5 % (GC), S7903, Sigma Aldrich, Finland) in 100 ml distilled water (10 % sucrose). The GG (Gelzan™ CM, Gelrite ®, G1910, Sigma Aldrich, Finland) solution was prepared by dissolving 250 mg of GG powder in 50 ml of 10 % sucrose solvent. Received concentration of GG solution was 5 mg/ml. SPM (Spermine trihydrochloride, BioXtra, ≥ 99.5 % (AT), 85578, Sigma Aldrich, Finland) was used as a cross-linker for the GG hydrogels. 14.0 mg of SPM powder was dissolved in 10 ml of 10 % sucrose solvent. The received concentration of SPM was 1.4 mg/ml. The SPM and sucrose solutions were stored in a refrigerator and the the GG solution was placed on a magnetic stirrer to dissolve overnight.

The GG solution is viscous at room temperature and heating the solution reduces its viscosity. This property was used during sterile filtration. The GG solution was heated (IKA®, RCT basic, safety control) in a water bath to 60 ˚C. Then the GG, SPM and sucrose solutions were filtered by Acrodisc® PF syringe filter with a 0.8/0.2 µm Supor® membrane (Cornwall, UK). After sterile filtering 1.4 mg/ml SPM was diluted with 10 % sucrose solution to 0.35 mg/ml concentration.

Hydrogel samples were produced into 5 ml cut syringes. The solutions were first heated in water at 37 ˚C before pipetting 750 µl of GG and 120 µl of SPM into the syringes (Figure 15). The solutions were prepared two at a time and mixed by pipetting. Heating facilitated the pipetting and mixing the solutions. Pipetting was done carefully to ensure homogenous samples and minimize air bubble formation.

Figure 15. Hydrogel samples gelling in molds.

Hydrogel samples were casted into cylindrical mold and kept on even base. The molds were self-made by cutting off the tip of the syringes. Before mechanical testing, hydrogels were kept at room temperature overnight to ensure complete gelling. The open surface of the mold was covered with a parafilm.

3.1.4 PLA Rod

PLA (70L/30D,L) rod was manufactured at Tampere University of Technology. The long PLA rod was cut into smaller samples (Figure 16). The length and diameter were measured by taking three different points and then using the average of the measured parameters. The measured diameter of the rod was 8.79±0.03 mm (n=25). The length of the PLA rod samples was 5.2±0.1 mm (for test with Instron E 1000 (n=20) and Instron 4411 (n=5)).

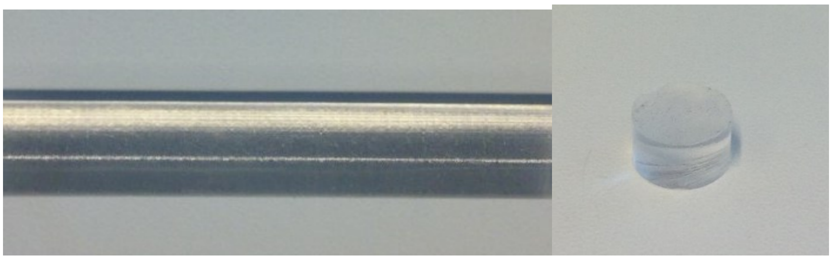

Figure 16. PLA rod and cut PLA rod sample.

The received samples had non-parallel surfaces after cutting. The percentage difference in measured lengths or surface tilt was calculated for every sample by using equation

$$Surface\ tilt\ \% = \left(\frac{h_{max}-h_{min}}{h_{min}}\right) * 100 \tag{12}$$

where h_{max} is the highest and h_{min} is the lowest measured length. The samples that were tested with Instron E 1000 had 1.1±0.6 % surface tilt and the samples tested with Instron 4411 had 3.9±1.3 % surface tilt.

3.1.5 Joint Scaffold

Ten batches of knitted scaffold structures, termed joint scaffolds, were received from Tampere University of Technology. Figure 17 illustrates the scaffolds of different sizes. One batch of the tested joint scaffolds were made of PLA (96L/4D) blended with 5 wt-% (mass percentage) PEG. PLA 96/4 + PEG 5 % scaffolds were not sterilized or heat treated. The rest of the joint scaffolds were made of PLA (96L/4D). PLA 96/4 joint scaffolds were heat treated in molds and sterilized by gamma irradiation. Table 9 gathers the batch numbers, sizes received from the manufacturer, measured diameter and length, materials, the date of manufacture and the number of samples.

Figure 17. Six different sizes of joint scaffolds.

Table 9. Gathered information of ten different joint scaffolds.

	Size (mm)	Apparent diameter (mm)	Apparent length (mm)	Material	Date of manufacture (mm/year)	n
Bionx						
S34	Φ8x3.6	8.2±0.3	3.6±0.1	PLA 96/4	03/2003	5
S37	Φ8x3.6	8.7±0.5	3.8±0.2	PLA 96/4	04/2003	4
S40	Φ8x3.6	8.6±0.4	3.8±0.2	PLA 96/4	04/2003	3
F22	Φ14x4.5	14.3±0.4	4.3±0.1	PLA 96/4	08/2002	8
Linvatec						
S54	Φ12x4	12.0±0.2	4.2± 0.1	PLA 96/4	06/2004	8
S54	Φ14x4.5	13.9±0.2	4.6±0.2	PLA 96/4	06/2004	8
S49/E68	Φ14x4.5	13.9±0.2	4.4±0.1	PLA 96/4	10/2003	7
S38	Φ16x4.5	16.0±0.3	4.4±0.1	PLA 96/4	04/2003	12
S38	Φ18x4.5	18.0±0.2	4.7±0.1	PLA 96/4	04/2003	9
Tampere University of Technology						
-	Φ14x10	14.0±0.3	10.0±0.2	PLA 96/4 + PEG 5 %	-	10

All the scaffolds were made by hand except for PLA of 96/4 joint scaffolds with batch number S54. The length and diameter were measured from three different points and the average was calculated. PLA 96/4 joint scaffolds were sterilized for two years after the manufacturing date.

3.1.6 Bioactive Glass Scaffold

Bioactive glass scaffolds were prepared in four steps: powder preparation, ink preparation, 3D-printing and sintering. The aim was to produce twenty uniform porous scaffolds. The glass had the following composition: 26.93 SiO_2, 26.92 B_2O_3, 21.77 CaO, 22.66 Na_2O and 1.72 P_2O_5 in mol %. The bioactive glass was labelled as B50 and was chosen for its favorable thermal properties [121].

The raw material for the glass was SiO_2, Na_2CO_3, $(CaHPO_4)(2(H_2O))$, $CaCO_3$ and H_3BO_3, received from Sigma-Aldrich®. The glass was prepared in a platinum crucible and melted in air. Electric furnace (Carbolite BLF 17/3, Carbolite® Ltd., UK) was heated up in steps to 1250 ˚C. The temperature was kept steady for 30 min when it reached 600 ˚C, 850 ˚C and 1250 ˚C. Figure 18 (a) illustrates the heating steps. Multiple isotherms allowed the release of H_2O, CO_2 and H_2 while preventing excessive foaming. After 30 min at 1250 ˚C, the melt was poured into a graphite mold and annealed in an electric oven (Nabertherm P330, Nabertherm GmbH, Lilienthal/Bremen, Germany) at 400 ˚C for 4 hours. The glass was cooled down to room temperature overnight. The solid glass was ground into fine powder. The particle size was controlled by sieving ground glass through a 38 μm mesh using a vibratory sieve shaker AS control 200 (Germany). Small particle size was used to enhance the flow consistency of the ink [122].

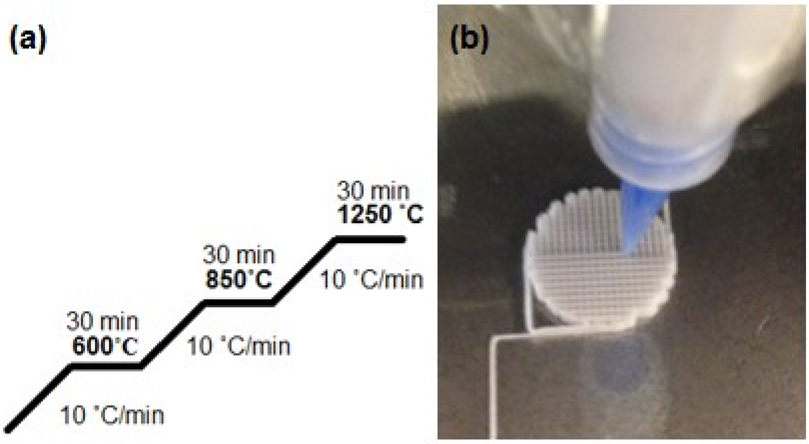

Figure 18. Heating steps for melting glass (a). Robocasting of bioactive glass scaffolds using layer by layer method (b).

Pluronic F127 is a thermoreversible synthetic copolymer that becomes fluid at low temperatures, but at room temperature it creates micelles and gels. Pluronic F127 (Sigma-Aldrich®) was used to bind the B50 glass powder together. 30 wt % Pluronic was prepared by dissolving 15 g of Pluronic F127 into 35 g of distilled water. Solution was left stirring for 24 hours in an ice bath. Then 2.349 g of B50 and 2.2407 g of 30 wt % Pluronic F127 were weighted and kept in the ice bath to keep Pluronic F127 fluid. Then solution was mixed by turn vortexing (Vibrofix VF1 Electronic, Janke & Kunkel IKA-WERK, Staufen, Germany) 30 s and cooling solutions 30 s in the ice bath. This was repeated until the powders were dispersed. Vortexing caused air bubbles, which were reduced by sonicating solution 40 s in an ultrasonic cleaning machine (FinnSonic M12, FinnSonic Oy, Lahti, Finland). After sonication tubes were placed in the ice bath and the ink was loaded into a 10 ml syringe.

The scaffolds were made using robocasting or in other words, direct ink writing method. The layer-by-layer method was used to build a 3D bioactive glass scaffold (Figure 18 (b)). The ink was robocasted by a computer controlled dispensing system (nScrypt Tabletop 3Dn, nScrypt Inc., Orlando, Florida). The diameter of the tapered dispense tip (Optimum® SmoothFlow™, Nordson EFD) was 0.41 mm. A colour laser printer and copier overhead transparency film (Folex®) was used as a substrate for the printed structure. The substrate provided sufficient adhesion for the first printed layer, which resulted in a stable ground layer. The scaffold was also easy to remove from transparency after drying. The 3D-printed scaffolds were left to dry for 48 hours at room temperature. Unnecessary edges were removed using a scalpel. Parameters of the 3D-printed scaffolds were measured to evaluate shrinkage after sintering.

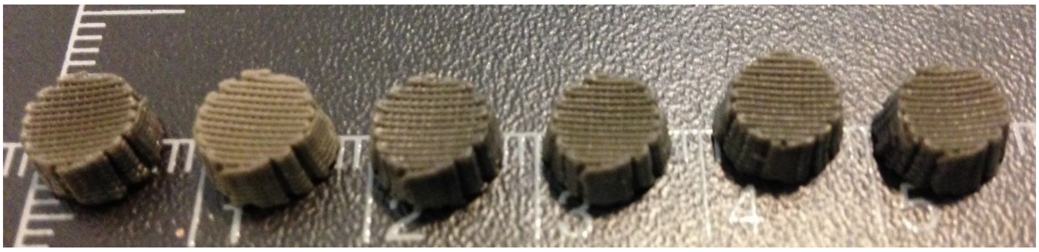

Figure 19. Sintered B50 scaffolds.

During sintering B50 powder particles coalescence into a denser structure as organics evaporate. In this study printed B50 scaffolds were placed into an electric oven (Nabertherm P330, Nabertherm GmbH, Lilienthal/Bremen, Germany) at room temperature and the oven was heated at rate 1 C°/min. When 515 C° temperature was reached, heating was stopped and the temperature was kept at steady state for 1 hour. Then oven was heated up to 585 C° at 1 C°/min heating rate and kept constant for 1 hour. The inaccuracy of the oven temperature was taken into account. Correct temperatures were about 15 C° less. Samples were cooled to room temperature. Figure 19 illustrates sintered B50 scaffolds. The length and diameter were measured from three different points of the samples and the average was calculated. The average of the measured diameters and lengths were 7.4±0.1 mm and 3.8±0.1 mm respectively. The scaffold shrinkage was measured from twenty-four samples using the same method. The received value was 21.2±3.6 %. Bioactive glass scaffolds were stored in a desiccator until the compression tests.

3.1.7 Cancellous Bone

Fourteen samples of cancellous bone were obtained from distal femur of a pig. Samples were taken from both lateral and medial femur (Figure 20 (a)). Pig's leg was left to thaw overnight. In order to keep pig's leg moist, it was placed in a plastic bag and kept in an air tight container. Tibia and femur were separated and femur was cleaned using a scalpel. Femur was stored into a freezer and taken out before sample preparation. Fresh frozen samples were machined using a band saw and a drill (Figure 20 (b)). The obtained cylindrical samples (Figure 20 (c)) were kept in a freezer until mechanical tests to keep them hydrated.

Buffer solution was prepared before mechanical test. Buffer was used during the mechanical test to keep samples moist enough. Sörensen buffer solution was made according to ISO 15814 [123]. Buffer contained 7.74 g of Na_2HPO_4 and 1.65 g of KH_2PO_4. The measured pH was 7.46 (Mettler-Toledo International Inc., Greifensee, Switzerland).

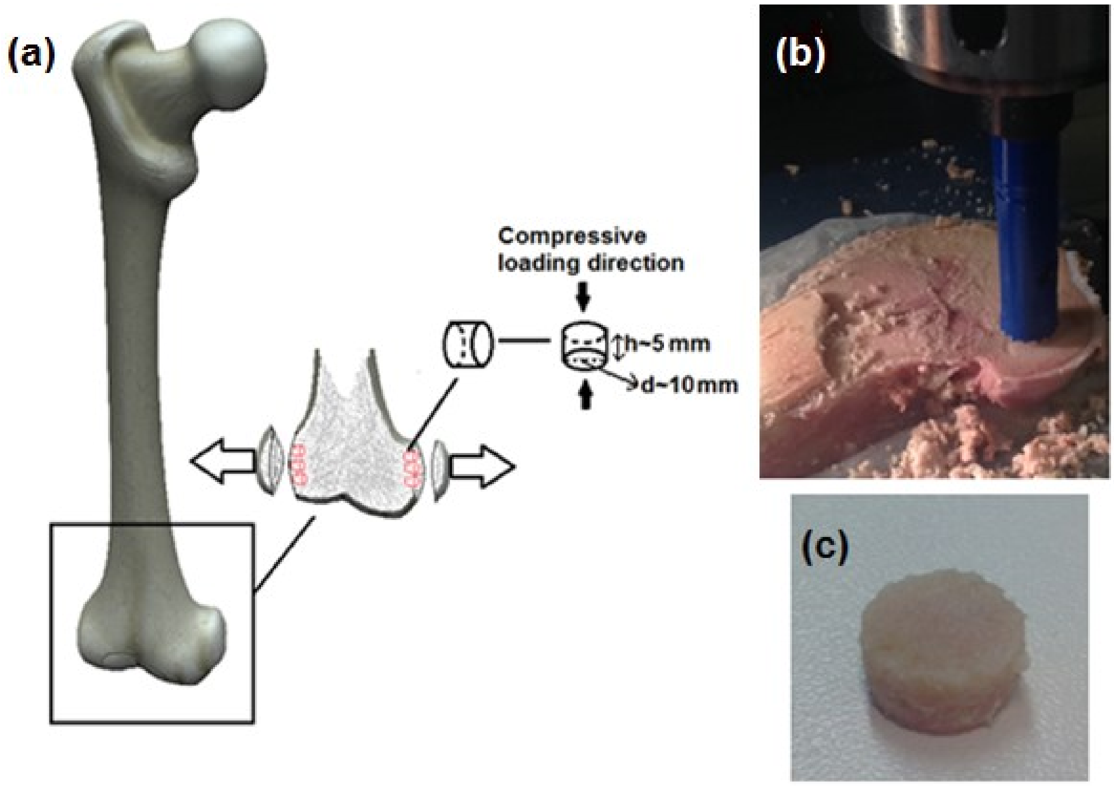

Figure 20 Cancellous bone samples were taken from pig's lateral and medial distal femur and prepared into ϕ10x5 samples (a). Samples were drilled (b) into cylindrical samples (c).

Samples diameter and length were measured before mechanical tests. Average of three measured points was used. Received diameter and length were 9.9±0.2 mm and 5.0±0.6 mm (n=14) respectively.

3.2 Compression test

Conventional quasi-static uniaxial compression tests were conducted using Instron Electropuls E 1000 (Instron®, High Wycombe, UK) (Figure 21 (a)) for all the materials. Additionally, Instron 4411 (Instron®, High Wycombe, UK) (Figure 21 (b)) was used for PET foam and PLA rod samples. The upper platen of Instron E 1000 was custom made at Tampere University of Technology. The diameter of the upper platen was 18 mm. In addition, the compressive parts of Instron 4411 were made at Tampere University of Technology. Other parts for the devices were provided by Instron®.

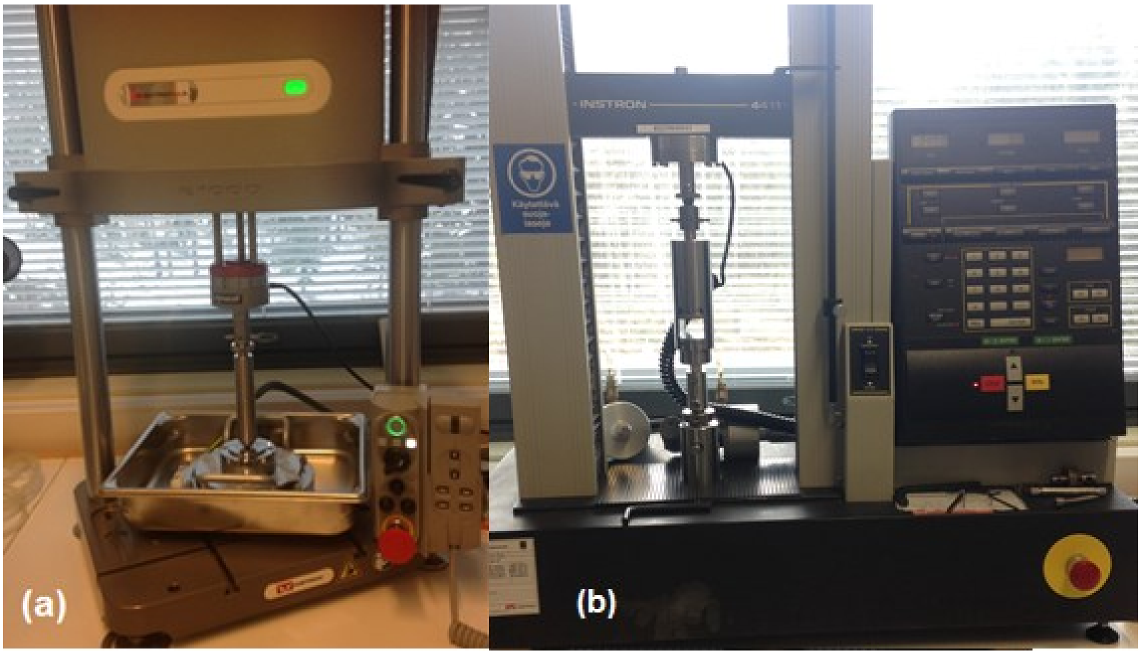

Figure 21. Testing machines Instron E 1000 (a) and Instron 4411 (b).

All the tests were performed at room temperature and in dry condition. The displacement of the test specimen was measured from the specimen platen interface. The gauge length for the tests were set as the length of the sample. The compressive strength and compressive modulus were analyzed from the stress-strain curves using an OriginLab software. In addition, the absorbed energy until yield was measured for PET foam, PU foam and cancellous bone samples. More detailed information of the compression test methods can be seen under tested material.

3.2.1 PET Foam

The compression tests for PET foams were performed using two different devices, Instron E 1000 and Instron 4411 (Figure 22). A 2 kN load cell was used for Electropuls E 1000 and a 5 kN load cell for Instron 4411. The tests were performed according to standard ISO 844 [127]. The cross-head speed was 10 % of the measured length, hence cross-head speed was about 0.5 mm/min. Additionally the rates of 0.1 mm/min and 1 mm/min were tested. Table 10 gathers testing device, cross-head speed, sample design (diameter, presence or not of the welding line and preparation method) and number of tested samples.

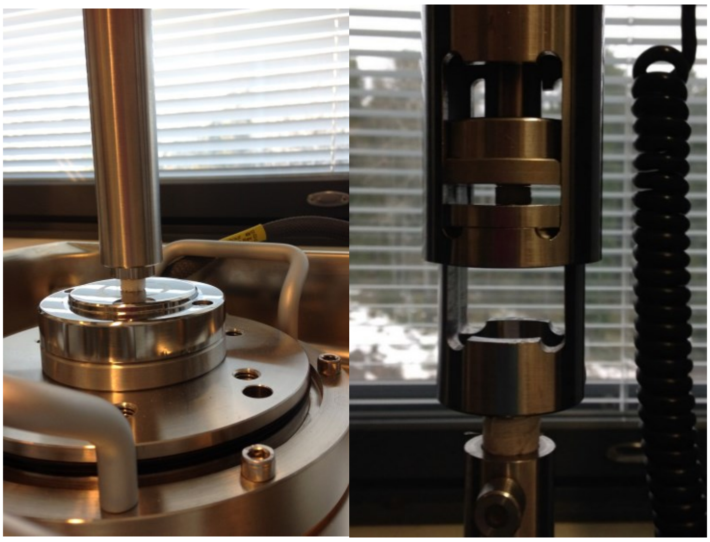

Figure 22. Compression tests of PET foam samples and mechanical testing devices Instron E 1000 and Instron 4411.

Table 10. Compression testing device, cross-head speed and number of tested PET samples with three densities, three diameters, welding line included or excluded and two preparation methods.

Compressive device	**Cross-head speed (mm/min)**	**Diameter (mm)**	**Welding line**	**Preparation**	**n**
PET foam 210 kg/m^3					
Instron E 1000	0.5	10	Yes+No	Punched	5+5
Instron E 1000	0.5	10	No	Punched & Silicone	5
Instron E 1000	0.5	14	Yes+No	Punched	5+5
Instron E 1000	0.5	6	Yes	Punched	5
Instron E 1000	0.52±0.01	10	Yes	Punched & Epoxy	5
Instron E 1000	1	10	Yes+No	Punched	5+5
Instron E 1000	0.1	10	Yes+No	Punched	5+5
Instron E 1000	0.5	10	Yes	Hand-carved	5
PET foam 135 kg/m^3					
Instron E 1000	0.5	10	Yes+No	Punched	5+5
PET foam 100 kg/m^3					
Instron E 1000	0.5	10	Yes+No	Punched	5+5
PET foam 210 kg/m^3					
Instron 4411	0.5	10	Yes	Punched	6
Instron 4411	0.55±0.02	10	Yes	Punched & Epoxy	6

The samples were compressed until 65-80 % strain depending on the sample density and compressive rate. The compressive strength was determined at 10 % relative deformation. The zero-deformation corresponded to the point where the stress reached 250 Pa.

Compressive modulus and absorbed energy until yield were determined using the method explained in theoretical background -section “2.1.1 Stress-Strain”. The fifth degree polynomial and its derivative was obtained using equation (5) and differentiating. The maximum of the derivative corresponds to the compressive modulus (see Figure 1 (b)). The yield point was found as described in Figure 1 (b). The absorbed energy until yield could be calculated by integrating the stress-strain curve up to the yield point.

3.2.2 PU Foam

The compression test for PU foam samples was performed using Instron E 1000. A 2 kN load cell was used for samples with densities of 160 kg/m^{3}and 320 kg/m^3. A 250 N load cell was used for samples with density of 80 kg/m^3. The tests were executed according to standard ISO 844 [124] similarly to the test performed for PET foam samples. The cross-head speed was 10 % of the measured length. Table 11 summarizes the test methods used for PU foams and the number of tested samples.

Table 11. Cross-head speed, compressive strain, capacity of the load cell and number of tested PU foam samples with three densities.

Density (kg/m^3)	Cross-head speed (mm/min)	Compression until strain (%)	Load cell (N)	n
80	0.50±0.01	75	250	20
160	0.52±0.01	75	1000	20
320	0.51±0.02	50	1000	20

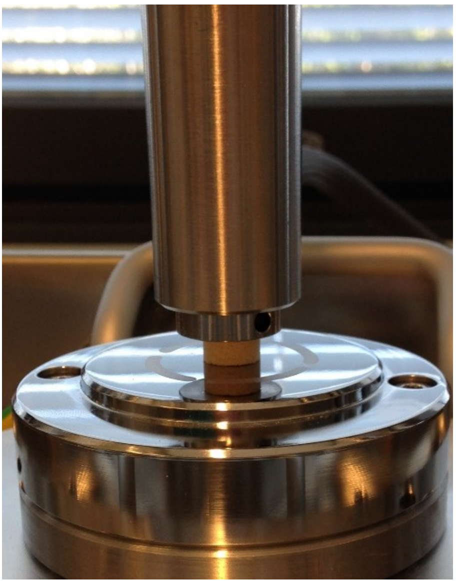

Figure 23. PU foam sample and starting position of a compression test.

The samples were compressed until 50-75 % strain depending on the sample density. The compressive strength was defined at 10 % relative deformation. Zero-deformation corresponded the point where the stress reached 250 Pa. Figure 23 illustrates the starting position of the compression test. The compressive modulus and absorbed energy until yield point was determined using the same method than for PET foams.

3.2.3 Hydrogel Scaffold

Thirty-two GG hydrogel scaffolds were compression tested using Instron E 1000 with the 250 N load cell. The upper and lower platen were covered with a thin piece of wet cellulose paper to increase friction between hydrogel and metal plates (Figure 24). The compression test was performed with a constant cross-head speed of 10 mm/min until 65 % strain. The method was obtained from literature [34, 35].

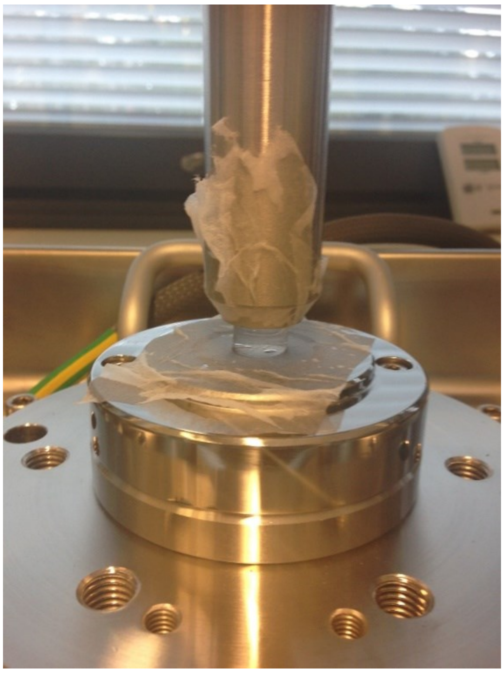

Figure 24. Setting of the compression test for hydrogel samples.

Samples were kept in molds until starting the compression tests. Before the test, sample was extruded out of the syringe on a plate. Extruded hydrogel sample can be seen in Figure 25. Three different zero-deformation points were used and referred as “A”, “B” or “C” position (see Figure 38 section “4.3.1 Considerations”). The gauge length of the A -position was the highest and C -position the lowest. The position “A” was achieved by carefully lowering the compressive platen until the hydrogel sample swell and adhere to the top platen. Seven samples were tested using the position “A”. The position “B” was achieved by lowering the compressive platen until platen touched the hydrogel and five hydrogel samples were tested. The position “C” was achieved by lowering the compressive platen until the gauge length was approximately the same as the sample length on the table before adhesion. Twenty samples were tested using the position “C”. Each length and diameter of the samples were measured three times prior the mechanical test and the average was calculated. The measured diameters for the positions “A”, “B” and “C” were approximately 12.3±0.1, 12.4±0.1 and 12.2±0.1 respectively. Measured lengths for positions “A”, “B” and “C” approximately 7.2±0.4 mm, 7.8±0.2 mm and 7.5±0.3 mm. Stress at zero-deformation point was slightly negative for all the three positions.

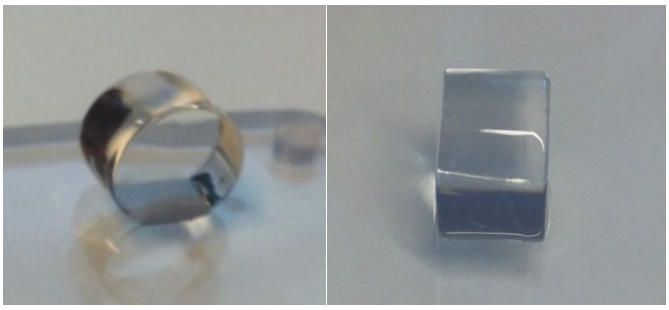

Figure 25. Hydrogel sample before the compression test.

The compressive strength was taken from the highest point of the stress-strain curve before a sudden drop. The compressive modulus was determined from the linear part of the stress-strain curve after a toe region approximately from 0.15-0.30 mm/mm strain.

3.2.4 PLA Rod

Instron E 1000 with a 2 kN load cell was used to test twenty PLA rod samples (Figure 26). Additionally, five PLA rod samples were tested with Instron 4411 with a load cell 5 kN. The compression test was performed using standard EN ISO 604 [125]. The compressive rate was 1 mm/min. Instron E 1000 was set to compress the samples up to 900 N and Instron 4411 up to 4 kN.

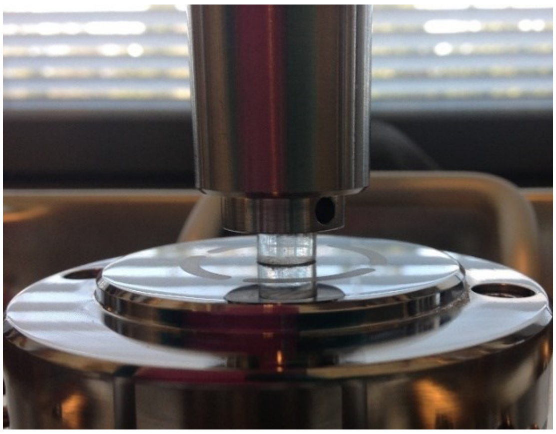

Figure 26. PLA rod sample in compression test.

The samples had slightly tilted surface. The gauge length corresponded approximately to the length of the sample. Zero-deformation corresponded to the point where the upper plate touched the sample (<0.0075 MPa). Compressive modulus was taken from the linear slope of the stress-strain curve (see Figure 43 section “4.4.1 Considerations and

Reliability”). PLA rod did not yield, hence the compressive strain at 900 N was taken for both devices.

3.2.5 Joint Scaffold

The joint scaffolds were compressed with Instron E 1000 using a 2 kN load cell. The compression test was performed by repeating previous study [126]. Joint scaffolds were compressed until 500 N at rate 2 mm/min. Zero-deformation corresponded to the point where the upper platen touched the sample while giving as little stress as possible (<0.0025 MPa) (Figure 27).

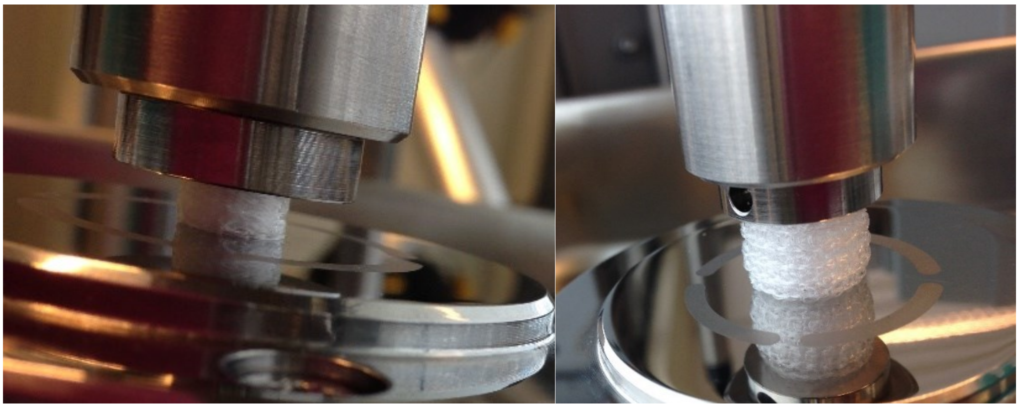

Figure 27. Smallest and highest joint scaffold set to compression test.

Th compressive modulus was determined approximately form 0-0.02 mm/mm strain. The compressive strain was determined from the points where the samples were loaded 80 N, 220 N and 440 N.

3.2.6 Bioactive Glass Scaffold

Twenty bioactive glass scaffolds were uniaxially compressed with Instron E 1000 (Figure 28). The used load cell was 2 kN and the compressive cross-head speed 0.5 mm/min. Instron E 1000 demands tuning of the specimen stiffness before compression test to optimize its performance for the test. Usually stiffness is tuned automatically, but for bioactive glass scaffolds the stiffness was manually set to 50 N/mm. The value was received from Instron® technician.

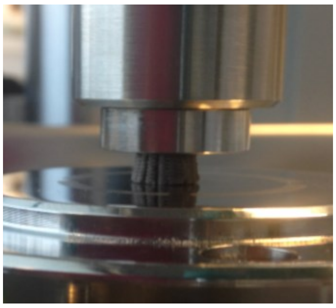

Figure 28. B50 scaffolds set to compression test.

The zero-deformation corresponded to the point where the upper platen touched the sample giving as little load as possible (<0.015 MPa). Scaffolds were compressed until breakage of the total structure. The compressive modulus was determined from the first linear slope of the stress-strain curve that reached higher than 0.5 MPa. The compressive strength was determined from the highest point of the stress-strain curve before a sudden drop.

3.2.7 Cancellous Bone

Fourteen cancellous bone samples taken from pig's femur were tested by Instron E 1000 with a load cell 2 kN (Figure 29). The samples were immersed in Sörensen buffer solution during the mechanical test to keep them moist. The buffer solution was warmed up to room temperature (22.5 ˚C) in a warm water bath (TW8, Julabo, Germany).

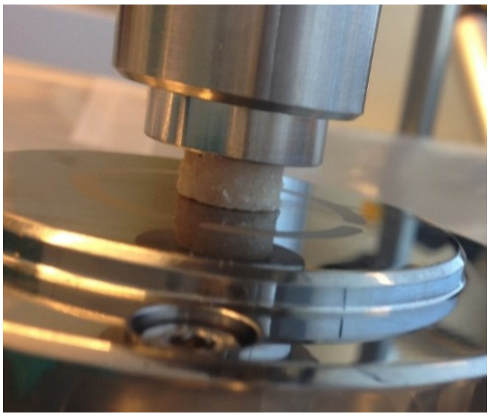

Figure 29. Cancellous bone sample at zero-deformation point during compression test.

The compressive test was performed as reported elsewhere [126]. The samples were compressed at a rate of 1 mm/min until 20 % compressive strain. The zero-deformation corresponded to the point where the upper platen touched the sample giving as little load as possible (<0.008 MPa). The compressive strength was the highest point of the curve. The compressive modulus was taken from the linear elastic part of the curve after a toe region from about 0.05-0.10 mm/mm strain. The absorbed energy was determined using the same method than for PET and PU foam.

3.3 Additional tests

Thermogravimetric analysis (TGA) and imaging were performed to understand better the structure-property relationship of the PET foams, PU foams, B50 scaffolds and the cancellous bone. Statistical tests were performed to support the evaluation of the data.

3.3.1 TGA

The inorganic content of the cancellous bone samples was analyzed using thermogravimetric analysis (TGA, Q500 TA Instruments, Delaware, USA). Five cancellous bone samples were as described elsewhere [126]. Tested pieces of the cancellous bone were 15-20 mg. The samples were heated up to 800 ˚C and kept 1 min at this temperature. The heating rate was 20 ˚C/min. The results were analyzed using Universal Analysis Software.

3.3.2 Imaging

The PET and PU foams with three densities were imaged with an optical microscope (Zeiss, West Germany). Additionally, micro computed tomography (µCT) was used to characterize the 3D microstructure and evaluate the porosity of the cancellous bone samples and B50 scaffolds. The analysis was made by the computational biophysics and imaging group at Tampere University of Technology. One sample was scanned for the materials.

3.3.3 Statistical Analysis

A statistical comparison was performed between compressive values by IBM SPSS statistics 23. The normality of the data was evaluated statistically (the Kolmogorov-Smirnov Test and the Shapiro-Wilk Test) and visually (Normal Q-Q plot). Table 12 summarizes the statistical methods used in the study depending on the data distribution and the number of groups. The null hypothesis was that no difference exists between the groups ($p>0.05$).

Table 12. Statistical methods used to evaluate the differences between data groups depending the data normality and the number of compared groups.

	Two groups	**More than two group**
Parametric	Independent t-test	One-way independent ANOVA
Non-parametric	Mann-Whitney test	Kruskal-Wallis test

The compressive strength of B50 scaffolds was characterized using Weibull statistics. Weibull modulus was calculated according to standard EN 843-5 [127]. Statistical analysis was performed using OriginLab software. First the compressive strength values were ranked in ascending order. Then the probability of each ranked strength value was determined using following equation:

$$P_{fi} = \left(\frac{i-0.5}{N}\right) \tag{13}$$

where P_{fi} is the i^{th} probability of each ranked strength value, i is the rank of the strength value in the strength value population and N is the total number of the strength values. The x-axis and y-axis was determined using equations

$$y_i = ln\left[\ln(\frac{1}{1-P_{fi}})\right] \tag{14}$$

$$x_i = \ln(\sigma_{fi}) \tag{15}$$

where σ_{fi} is the i^{th} strength of the ranked test sample, y_i is the i^{th} ranked data point for y-axis and x_i is the i^{th} ranked data point for x-axis. Data points were plotted and a linear fitting was performed for the plotted points. The Weibull modulus was the slope of the fitted line.

4. RESULTS AND DISCUSSION

In this section, the results are reported and the reliability and limitations of the compression test are discussed. The results are represented using mean and standard deviation.

4.1 PET Foam

The performance of the mechanical testing device Instron E 1000 was evaluated by comparing the measured compressive values of PET-foam samples with the compressive values provided by the manufacturer (AIREX®). The compressive values are termed as reference values and can be seen from Appendix 1. Additionally, the performance and limitations of the Instron E 1000 was evaluated by testing the same materials with another testing device. At least five samples were tested per variation in method, device, sample size or sample structure. The results are gathered in Appendix 2.

4.1.1 Specimen Design and Device Performance

PET foam with three different densities (100 kg/m^3, 135 kg/m^3 and 210 kg/m^3) were compression tested. Porosities were estimated using equations (10) and (11) (see section "3.1.1 PET Foam"). The porosities from the lowest foam density to the highest were approximately 93 %, 90 % and 85 %. Figure 30 shows the microscopic images of the cut open cell structures (a-c) and stress-strain curves of PET foams (d). The increase of density resulted in steeper and higher slope and indicated an increase in stiffness and strength. In the stress-strain curves, we can see a plateau region for all the foams after an elastic phase. During this phase, the pore walls bend and collapse gradually. For the densest material, the plateau region is the shortest as there are probably less cells being crushed. Eventually, the cell walls touch each other and a densification phase begins. [128] The densification phase can be seen as a steep increase in the slope.

The manufacturer tested 100x100x50 mm sized cubic PET samples that had a welding line in the center of the sample and a thin glued epoxy layer on the top and bottom surfaces. The compressive method was obtained from standard ISO 844 [124] and the same method was attempted to use in this study. However, this was not possible with our instrument. The diameter of the compressive platen was 18 mm. Therefore, the PET samples in this study were ten times smaller than reference samples. Additionally, the design was cylindrical not cubic. The same standard was applied in this study and the suggested compressive rate was 10 % of the sample length [124]. Therefore, some differences in compressive properties were expected due to the differences in size, design and cross-head speed.

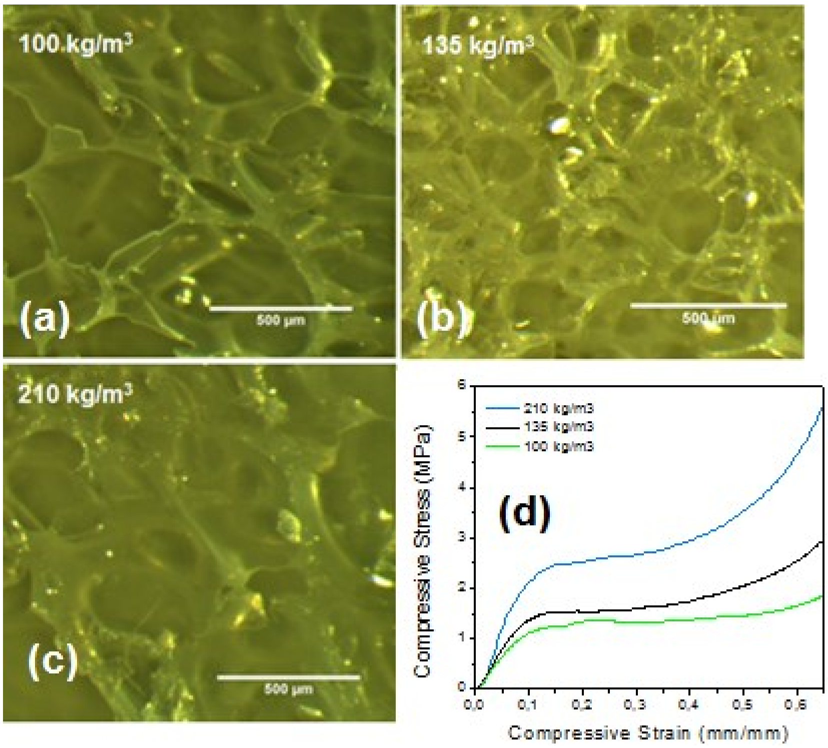

Figure 30. Optical microscope images illustrating the structure of PET foam specimens (a-c). Stress-strain curves of the investigated PET foams. (d).

As explained previously, the manufacturer had included the welding line in the center of the samples. In this study, we tested samples with and without the welding line. Figure 31 illustrates the compressive strength (a) and compressive modulus (b) for the tested samples along with the reference values. The difference between the reference value and the measured one are expressed in %. An increase in density results in a higher compressive strength and compressive modulus. Slightly more variation in the standard deviation can be seen for the densest foam, which could be due to an increase of non-homogeneity in the pore structure of the densest foam. Indeed, the cell shape, cell size, cell distribution and cell wall thickness in the foams were random. Nevertheless, an increase in density and the following decrease in porosity is expected to lead to increased mechanical properties [51, 129-132].

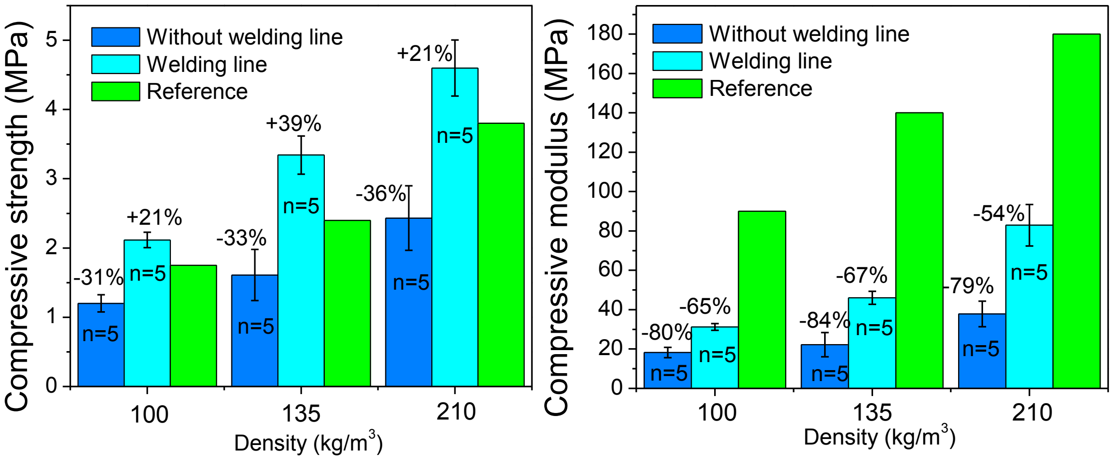

Figure 31. Compressive strength and compressive modulus of PET foam with three different densities, with and without welding line. Blue columns indicate samples without the welding line, the light blue are columns with the welding line and the green columns are the reference values. The % above the columns are differences between measured values and reference values. The number of samples are in the columns.

The compressive strengths for the samples without the welding line were 31 to 36 % lower than the reference value. This was expected as the manufacturer had included the welding line in the center of the samples. However, the presence of the welding line in the center of the samples had significant influence on the mechanical properties. The measured compressive strength was 21 % to 39 % higher than the reference value when the samples were tested with the welding line. In this study, the size of the samples is not comparable to the samples tested by the constructor. The reference values were obtained by testing ten times bigger samples. The over-estimated compressive strength can be to the welding line having more impact on small samples compare to larger samples. The effect of the sample size and the design on the structure of the samples was evaluated. The apparent densities for the samples used in this study were calculated using equation (9) (see section “3.1.1 PET Foam”). The apparent density of the samples without welding line was 193±2 kg/m^3 and with the welding line 240±67 kg/m^3. The reference material had the density ranging from 200 to 220 kg/m^3 [117]. The samples without the welding line had logically lower density that resulted in lower compressive strength. The higher density for our samples with welding line compare to the one reported by the manufacturer confirm that the welding line will have more impact on small samples than on larger ones. Figure 32 illustrates the differences in the design and density of the tested and reference samples.

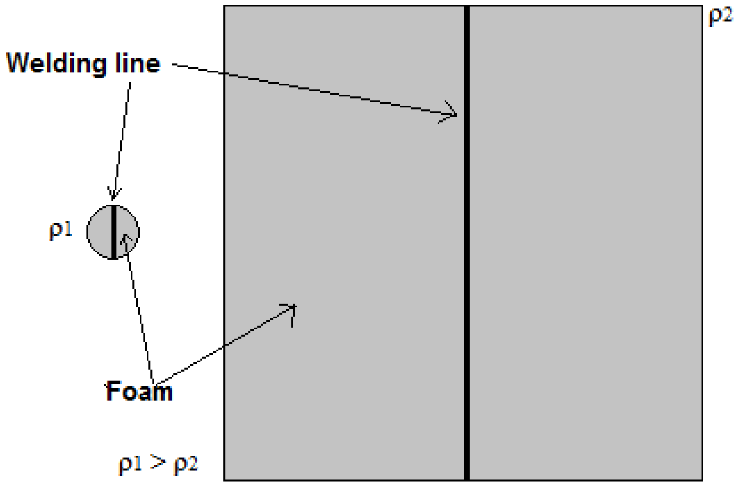

Figure 32. The part of the foam in a bigger and cubic sample is higher than in a smaller and cylindrical sample, which leads to a lower density. The width of the welding line stays the same.

The measured compressive modulus for the samples with different densities showed great difference (>50 %) when compared with the reference material. Again, less difference was in the compressive modulus of the samples with the welding line compared with the samples without a welding line, which was expected as the reference values were received with the welding line. However, the huge difference in the compressive modulus raised questions on the methodology used for testing our samples.

The samples with 6, 10 and 14 mm diameters were tested to study the impact of the sample size in the compressive results. All the tested samples included a welding line. The compressive results of three different specimen sizes are shown in Figure 33. A significant difference between different sizes can be seen for compressive strength (p=0.022) and compressive modulus (p=0.005). According to these results, the smallest specimens had the highest compressive strength and compressive modulus. Then again, the specimens with the highest diameter had the lowest compressive modulus and compressive strength. Generally, it is known that the specimen size has effect on compressive properties [3, 9]. For example, specimens may exhibit buckling when the relationship of the specimen length and diameter is less than 2:1. Chen and Fleck reported smaller metallic foam samples having higher mechanical properties [133]. Their results did support the results received in this study. However, Andrews et al. reported that the compressive stiffness and strength of aluminum foams reduce with decreased sample size [134]. Thus, the size effect needs to be taken into consideration.

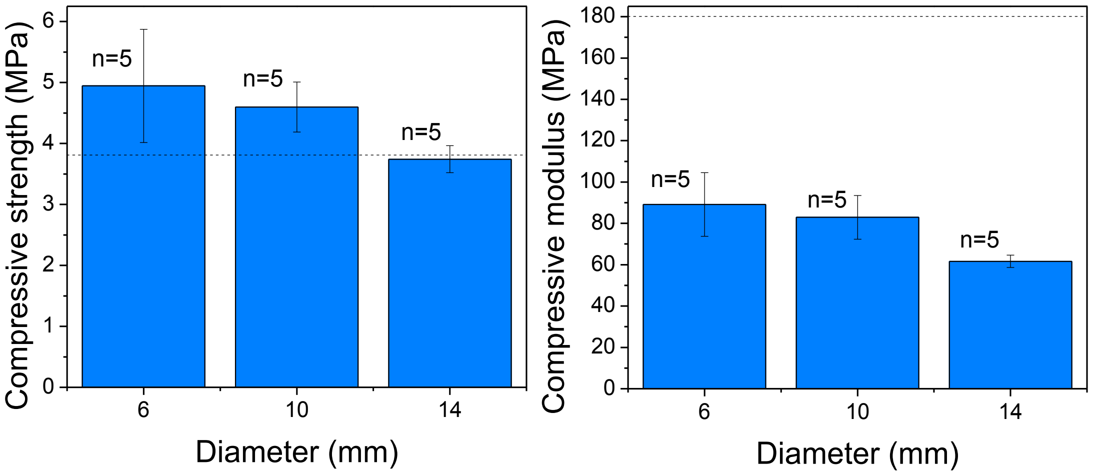

Figure 33. Compressive strength and compressive modulus of three different diameters of 210 kg/m^3 PET foam. Dotted lines represent the reference values. The number of samples are above the columns.

Again, greater difference can be seen in the compressive modulus than in the compressive strength when the reference values and measured values are compared in Figure 33. According to the results, the decrease in the sample size caused bigger standard deviation in the compressive modulus. This could be due to the punching preparation method, that may have caused some inconsistency and damage in pores and could in smaller samples have higher impact on the total structure and on mechanical properties.

Experimental errors were studied in two ways. Due to the uncertainty of the structure consistency of the punched samples, we prepared samples using a scalpel in order to minimize the risk of the damage. Additionally, during the compression test, the device assumes that the compressive platen gives load on a sample with a solid surface. This causes inaccuracies with porous materials as the platen loads the cell walls, not the total surface area of the foam sample. Hence, the surface pores on both sides of the foam samples were closed by a thin layer of silicon or epoxy glue. The cross-head speed was set to 0.5 mm/min (for 5 mm high samples) as suggested in the standard ISO 844 [124]. The impact of the cross-head speed was also investigated by testing the PET foam samples (punched, open cell surface, ϕ=85 %) at 0.1 and 1 mm/min.

The results of the compressive strength and compressive modulus of PET foam with density 210 kg/m^3 are gathered in Figure 34. The samples with the welding and without the welding line are separated by large squares. The result of the faster compressive rate (1 mm/min) is coloured light blue and the slower compressive rate (0.1 mm/min) is coloured green. The dotted line presents the reference value obtained from the manufacturer.

The samples with the welding line exhibited slightly higher compressive strength than the reference value. On the contrary samples without the welding line had slightly lower values. Two values of the compressive strengths were overlapping the reference value in

Figure 34. One of these values was received with the compressive rate of 0.1 mm/min and another was with a bigger (14 mm) diameter. A reversed effect on results can be seen by increasing the compressive rate or decreasing the diameter. Generally, sensitivity to the strain rate is a sign of viscoelastic behavior, but also the closed cell structure might have some effect if gases are trapped inside the cells [135].

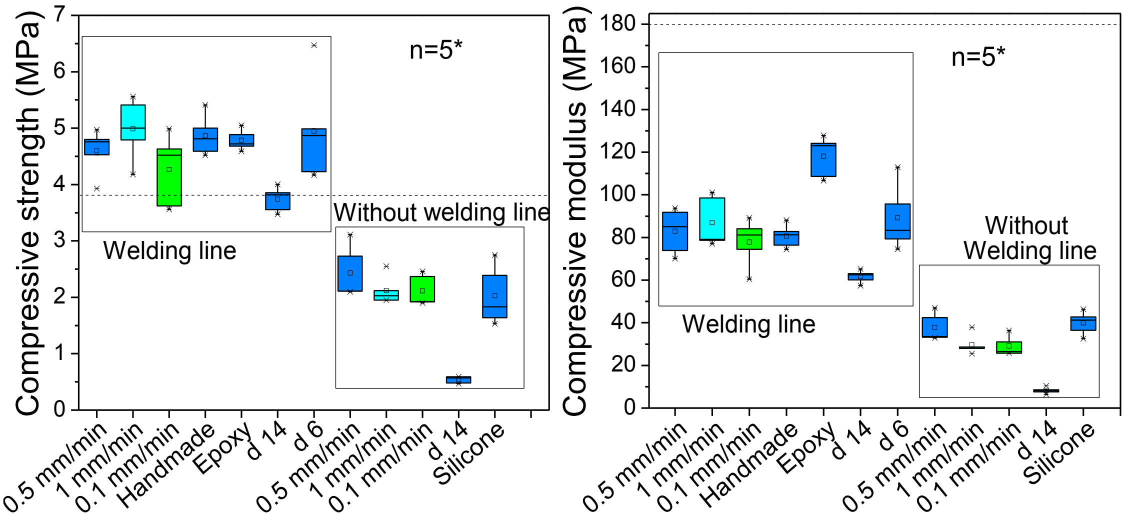

Figure 34. Compressive strength and compressive modulus of 210 kg/m^3 PET foam. The results with and without the welding line are separated. The blue colour represents the compressive speed of 0.5 mm/min, light blue 1 mm/min and green 0.1 mm/min. The dotted line indicates the reference value. *The number of specimens was five for each variation.

The difference between the measured and reference values of the compressive modulus was remarkable (Figure 34). The epoxy glued samples showed slightly more accurate results for the compressive modulus, but flexible silicone samples did not show an increase in the modulus (Figure 34). Silicone glue might not be as stabilizing glue as epoxy. However, even the use of epoxy did not improve the measured compressive modulus enough. Similar inaccuracies have been reported in the literature [5]. According to Keaveny et al., the error in the compressive modulus could be explained by the specimen surface artifacts in case the change in length is measured from specimen-platen interface [5].

Generally, the term surface artifact is used when there is a discussion about the experimental errors of the conventional compression test. Surface artifacts may refer to three different experimental artifacts: friction artifact, damage artifact and compliance artifact [5]. The term friction artifact is used when there is friction between the sample surfaces and compressive platens. The friction results in non-uniform stress distribution during the compression test. For example, bulging of a specimen is a cause of friction artifact. The damage artifact refers to the phenomena on the end surfaces of the sample. [5] The damage can result from cutting the sample surfaces, such as discussed with the

PET foam samples. Compliance artifact is occurring due to the high stiffness of the load frame and compliance of the load cell [5, 136]. Table 1 in section 2.2.3 “Specimen” gathers general problems and some methods to minimize the artifacts.

According to the manufacturer, the compressive values of PET foams in their Technical data sheet [117] were conservative. Hence, the accuracy of the compressive strength was good. However, the use of glue did not sufficiently improve the accuracy of the compressive modulus. The cut sample surfaces affected the measurement, as the samples were most likely too thin. For biomaterials, there are other suggested methods to exclude the surface artifacts. Extensometer can be used to measure the strain precisely from the intact center part of the specimen [3, 24]. There are contact and non-contact extensometers. The contact-extensometers have two challenges. The tested specimens should be larger than the ones we can use with our instrument. The second problem is that mostly the biomaterials breaks under compression and the breakage may cause inaccuracies in the measurements when the extensometer is in contact with the specimen. The solution could be an optical extensometer that can measure the strain by a laser or with video images without touching the sample. Additionally, a self-aligning platen could be used to minimize non-uniform stress distributions if the sample surfaces are non-parallel.

4.1.2 Comparison of Devices

Two compressive testing devices (Instron E 1000 and Instron 4411) were compared. The testing method and samples were the same. Five samples of 210 kg/m^3 PET foam with and without epoxy glued surfaces were tested with both devices. Figure 35 shows the compressive results. The dotted line illustrates the reference value. The results of the compressive properties were controversial. Instron 4411 showed more accurate results on compressive strength but Instron E 1000 showed more accurate results on compressive modulus. Instron E 1000 has a patented algorithm for stiffness tuning, which automatically optimizes the system before the test by measuring the stiffness of the specimen. This facilitates the testing and could be a factor that enhances the precision of the compressive modulus. A high standard deviation can be seen for the epoxy glued samples tested with Instron 4411 (Figure 35). This could be due to the difficulties in determining the zero-deformation point as the surface of the glued samples was slightly uneven and the gauge length needed to be measured by hand using a Vernier caliper. Similar problems were not experienced with Instron E 1000, as Instron E 1000 had a fine cross-head adjusting system simplifying the determination of the zero-deformation point.

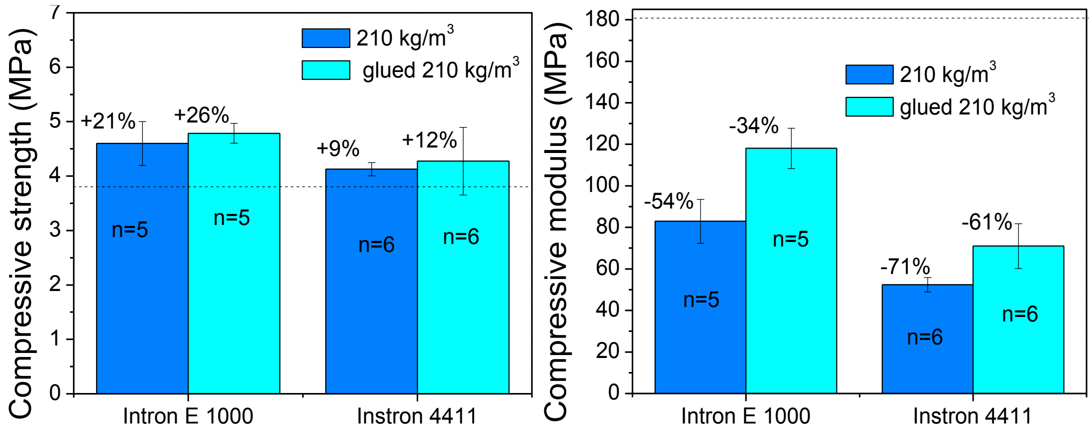

Figure 35. Comparison of two mechanical testing devices, Instron E 1000 and Instron 4411. The blue columns are the compressive strength and compressive modulus of samples with a welding line. The light blue columns are the compressive strength and compressive modulus of the same samples with epoxy glued surfaces. The dotted lines represent the reference values. The number of samples are in the columns.

No significant difference was seen between the compressive strength of non-glued and glued samples either for Instron E 1000 ($p=0.374$) or Instron 4411 ($p=0.578$). When the devices are compared, a significant difference between the compressive strength of non-glued samples ($p=0.023$) can be seen, but not between glued samples ($p=0.112$).

A significant difference was seen in the compressive modulus of the non-glued and glued samples for Instron E 1000 and Instron 4411, and between the devices ($p<0.002$). Altogether, Instron E 1000 shows more accurate results compared with Instron 4411 when both compressive strength and compressive modulus are considered. The use of glue decreased changes in the compressive strength, but did not give satisfactory improvements in the compressive modulus as both devices underestimated the compressive modulus by at least 34 %.

4.2 PU Foam

PU foam was the second reference material that was used to evaluate the performance of compression testing device Instron E 1000. The compressive results were compared with the reference values provided by Sawbones® (see Appendix 1). The structural properties to the mechanical test were discussed. At the end of this section, the limitations and reliability of the test results of both reference foams were evaluated.

4.2.1 Reliability and Limitations

Twenty samples of three different foam densities (80 kg/m^3, 160 kg/m^3, 320 kg/m^3) were tested. Foam porosities were estimated using equations (10) and (11) (see section "3.1.1) PET Foam"). The approximate porosities for PU foams were 93 %, 86 % and 71 % from the lowest density to the highest. An optical microscope was used to image the microstructures of the foams. The structural differences between the PU foams and the effect on the stress-strain curves are shown in Figure 36. According to the optical microscope images, the pore size decreased when the density increased, which logically caused strengthening of the material [3]. The pore structure was different between PET and PU foams. However, the compressive behavior was similar. Again, the denser foam presented a steeper slope and a shorter plateau region on the stress-strain curve. The smaller cells in the densest PU foam were most likely to deform and close at faster rate [137]. Therefore, densification initiated at earlier strain for denser PU foam. Additionally, compressive results in Figure 37 showed that the densest foam had higher standard deviation as was the case with the densest PET foam. Thus, the variation in compressive properties could be dependent on porosity parameters. Meille et al. reported similar results [19]. However, the fraction mechanism of non-homogeneous and porous materials is complicated and needs more research.

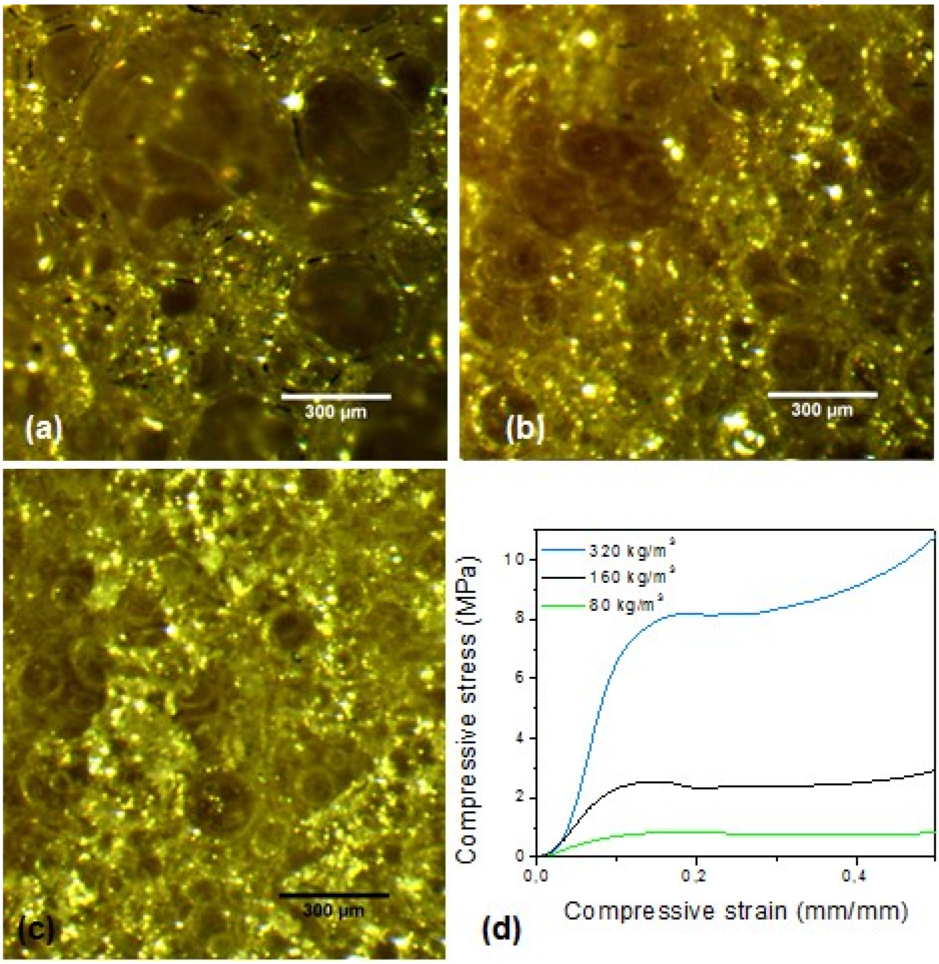

Figure 36. Optical microscope images of the cut open pore structure of PU foam specimens with three different densities (a-c), and the stress-strain curves of the investigated samples (d).

The manufacturer tested cubic 2x2x1 inch (~50x50x25 mm) sized PU samples according to ASTM F1839-08. Similar method was attempted to use in this study, but as earlier discussed the diameter of the compression platen limited the sample size. The samples in this study were cylindrical and about five times smaller than the reference samples. The suggested compressive speed was 10 % of the sample length [124]. Therefore, some differences in compressive properties were expected due to the differences in size, design and cross-head speed.

Figure 37 summarizes the compressive strength and the compressive modulus of the measured and reference values. The % value above the columns represents the difference between the measured and reference values. Similarly to the first reference material, the compressive modulus measured using Instron E 1000 underestimated the compressive modulus, but the compressive strengths were more accurate (Figure 37). Depending on the density, the error in the compressive modulus were about 40 %. Additionally, some differences in the compressive strength could be seen, which could be due to many reasons such as the small sample size, difference in design or surface artifacts on the specimen-platen interface like earlier discussed.

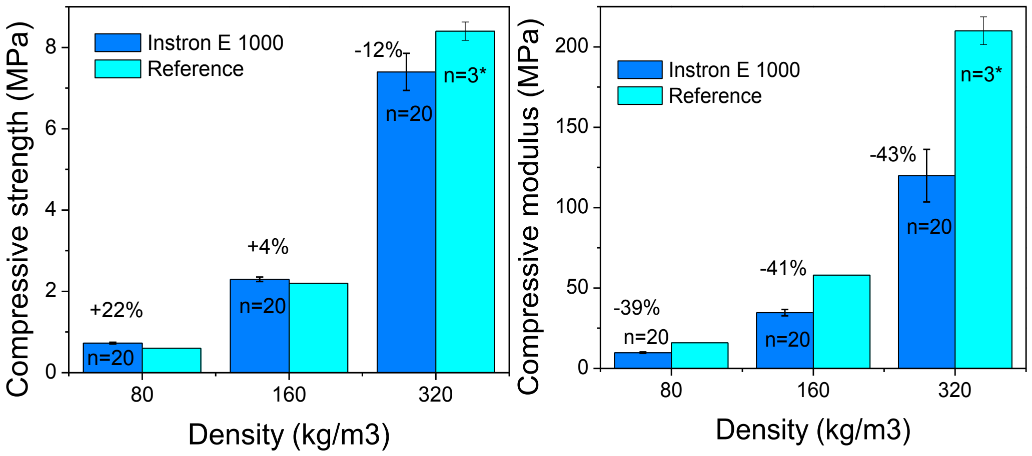

Figure 37. Compressive strength (a) and compressive modulus (b) of the tested samples along with the reference value. Twenty samples of each densities (80 kg/m^3, 160 kg/m^3 and 320 kg/m^3) were tested. *A data obtained from manufacturer for the densest foam had three samples.

Table 13 summarizes the errors in the measured compressive modulus for the PET and PU foams. Additionally, the absorbed energy until yield is represented. The values can be compared with other quasi-static compression test results of PVC and PU [10, 11]. The compressive modulus and the absorbed energy were measured for all studies using the gradient of the stress-strain curve (see section “2.1.1 Stress-Strain”).

Oroszlány et al. compressed closed cell PVC foam samples at rate 0.15 m/s [10]. They used cube-shaped 10x10x10 mm samples and a self-aligning compression platen to minimize non-uniform stress distributions. Patel et al. used a compressive strain rate of 0.0033 s^{-1} and had two different lengths of cylindrical samples with a diameter of nine mm [11]. 90 kg/m^3 PU foam samples had an open cell structure, but the other foams in

Table 13 had closed cell structure. The colours in Table 13 simplify the comparison of the results.

Table 13. Compressive modulus and absorbed energy until yield for different polymer foams. Additionally, the error in the compressive modulus is summarized. The colours highlight the foam similarities.

	Size (mm)	**Material**	**E (MPa)**	**Error in E**	**U_y (kJ/m^3)**
Present study	ϕ10x5	80 kg/m^3 PU	9.8±0.5	39 %	8.3±1.2
		160 kg/m^3 PU	34.5±1.5	41 %	19.4±3.9
		320 kg/m^3 PU	119.9±16.3	43 %	71.7±19.5
Present study	ϕ10x5	100 kg/m^3 PET	31.3±1.7	65 %	24.7±3.3
		135 kg/m^3 PET	46.0±3.3	67 %	39.9±7.1
		210 kg/m^3 PET	82.9±10.6	54 %	39.1±8.8
Patel et al. [11]	ϕ9x3.9 ϕ9x7.7	90 kg/m^3 PU (open cell)			
		3.9 mm length	0.3±0.2	95 %	0.8±0.6
		7.7 mm length	0.7±0.2	89 %	1.5±1.4
		160 kg/m^3 PU			
		3.9 mm length	19±3	67 %	27.3±10.0
		7.7 mm length	41±3	29 %	10.6±2.7
		320 kg/m^3 PU			
		3.9 mm length	66±13	69 %	96.6±47.9
		7.7 mm length	145±6	31 %	26.5±14.4
Oroszlány et al. [10]	ϕ10x10x10	100 kg/m^3 PVC	53.7±5.0	57 %	17.8±1.5
		130 kg/m^3 PVC	66.4±5.1	61 %	42.4±6.0
		200 kg/m^3 PVC	123.2±14.9	56 %	41.2±11.4

As previously discussed, both values of the measured compressive modulus of PU and PET foam have a significant error when compared with the reference values. Similarly, a large error can be seen in Table 13 in the values of the compressive modulus reported by Oroszlány et al. and Patel et al. [10, 11]. The displacement was measured in these studies without optical extensometer from the interface between platen and the sample surface, such as in the present study. Hence, the compressive results should be more comparable. The measured values of the PU foams of 160 kg/m^3 and 320 kg/m^{3}and the values reported by Patel et al. of the same foams showed fairly similar results. The measured results go in the middle of the values Patel et al. reported. 90 kg/m^3 PU foam had an open cell structure and showed lower compressive modulus and absorbed energy compared with the measured values of 80 kg/m^3 PU foam. This was expected, as the cell walls in an open cell structure are generally weaker than in a closed cell structure [138, 139].

PET and PVC foams are used as a protective sandwich structures and the PET foam is considered as a competitive material for PVC foams [140]. Oroszlány et al. studied PVC foams that had similar densities than the PET foams in the present study (see Table 13). The values of the absorbed energy until yield are similar for the PET and PVC foams. The absorbed energy until yield tells about the ability of the material to bear loads elastically. The results suggested that the foam cells can absorb similar amounts of energy before plastic deformation and hence are equally good materials for load protecting applications.

The comparison of the errors in the measured compressive properties of PU and PET foams showed that the results of the PU foam were more accurate compared with the measured values of the PET foam. The microstructural architecture controls the mechanical response of the foams [19, 51, 139], thus the higher inaccuracy measured from the PET foam could be due to greater non-homogeneities in the structure. Altogether, the reference materials indicated that the density, pore geometry, sample size, strain rate and other structural design properties caused variation in mechanical properties and cannot be neglected.

4.3 Hydrogel Scaffold

The hydrogel scaffold preparation and the compression test were conducted according to Koivisto et al. and Salonen [34, 35]. Thus, the measured and reported compressive values for GG bioamine hydrogel scaffolds were compared. The reliability and limitations of the compression test was discussed and the mechanical testing devices were compared.

4.3.1 Considerations

The hydrogen ions in water exhibit adhesive property to reach towards opposite charged molecules. As the GG bioamine hydrogel scaffolds had high water content, scaffolds were adhesive toward upper platen causing some tension in the structure. This phenomenon caused difficulties on determining the zero-deformation point. As no clear guideline was found, three different zero-deformation points and their effect on the compressive values were evaluated as shown in Figure 38. The position “A” had the highest gauge length and the position “C” the lowest. The position “C” was achieved by lowering the compressive platen until the gauge length was approximately the same as the sample length on the table before adhesion. The difference between the positions “A” and “B“ was that at position “A” the hydrogel sample itself reached toward the platen. On the contrary the position “B” was achieved by lowering the compressive platen until platen touched the hydrogel. The compressive strength and compressive modulus of similar GG hydrogel scaffolds depending on the starting positions (A, B and C) can be seen in Figure 39.

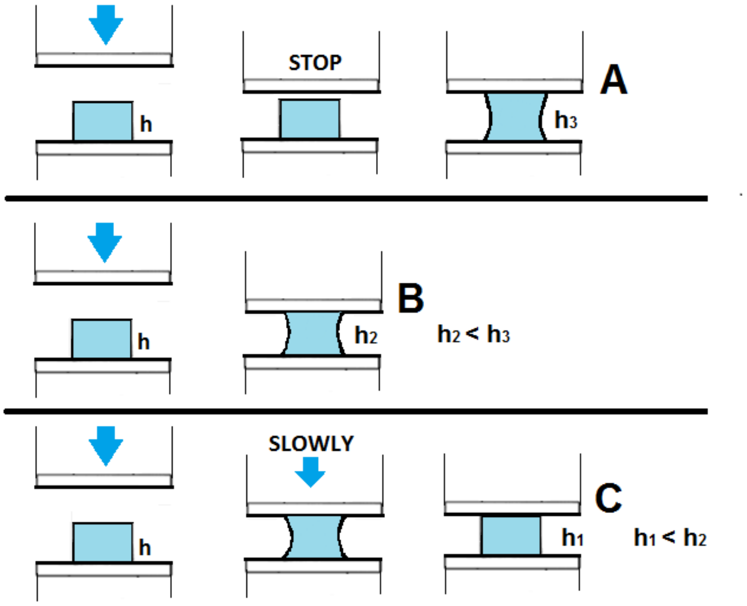

Figure 38 Different zero-deformation points that were used in this study are illustrated. The initial length of the sample on the table is h. The gauge length of position "A" is h_3. The gauge length of positions "B" and "C" is h_2 and h_1 respectively.

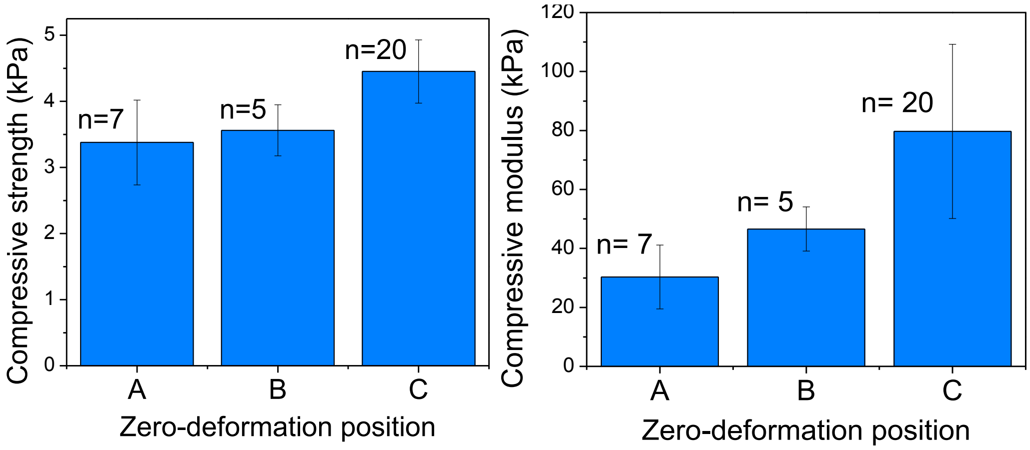

Figure 39. Compressive strength and compressive modulus of GG bioamine hydrogel samples tested with different gauge lengths (A, B, and C). The number of samples are above the columns.

The lowest gauge length "C" showed higher compressive strength and compressive modulus, which could be due to some preload on the scaffold at the "C" zero-deformation point. The higher standard deviation was found for compressive strength in position "A" and for compressive modulus in the position "C". The high standard deviation for the position "C" was attributed to the difficulty in assessing the starting point accurately. However, despite this challenge the position "B" showed less variation in both compressive strength and compressive modulus than the position "A" even though the position "A" was easier to repeat. Statistical differences between the compressive results of the positions are gathered in Table 14.

Table 14. Results of statistical difference between A, B and C zero-deformation positions for compressive strength and compressive modulus.

Comparison of positions	Compressive property	P-value
A, B, C	σ_{max}	<0.001
	E	0.001
A, B	σ_{max}	0.586
	E	0.215
B, C	σ_{max}	0.006
	E	0.018
A, C	σ_{max}	0.006
	E	0.001

One way ANOVA test showed significant difference between all the three positions for the compressive strength and compressive modulus. The independent t-test was performed to evaluate the differences more closely. Only the results of the positions "A" and "B" showed no statistical difference. Thus, the effect of the zero-deformation point on the compressive results is considerable.

4.3.2 Comparison of Devices

The hydrogel scaffolds were prepared and tested using exactly the same method as Koivisto et al. and Salonen [34, 35]. The only difference was that in the present study the used compression testing device was Instron E 1000 and in the other studies the device was Bose Electroforce Biodynamic 5100. The term Bose 5100 is used to refer to this device. Bose 5100 is intended for characterizing biomaterials, cellular scaffolds, acellular scaffolds, tissue samples or tissue mimicking constructs. Thus, the device should be suitable for mechanically testing the GG bioamine hydrogel scaffolds engineered for neural tissue.

The compressive strength and compressive modulus for all hydrogel samples can be seen in Figure 40. Instron A, Instron B and Instron C represent the present results of different compressive starting positions (A, B, and C). Bose 1 represents the results reported by Koivisto et al. [34] and Bose 2 the results reported by Salonen [35].

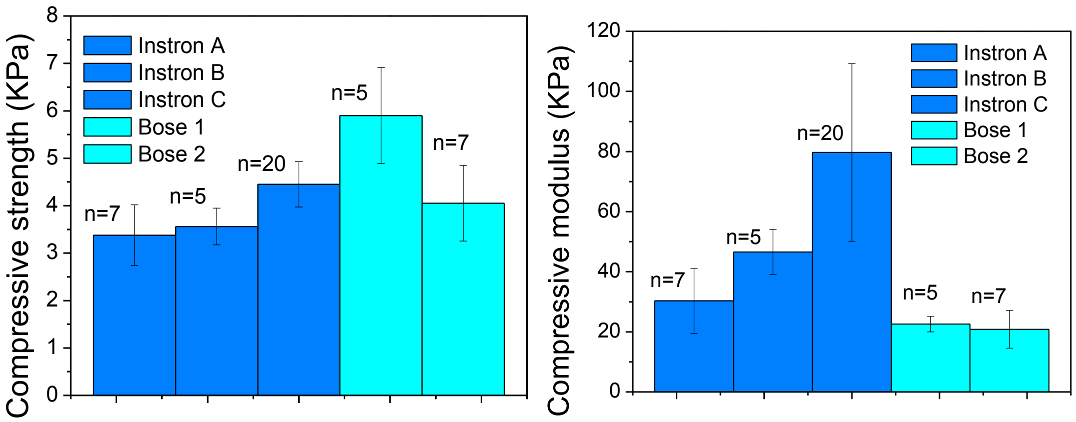

Figure 40. Compressive strength and compressive modulus of hydrogel scaffolds tested in the present study (Instron A, Instron B, Instron C) and in the previous studies (Bose 1, Bose 2). The colours represent the compressive testing devices. The number of test samples can be seen above the columns.

As previously demonstrated, the effect of a zero-deformation position cannot be neglected. According to Koivisto et al. and Salonen, the used zero-deformation point was the position where platen touched the sample surface [34, 35]. Thus, the reported compressive results should be comparable to the present results of Instron A or Instron B. Table 15 gathers P-values of statistical differences between the compressive results. Visually Figure 40 shows that the compressive strengths of Bose 1 and Bose 2 are closer to the value received using the position “C”. Statistically there is still a significant difference (Table 15). However, when the comparability with the present study and Bose 2 alone is evaluated there is no significant difference between the compressive strengths.

Table 15. Results of statistical differences between compressive values of the present study (Instron A, Instron B, Instron C) and previous studies (Bose 1, Bose 2).

Test	**Compressive property**	**P-value**
Instron C, Bose 1, Bose 2	σ_{max}	0.019
C, Bose 1	σ_{max}	0.008
C, Bose 2	σ_{max}	0.619
A, Bose 2	σ_{max}	0.110
	E	0.009
A, Bose 1, Bose 2	E	0.020
A, Bose 1	E	0.042
B, Bose 1	E	0.009
B, Bose 2	E	0.004

As all studies were conducted at Tampere University of Technology, within the Biomaterials and Tissue Engineering Laboratory, the raw data were available also for the previous studies. The stress-strain curves in Figure 41 illustrate the stress-strain curves received from different compressive testing devices. Bose 5100 showed more noise and sensitivity in the stress-strain curves than Instron E 1000. However, Bose 2 showed less noise than Bose 1 even if no difference in the equipment's parameter or sample morphology could be identified. The only difference was the increased number of data points in the case of Bose 1. According to the instruction manual of Bose 5100 [25], the system is sensitive to noises and for example might get resonance from the device position. The amount of data points recorded with Instron E 1000 was higher than Bose 1 and maintained lower noise to signal ratio. Additionally, Instron E 1000 was adjusted to retain all peaks or trend changes resulting in extra data points. The high peaks in the stress-strain curves of Bose 1 may have caused some inaccuracy in the analysis of the compressive strength values, but no great difference could be seen when averaging the highest peaks.

The compressive modulus showed a significant difference between the measured results and the results reported by Koivisto et al. and Salonen (Figure 40). The differences between the results of the compressive modulus were partly due to different methodology to analyze the compressive modulus as the combination of viscoelasticity of the hydrogel scaffolds and noise in the stress-strain curves (see Figure 41) caused some problems on determining the elastic region (as shown in Figure 42). Figure 41 illustrates the measured stress-strain curve when starting our test in position "A" and the received stress-strain curves of the previous studies Bose 1 and Bose 2. The stress-strain curve in Figure 42 illustrates the difference in methodologies that were used to analyze the compressive modulus in the present and previous studies. The compressive modulus was taken in the previous studies from the entire part of the ascending trend (Figure 42 (a)). However, no clear beginning and end of the elastic region could be determined. In this study, the analysis was planned to be done according to the previous studies (Koivisto et al. and Salonen). However, the stress-strain curves of the present study showed repeatedly distinct linear part, which was assumed to correspond to the elastic deformation and the compressive modulus was taken from that region (Figure 42 (b)). Figure 42 (b) illustrates the stress-strain curves of the positions "A" and "C". The position "B" had similar curves as the position "A".

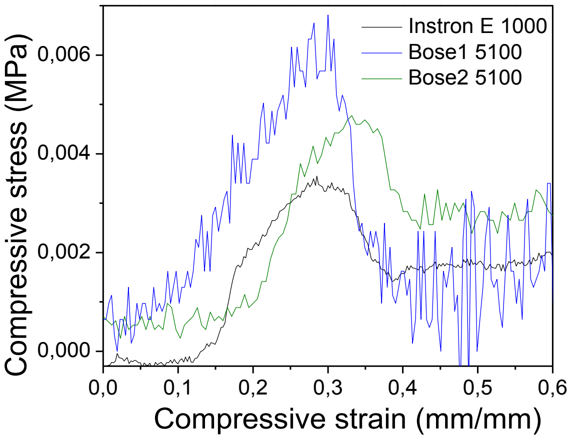

Figure 41. Stress-strain curves for similar hydrogel scaffolds. Two different compression testing devices (Instron E 1000 and Bose 5100) was used.

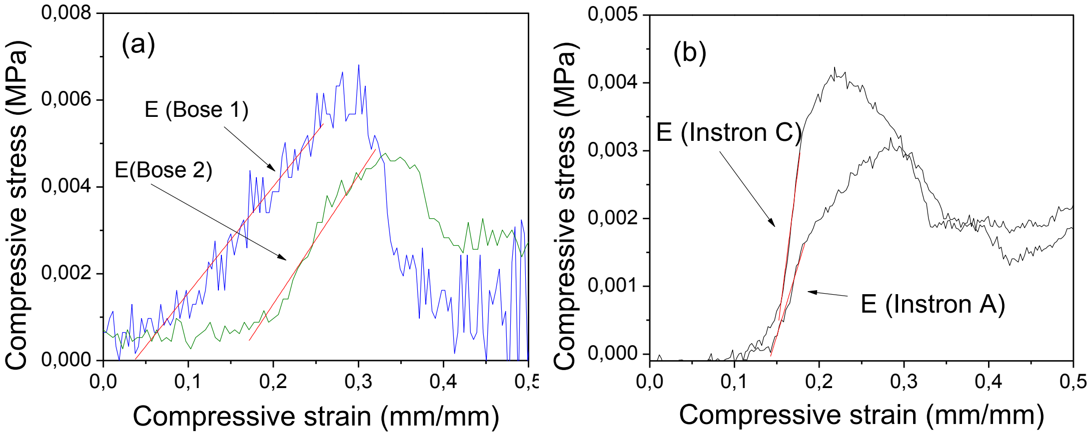

Figure 42. Analysis of compressive modulus. (a) Stress-strain curves from the previous studies (Bose 1 and Bose 2) and (b) from positions "A" and "C" obtained using Instron E 1000.

The viscoelastic and self-adhesive properties of the hydrogel scaffolds complicated the repeatability of the compression test and reliability of the results. A significant difference in the compression strengths of the present study and two other studies could be seen even if the study was repeated using the exact same methods. No reliable comparison between the results of the compression modulus could be performed due to differences in the stress-strain curves and analyzed methods. In general, the compressive testing device Instron E 1000 presented lower noise to signal ratio and more reproducible dataset.

4.3.3 Comparison with Other Studies

The mechanical properties of hydrogels can be modified by changing the degree of a cross-linker polymer [35, 57]. An increased amount of cross-linking chains leads to stiffer structure. In the literature, the mechanical properties of GG hydrogels have been tuned for different tissues, such as cartilage tissue [61] and softer neural tissue [34]. The network formation of GG has shown to be dependent on the quantity of the cations [141, 142]. The binding network of GG hydrogels can also be modified by using additives [142]. Sowrn and Kasapis compression tested a wide range of 0.5 wt-% GG hydrogels and studied the effect of sugars and/or calcium on the mechanical properties. Depending on the amount of sugars and/or calcium, the compressive modulus varied from 0.35-2 kPa. Sowrn and Kasapis suggested that an increase of sugar-solution could have influence on the polymer aggregation and give flexibility to the chains [142]. Coutinho et al. used physical and chemical mechanisms to cross-link GG hydrogels in order to improve the mechanical properties [143]. The compressive modulus of GG varied from 0.15 to 148 kPa depending on the used ion concentration, cross-linking mechanism and polymer concentration. In this study, the measured compressive modulus ranged from 30-80 kPa depending on the zero-deformation position of the compressive platen. The measured compressive modulus had similarities with the results reported by Coutinho et al. However, hydrogels are viscoelastic and hence the mechanical properties are dependent on the compressive rate and temperature [8, 13, 15]. Coutinho et al. tested three samples per variation and the compressive rate was 0.2 mm/min. The compressive rate in the present study was 10 mm/min. As previously discussed, also the performance of the testing device might have influence on the results (see Figure 41 and 42). Additionally, there was no mention of slipping of the hydrogel scaffolds, that may happen due to slippery surfaces of the hydrogel samples on the compressive platen. In the present study, the slipping of the hydrogel samples was prevented using cellulose paper between the specimen and compressive platen. As there are many factors effecting on the compressive results of GG hydrogels, the compressive tests are suggestive and the comparison between studies need to be done with caution.

4.4 PLA Rod

PLA rod samples were compression tested using Instron E 1000. Instron E 1000 could deliver load up to 1000 N. Due to the limitation in the maximum load Instron E 1000 can deliver and the accuracy of the measurements at higher load, PLA rod samples were tested also with Instron 4411, for which the 5 kN load cell could be used. The reliability and limitations of sample geometry and devices were discussed.

4.4.1 Considerations and Reliability

Twenty PLA rod samples were compression tested with Instron E 1000 and five with Instron 4411. Figure 43 illustrates the stress-strain curves obtained using Instron E 1000 and Instron 4411. Red lines present the regions of the compression modulus. No failure could be detected from the stress-strain curves. The stress-strain curve received using Instron E 1000 showed steeper slope. However, due to the limitation of the load cell capacity, the curve ends earlier than the curve of Instron 4411. Instron 4411 had a toe region and a long elastic slope until the compression test ended. A significant difference could be seen between the compressive results of the devices. The results of the compressive strain at 900 N (ε_{900N}) and compressive modulus are gathered in Table 16.

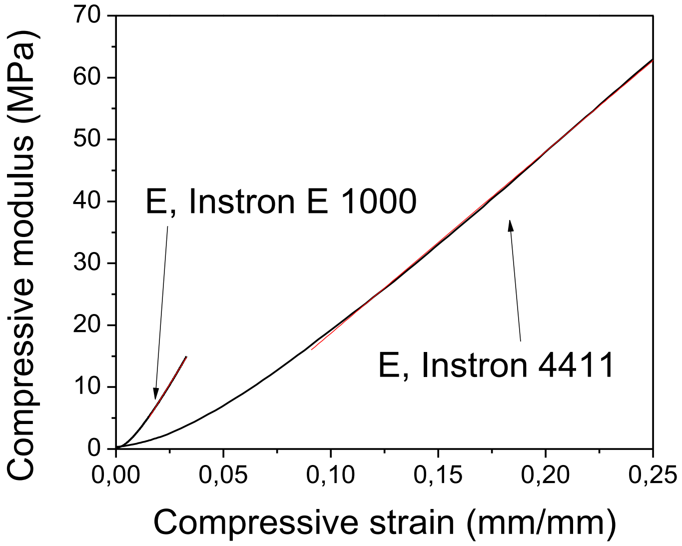

Figure 43. Stress-strain curves of PLA rod samples recorded with two different compressive testing devices (Instron E 1000 and Instron 4411). Red line represents the region of the compressive modulus.

Table 16. Surface tilt, strain at 900 N, compressive modulus and P-values for PLA rod samples tested with two compressive testing devices.

Device	Surface tilted (%)	ε_{900N} (%)	P-value	E (MPa)	P-value
Instron 1000	1.1±0.6	3.1±0.3		554.5±56.5	
Instron 4411	3.9±1.3	4.6±1.1	0.03	357.7±52.0	0.002

Figure 44 illustrates the problems in sample design. The prepared PLA rod samples had tilted surfaces and the compressive platen could not deliver parallel load at the surface of full samples cross-section. The % surface tilt was calculated using equation (12) (see section “3.1.4 PLA Rod”). The results are gathered in Table 16. Samples tested with Instron E 1000 had 1.1±0.6 % difference in the minimum and maximum length and samples tested with Instron 4411 had 3.9±1.3 % difference in the minimum and maximum length. Larger surface unevenness in PLA rod samples tested with Instron 4411 resulted in higher strain at 900 N. There were also difficulties on determining the zero-deformation point when using Instron 4411 that caused variation on the starting positions of the compression tests. The linear elastic region of stress-strain curve was used to determine the zero-strain point and the curved region was removed from the analysis of stress-strain curve as standard EN ISO 604 suggested [125].

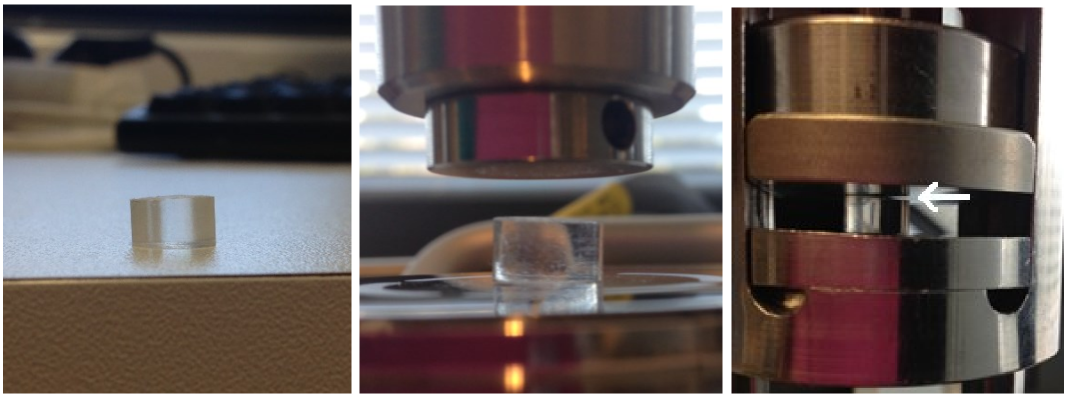

Figure 44. Tilted surface of a PLA rod sample that results in an uneven stress distribution during the compression test.

In the literature Felfel et al. [144] compressed a pure PLA rod with a diameter of 4mm, but reported only the stiffness value (~5kN/mm). Stiffness value is not sensible to compare with the compressive modulus as stiffness is dependent on geometrical parameters when the compressive modulus describes better the material properties. Generally, a three-point bending test is used for mechanically testing beams such as polymer rods [29]. Preparing uniform and parallel samples of a strong and stiff PLA rod for a compression tests is problematic. Hence, the three-point loading test could be considered as a good alternative method.

The tilted sample surface and the fixed uniaxial compressive platen caused uneven distribution of load on the specimen during the compression test. Thus, inaccuracies in compression test results may exist. The cross-head adjusting system of Instron 4411 was not as easy to use compared with the one in Instron E 1000. A significant difference in the received results between two different testing devices was found. The PLA rod samples tested with Instron E 1000 had a less tilted surface and the ease of use Instron E 1000 improved the repeatability of the tests. Thus, the compressive results of Instron E 1000 are considered more accurate than the results of Instron 4411. However, with stronger samples the displacement becomes harder to measure. Some inaccuracy in compressive modulus could exist as no optical extensometer was used. The reliability of the test results could have been improved by grinding or polishing the sample surface [33, 145-147].

4.5 Joint Scaffolds

Various sizes of joint scaffolds and two different joint scaffold materials (PLA 96/4 and PLA 96/4 + PEG 5 %) were compression tested. Exactly the same compression method and testing device was used as Karjalainen [126]. The reliability and limitations of compression testing on knitted joint scaffolds were discussed. Also, the results received in the present and previous study are compared. All the results can be seen in Appendix 3.

4.5.1 Structural Limitations

Three batches of ϕ14x4.5 mm sized joint scaffolds were compression tested. The results of the compressive strain at 80 N, 220 N, and 440 N and the compressive modulus are shown in Figure 45. A significant difference was observed between different batches and compressive strain at 80 N, 220 N, and 440 N ($P<0.002$), but not between the results of compressive modulus ($P=0.185$).

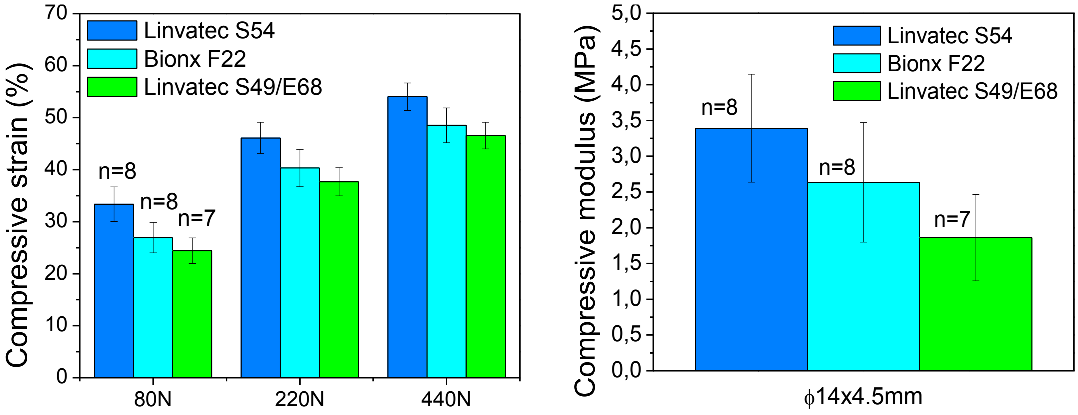

Figure 45. Compressive strain at 80 N, 220 N and 440 N (a) and compressive modulus (b) for three batches (S54, F22, S49/E68) of ϕ14x4.5 mm sized joint scaffolds. The number of samples tested are presented above the columns.

Linvatec S54 was manufactured in 2004, Bionx F22 in 2002 and Linvatec S49/E68 in 2003. All the scaffolds were more than ten years old (see Table 9 section "3.1.5 Joint Scaffold"). No consistency on the manufacturing year and mechanical properties was detected. However, some differences in the compressive results were found. It is known that the manufacturing process may cause variation in the joint scaffold structure. The detailed manufacturing process can be found in the literature [148, 149]. For example, the level of gamma irradiation during sterilization [149] and differences in thermal treatments [148] have shown to effect on the mechanical properties of joint scaffolds. Linvatec S49/E68 and Bionx F22 were reeled by hand, but Linvatec S54 was mounted in a reeling instrument. The knitted jersey in the scaffold is flexible. Thus, there could have been more variation in the tension of jerseys that were hand reeled. Additionally, if the scaffold's fibers were from different manufacturing lots, there might have been some variation in the thickness of the fibers. However, different joint scaffold batches and their mechanical properties had similar standard deviation (Figure 45), which suggest that experimental artifacts in the batches are similar.

The structural differences in the old knitted scaffolds have been studied. Karjalainen demonstrated that in 8 to 15 years the crystallinity of the joint scaffolds might change resulting in a stiffer structure [126]. In this study, some differences were detected visually in the joint scaffold structure such as differences in the tightness of the loops in the joint scaffold jersey and as an uneven cross-sectional surface. Differences in jersey tension could cause differences in density and effect on the mechanical properties. The zero-deformation point was the position where the cross-head touched the specimen surface, hence the unevenness of the samples might have caused inaccuracies during the compression test. Indeed, some unevenness was detected as a hollow middle part. However, as the joint scaffolds were soft, the surface unevenness did not have as big of an effect on mechanical properties as strong samples would have had [24].

The compressive strain at 80 N, 220 N, and 440 N and the compressive modulus for different sizes of tested joint scaffolds can be seen in Figure 46. The same colour is used for the columns of the same sized joint scaffolds.

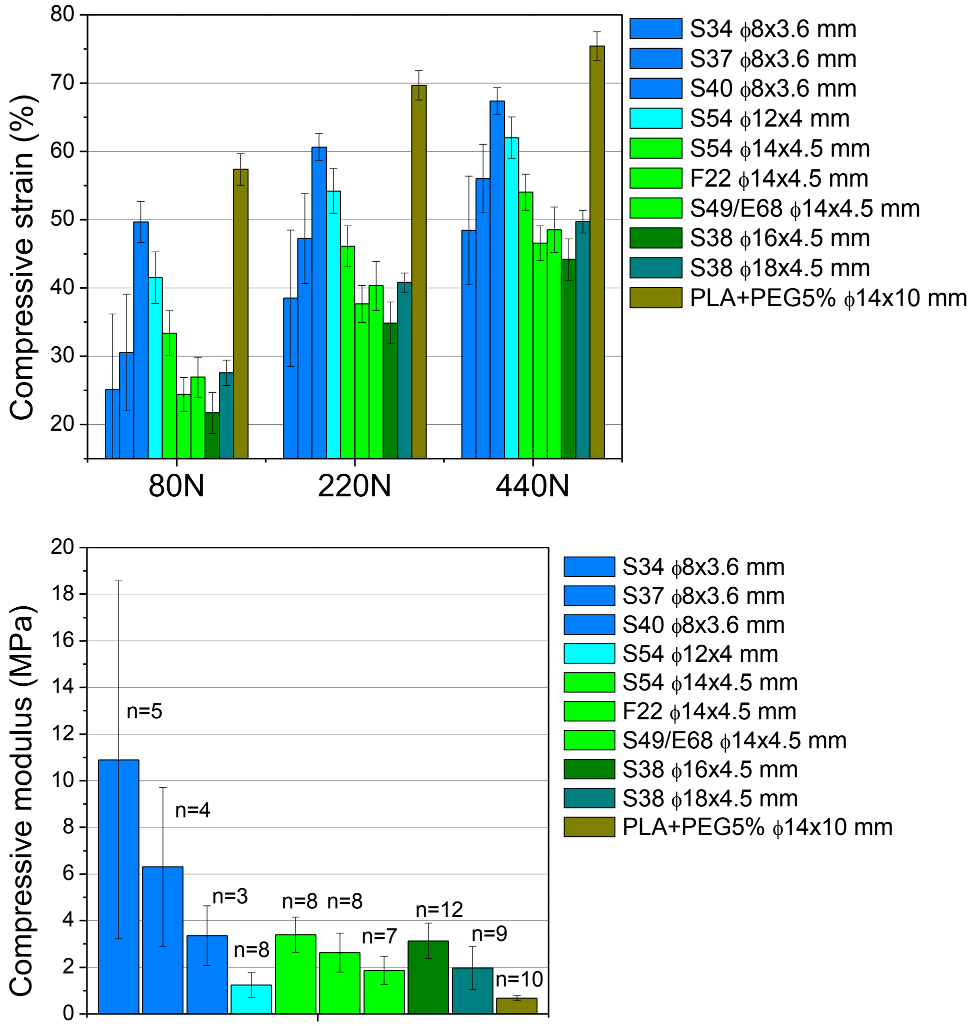

Figure 46. Compressive strain at 80 N, 220 N, and 440 N and compressive modulus for all tested joint scaffolds are gathered. The same sizes of joint scaffolds are represented with the same colour. The number of the samples are presented above the columns in (b).

The size of the scaffold was modified during manufacturing by altering the number of jersey loops. According to the results, an increase in size resulted in a higher compressive modulus and logically lower compressive strain. The exception to this was the ϕ18x4.5

sized joint scaffolds that had lower compressive modulus than ϕ16x4.5 sized joint scaffolds. However, the structure of ϕ18x4.5 sized joint scaffolds had more loops of jersey than smaller joints, which complicates the manufacturing. Variation in the structure and in the tension of the jersey of ϕ18x4.5 sized joint scaffold was detected (Figure 47 (a)). Additionally, the diameter of the compressive platen was the same as the diameter of the biggest joint scaffold. Hence, the compressive platen could not deliver the load at the sample of the full sample cross-section as the joint scaffold started bulging during the test (Figure 47 (b)). This increased the inaccuracies of the compressive results of the ϕ18x4.5 joint scaffold.

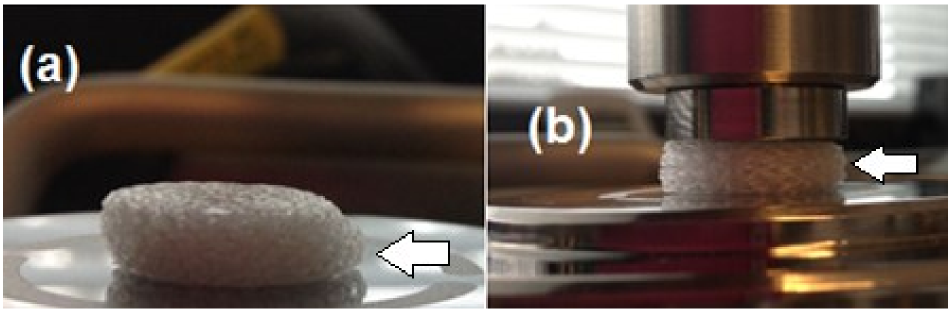

Figure 47. Non-homogeneous structure of the knitted Φ18x4.5 mm sized joint scaffold (a). Small diameter of the compressive platen had limitations on delivering load throughout the Φ18x4.5 mm sized sample (b).

The addition of PEG in PLA 96/4 joint scaffolds increased the hydrophilicity [47] and resulted in a softer structure, which can be seen in the results (Figure 46). The compression tests showed lower stiffness and higher strain compared with the other joint scaffolds. The compressive results were related to the structural differences as the length of the PLA + PEG 5 % joint scaffolds were more than double (10.0±0.2 mm) than the length of other joint scaffolds (<5 mm, see Table 9 in section”3.1.5 Joint Scaffold”).

4.5.2 Comparison with Other Studies

As previously shown three batches of the PLA 96/4 joint scaffolds in size of Φ8x3.6 were compression tested. The initial idea was to combine the results in one, as the number of the samples were small. However, the received mechanical properties had great difference and the results could not be merged. Additional information and compressive results of Φ8x3.6 sized joint scaffolds are gathered in Table 17. ε_{80N} is the strain at 80 N, ε_{220N} the strain at the 220 N and ε_{440N} is the strain at 440 N.

Table 17. Measured parameters of Φ8x3.6 sized joint scaffolds and compressive strain at 80 N, 220 N, and 440 N and compressive modulus from this study and a previous one.

	Φ (mm)	**l_0 (mm)**	**ε_{80N} (%)**	**ε_{220N} (%)**	**ε_{440N} (%)**	**E (MPa)**
Present study						
Bionx S34	8.2±0.3	3.6±0.1	25.1±11.1	38.5±10.0	48.4±8.0	10.9±7.7
Bionx S37	8.7±0.5	3.8±0.2	30.5±8.6	47.2±6.6	56.0±5.0	6.3±3.4
Bionx S40	8.6±0.4	3.8±0.2	49.7±3.0	60.6±2.0	67.4±2.0	3.4±1.3
Karjalainen [126]						
Bionx S21	7.7±0.05	4.0±0.3	44.1±2.4	56.9±2.6	66.1±2.4	0.52±0.07
Linvatec S64	7.7±0.1	3.5±0.1	25.9±4.7	40.4±5.3	48.7±1.9	10.7±3.4
Kulmala [149]	13	3-3.5	35±5	43±5	49±10	-
Kulmala [149]	12	3-3.5	50±5	62±5	69±5	-
Kulmala [149]	11	3-3.5	42±10	50±10	56±7	-
Mutanen [148]	8	3.6	39±7	53±7	63±7	-

The received compressive results could be compared with compressive results reported by Karjalainen [126], Kulmala [149] and Mutanen [148]. Kulmala tested joint scaffolds with bigger diameter (11-13 mm). Otherwise all the scaffolds were similar in size. Variation in the compressive strain at 80 N, 220 N, and 440 N can be seen between all the studies. Differences are examined more closely between the present study and the previous study reported by Karjalainen, as the same compressive device was used for both. Figure 48 illustrates the compressive strain at 80 N, 220 N and 440 N and compressive modulus for the present and study reported by Karjalainen. A great variation can be noted between batches for compressive strain at 80 N, 220 N and 440 N and for the compressive modulus. The increase in joint scaffolds' stiffness seems to result in an increase in the standard deviation. All but one of the batches had less than five samples tested. Hence, the small number of tested samples hampers the reliability of the results.

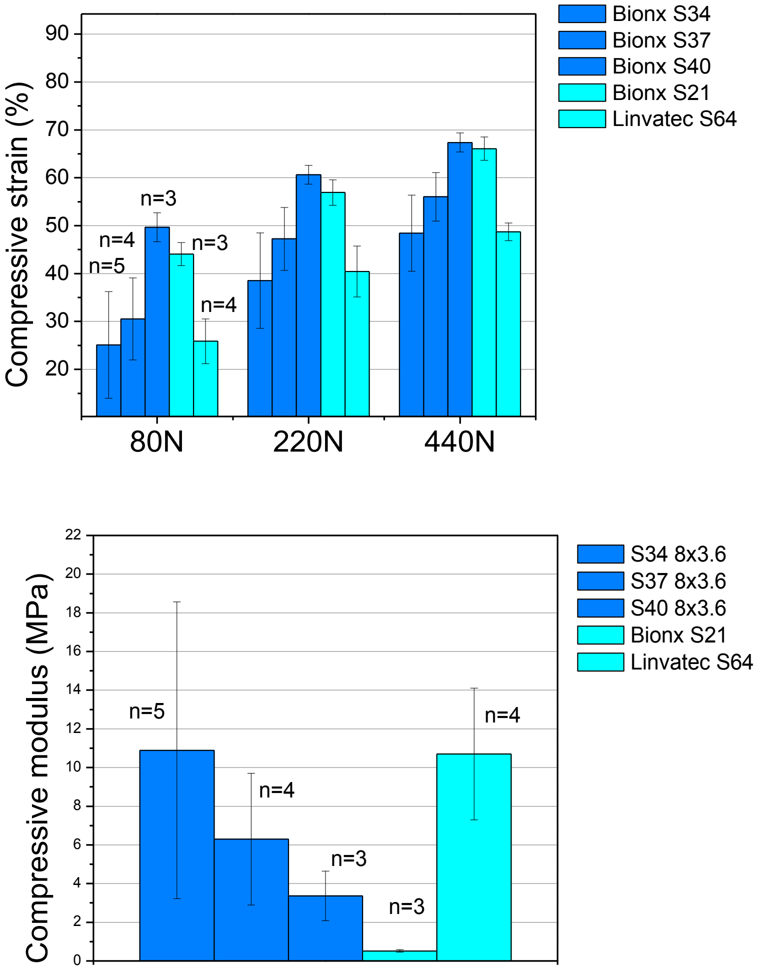

Figure 48. Compressive strain at 80 N, 220 N and 440 N and compressive modulus of Φ8x3.6 sized joint scaffolds. The blue colour represents the present study and the light blue the previous study. The number of samples are above the columns.

The variation in the compressive strains and the compressive modulus could be due to differences in the physical or chemical structure of the joint scaffolds. Karjalainen [126] reported that the DSC tests showed differences in the crystallinity of the tested joint scaffolds. Crystallinity of Linvatec S64 was 38.4±0.5 J/g and the crystallinity of Bionx S21 was 36.6±1.6 J/g. Generally, higher crystallinity increases the stiffness of the material, as Karjalainen demonstrated [126]. As the tested joint scaffolds were manufactured more than ten years ago, some changes might have happened in the crystallinity during the time. However, due to many steps in manufacturing, there could have been some chemical or physical differences already before packaging. All the joint scaffolds were reeled by hand, heat treated in molds and sterilized by gamma irradiation. As before discussed, these factors could have had effect on the structure and hence on the mechanical properties. The measured parameters proved that there were some differences in the physical structure, but other additional studies were not conducted.

Karjalainen tested PLA 96/4 scaffolds blended with PEG, but the amount of used PEG was 15 % when in this study it was 5 % [126]. Additionally, the present study had about 1 mm bigger joint scaffolds in length and diameter. The comparison of the compressive strain at 80 N, 220 N, and 440 N, and the compressive modulus can be seen in Figure 49.

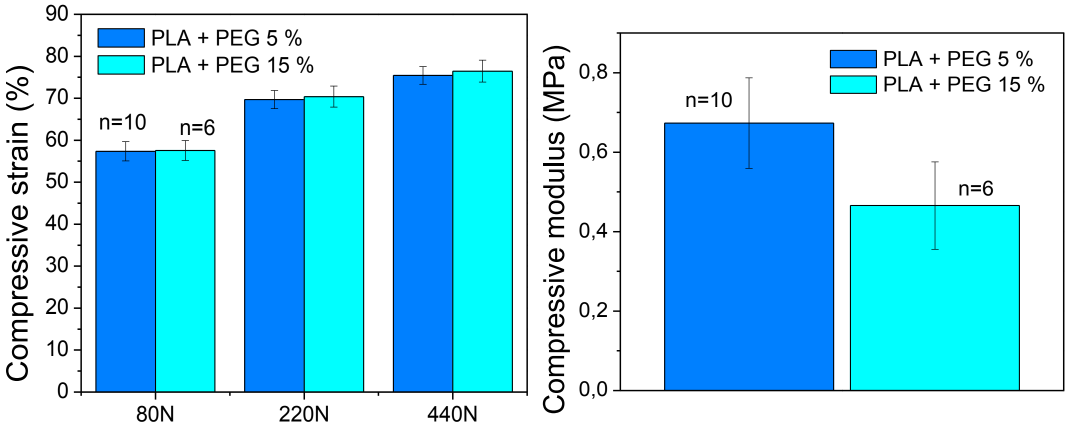

Figure 49. Compressive strain at 80 N, 220 N, and 40 N and compressive modulus of PLA 96/4 joint scaffolds blended with PEG 5 % and 15 %. The blue colour represents the present study and the light blue the previous study. The number of samples are above the columns.

As already discussed the addition of PEG seemed to make the joint scaffold softer. Consistently PLA + PEG 15 % had lower modulus compared with PLA + PEG 5 % and a slightly higher mean strain at 80 N, 220 N, and 440 N even if the PLA + PEG 5 % samples were slightly taller. No big difference in the standard deviation could be detected.

Some chemical changes were expected in the joint scaffold structures as the manufacturing date was more than ten years ago and the manufacturing process is challenging. Variation in the mechanical properties of the same sized joint scaffolds could be seen, but due to the low number of tested specimens and the lack of supportive experiments, the results were unreliable. The size effect on mechanical properties could be assessed when comparing different sized PLA 96/4 joint scaffolds. The smaller sized samples had a higher modulus and led to a lower strain under a specific load. The exception was the ϕ18x4.5 joint scaffold that had structural variation and compressive test limitations due to small size of the compressive platen. For reliability, the sample size should not be bigger or equal to the diameter of the compressive platen.

4.6 Bioactive Glass Scaffold

Twenty 3D-printed B50 scaffolds were compression tested until breakage using Instron E 1000. The production of the B50 scaffolds and the structure-property limitations were discussed, as the study was about the reliability and mechanically testing bioactive glass scaffolds. All the B50 scaffolds were produced with similar mass. Additionally, the received mechanical properties were compared with previous studies and the limitations and reliability were discussed.

4.6.1 Structure-Property Limitations

Even if the robocasting method is generally considered as a good method to control scaffold architecture and attain mechanically strong and homogenous ceramic scaffolds [102, 150], there are many considerations to keep in mind. The production of bioactive glass scaffolds has many steps and factors that may cause changes in the scaffold's mechanical properties. Just to mention a few, binder [104], glass composition and particle size [122], strut size [151], pore size [152], scaffold size, scaffold design [152] and sintering temperatures [153] have effect on the mechanical properties. In this study, the size of the scaffolds was smaller (ϕ7.4x 3.8 mm) than planned due to the increasing difficulties of printing and sintering larger scaffolds (ϕ10x5 mm). However, two main problems that were experienced in this study were ink preparation and sintering. These two challenges are discussed more closely.

According to Rice, defects have dominant effect on the mechanical properties of porous materials, not the pores [51]. Hence, achieving homogenous and consistent ink was important to prevent defect formation in the scaffold. Air bubble formation could not be avoided during mixing the ink. Hence, the ink was sonicated in order to mechanically collapse the air bubbles [154]. However, this method could not eliminate all the bubbles. According to Franco et al. the mechanical strength of the 3D-printed scaffolds is influenced on the density of the printed lines [150]. In the present study, we experienced problems during 3D-printing due to the air bubbles. The air bubbles caused drops in the pressure and reduced the consistency of the printed struts.

The B50 scaffolds were sintered. The sintering is a thermal processing method that is used to bond glass particles. Differential thermal analysis (DTA) is generally used to characterize the crystallization process and determine sintering temperatures. DTA records differences in temperatures between a sample and a reference material during an increase of temperature (see Figure 50) [20]. The sintering of the glass particles happens above the glass transition temperature (T_g) at which the particles undergo viscous flow. However, if the temperature rises above a certain limit the bioactive glass starts to crystallize and the bioactivity declines. The temperature after which crystallization occurs is called onset of crystallization (T_x). The range between T_g and T_x is called hot working domain (see Figure 50) and is determined to sinter glasses while preventing crystallization [155, 156]. The highest exothermic peak in the DTA curve in Figure 50 is called crystallization peak (T_p). At temperature higher than the crystallization melting of the glass occurs. The microstructure of the bioceramic is an important feature for the mechanical properties, hence sintering is used to fuse glass particles into a denser and stronger structure [20].

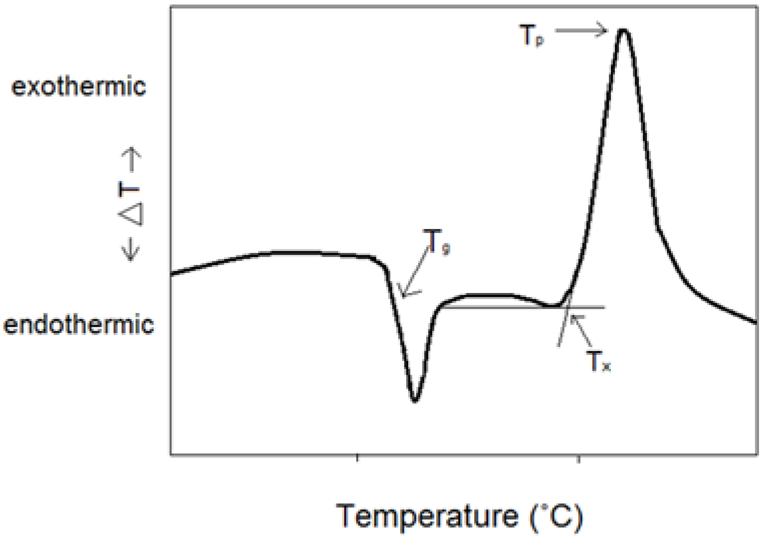

Figure 50. DTA thermogram showing the glass transition temperature (T_g), onset of crystallization (T_x) and crystallization peak (T_p) in DTA curve [121].

The scaffolds were heat treated to first burn the organic material and then sinter the B50 particles. During the sintering process, the powders were compacted. However, big gaps in the printed lines left defects in the structure. Additionally, the hot forming domain between T_g and T_x of B50 caused difficulties. The temperature was raised to 500 ˚C to burn organic material. Then the temperature was further increased to reach viscous flow and sinter the glass particles. However, after sintering the scaffolds turned out to be grey. The grey colour is most likely due to silicon carbide (SiC) and boron carbide (B_4C) formation upon organic dissociation. Lower temperatures did not show improvements and the increase of the burning time or temperature could have activated an unwanted crystallization process. Thus, as the burning temperature of the organics and the sintering temperature of B50 were close to each other, the greyness of scaffolds could not be avoided. Additionally, the rate of organics burning was linked to the uneven temperature distribution inside the oven, which led to visual variation of the sintered scaffolds. Different shades of scaffolds' greyness are shown in Figure 51.

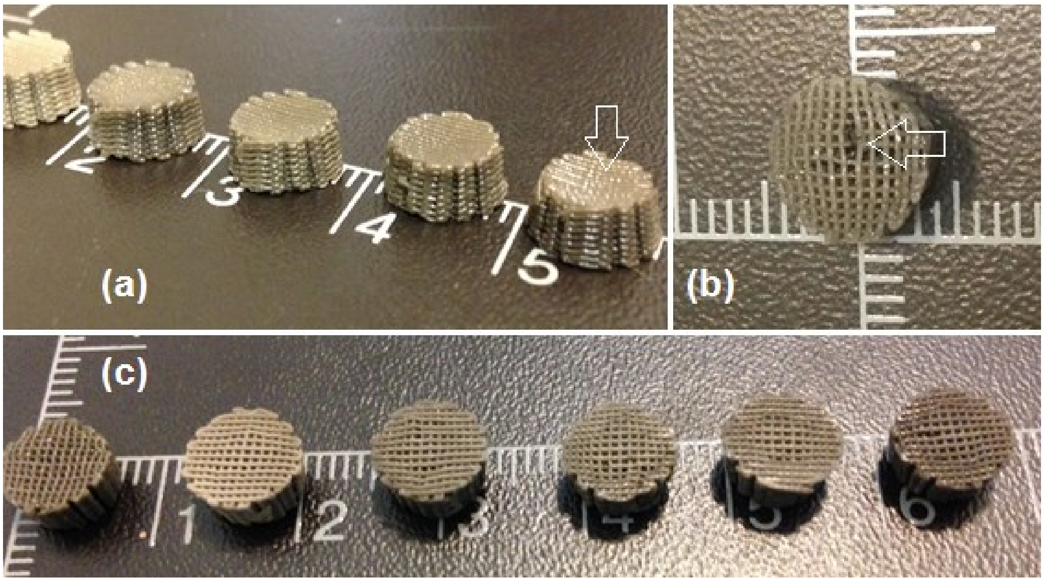

Figure 51. Photograph of the top surface of the B50 scaffolds (a) and bottom surface (b) and (c). The arrows point out collapsed middle part (a) and cracked struts (b).

Figure 51 (b) shows the bottom of the scaffold, that undergo significant changes during sintering. The problem was the evaporation of the organics that caused pressure in the middle of the scaffold and then distorted the struts. The pressure during the sintering widened the pores in the center part causing the struts to crack (Figure 51 (b), (c)). The uneven evaporation also resulted in a collapsed middle part of the scaffolds (Figure 51 (a)). µCT images show structural defects (see Figure 52). At some parts of the scaffold, the struts are not aligned on top of each other. The structural difference at the bottom and top of the scaffold is shown clearly in µCT images. The pore sizes are greater at the center of the bottom surface than at the center of the top surface.

The compression device Instron E 1000 had difficulties in performing compression tests. Instron E 1000 has a patented automatic tuning system that is capable of controlling the machine and providing more accurate results. Normally, the specimen's stiffness is determined before testing and does not cause any damage to the specimen. However, B50 scaffolds were strong and brittle and the tuning of the device could not be conducted due to sudden changes in stiffness that caused instability of the device and breakage of the specimen. The stiffness of the specimen was manually set to 50 N/mm to enable the compression tests. The value was received from Instron® technician. The device used this value to optimize its performance. As this was not probably the real stiffness for B50 scaffolds, it might have had some effect on accuracy of the results. However, the tuning would have been more critical in fatigue tests where the device needs to be able to respond to quick changes in the load and strain. [157]

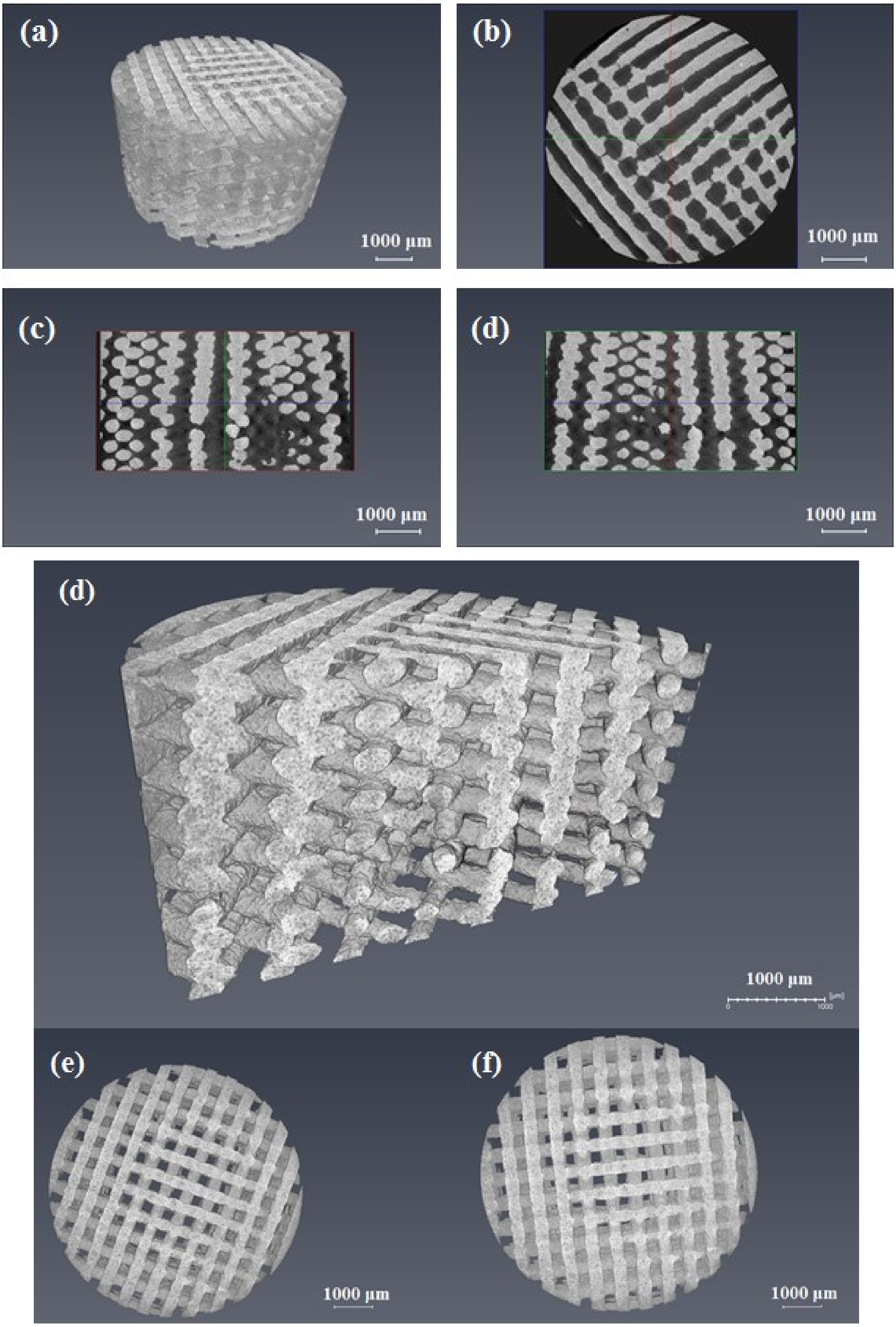

Figure 52. µCT images of B50 scaffold; 3D structure (a), the sectional view (d), 3D top (e) and the bottom (f), 2D structure top (b) and the cross-sections (c, d).

Additionally, the nonuniform scaffold surface caused difficulties during the compression test. As already discussed, the middle part of the scaffold was stacked, leaving the edges to carry the load during the compression test. Some scaffolds had a small node at the edges where printing ended. Any defect in the corner structures would have had harmful effect on compression tests [20]. The platen could not distribute the load evenly throughout the scaffold, which may have caused unequal stresses into the unevenly unaligned columns and led to the fracture of the unsupported centrum part.

Figure 53 illustrates two stress-strain curves received from the compression tests and the red line represents the region of the compressive modulus. The analysis of the compressive modulus was challenging due to great variation and sudden drops in the stress-strain curves. The sudden drops in the stress-strain curves were fractures of non-critical struts or fractures of critical struts as shown in Figure 53. When the stress-strain curve went to zero stress, the compressive platen did not receive any stress. This means that there was some kind of failure of the structure and the structure had given away under the platen.

The stress-strain curve in Figure 53 (a) shows in the beginning a small increase in the compressive stress before a sudden drop. As the stresses are quite small, this could be a fracture of a small node at the edge of the scaffold. Thus, the compressive modulus was analyzed from the next steep increase in the curve. Additionally, the stress-strain curve on the left has many sudden drops that goes to zero stress. As the pillars were unaligned, the failing could be due to the fracture of the bottom struts. Some stress-strain curves showed a plateau phase that could characterize a small crack propagation. The crack propagation was fast and the fractures sudden. If accurate conclusions of the behavior of the B50 scaffold under a compression test are desired, the compressive process could be imaged for example with non-contact video extensometers. Even an x-ray tomography has been used during a compression test to confirm the mechanical behavior of porous ceramics [19].

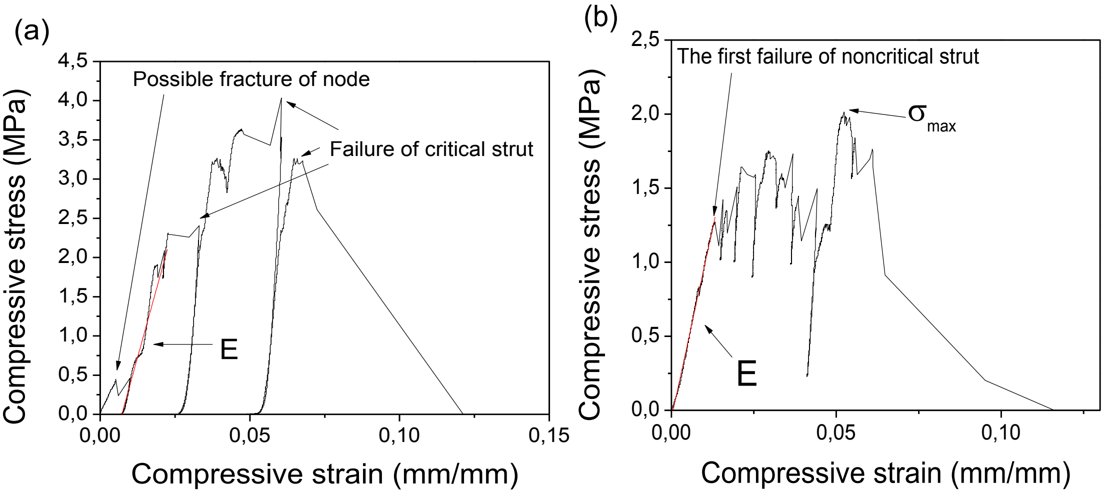

Figure 53. Stress-strain curves of B50 scaffold. The red line illustrates the analyzed region of the compressive modulus.

According to the stress-strain curves, the propagation of the cracks and the failure of the scaffold seems to depend on the structure and defects. The weakest strut that has the largest defect is the first to fracture. According to Genet et al., the failure of a quasi-brittle material depends on the critical struts, hence having the fractures of the non-critical struts before the failure of the total structure [151]. Then again, the failure of the brittle material is a sudden drop in the stress-strain curve after a steep slope. Thus, the term quasi-brittle characterizes better the behavior of the B50 scaffolds tested in this study. However, the criteria of the brittle or quasi-brittle fracture of materials is still widely researched as the fracture process is complicated [158].

The compressive strengths of B50 scaffolds were scattered. Weibull modulus was calculated according to standard EN 843-5 [127] using equations (13-15) (see section “3.3.3 Statistical Analysis”) The plotted graph can be seen in Figure 54 (a). The received Weibull modulus was 3.8. Similar results have been reported in the literature for other 3D-printed ceramic scaffolds [159, 160]. Low value is typical for brittle materials and it indicates that there is statistically high probability to find flaws in the structure. In contrast, Liu et al. and Roohani-Esfahani et al. reported higher values for the Weibull modulus (12-17) [33, 147]. The Weibull modulus for solid bioactive glasses and ceramics has been varying in range 5-20 [161, p. 303].

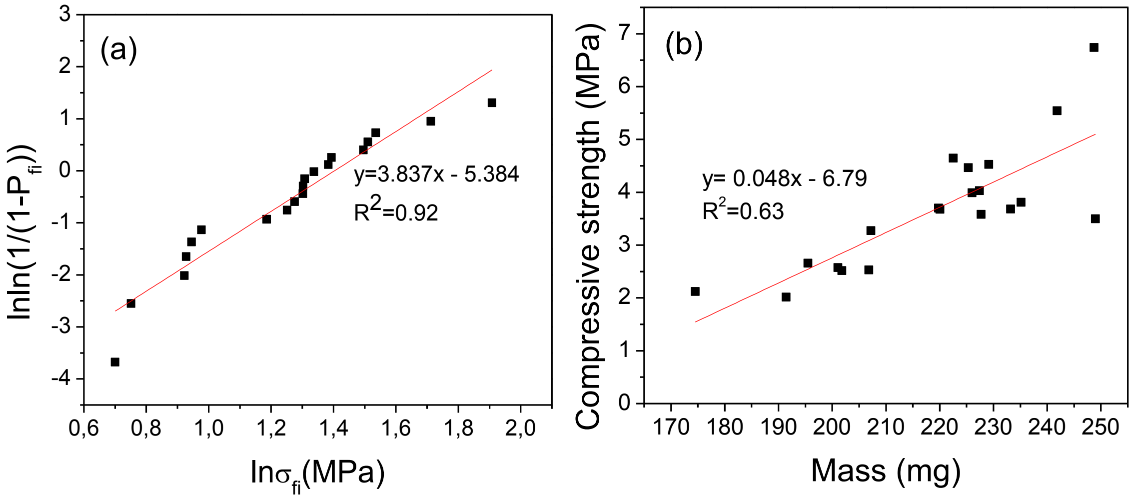

Figure 54. Distribution of the compressive strengths (a) and relationship between mass and compressive strength (b).

Genet et al. proposed that the mechanism of a final failure could depend on the strut diameter [151]. Additionally, a greater amount of bubbles or less B50 particles could have lowered the mass of the scaffolds and caused structural variation in the printed struts resulting in lowered compressive strength. Hence, even if the fracture strength is greatly dependent on structure and defects, the variation in mass was examined. The relationship between the compressive strength and mass is illustrated in Figure 54 (b). The low correlation coefficient (R^2) indicates that there would not be correlation between the mass and compressive strength.

4.6.2 Comparison with Other Studies

The received results could be compared with literature. Table 18 summarizes the studies. All the compression tests were conducted dry using the static compressive rate ranging from 0.5 to 0.6 mm/min. The compressive directions were perpendicular to the printed struts. Glass compositions are explained in Table 19.

Table 18. Compressive properties of robocasted bioactive glass scaffolds compared. The glass composition, binder, porosity, compressive strength, compressive modulus, Weibull modulus and the number of the samples are summarized.

	Composition	**Binder**	**$\sim\phi$ (%)**	**Size (mm)**	**σ_m (MPa)**	**E**	**m**	**n**
Present	B50	F-127	52	7.4x3.8	4±1	178±82 MPa	3.8	20
Liu et al. [147]	13-93	F-127	47	6x6x6	86±9	13±2 GPa	12	30
Fu et al. [152]	6P53B	F-127	60	3x3x3	136±22	-	-	8
Eqtesadi et al. [146]	45S5	CMC(a)	60	3x3x6	11-13	-	-	9
Deliormanli & Rahaman [145]	13-93	EC(b)	50	7.5x7.5x7.5	142±20	-	-	5
	13-93B3	EC(b)	50	7.5x7.5x7.5	65±11	-	-	5
Wu et al. [101]	HgSi/Ca/P	PVA(c)	60	10x10x10	16±2	155±15 MPa	-	4

(a)Carboxymethyl cellulose
(b)Ethyl cellulose
(c)Poly(vinyl alcohol)

Table 19. Bioactive glass compositions in mol % [101, 145-147, 152].

Composition	**SiO_2**	**Na_2O**	**K_2O**	**MgO**	**CaO**	**P_2O_5**	**B_2O_3**
B50	26.93	22.66	-	-	21.77	1.72	26.92
13-93	53	6	12	5	20	4	-
6P53B	52.7	10.3	2.8	10.2	18.0	6	-
45S5	45	24.5	-	-	24.5	6	-
13-93B3	-	5.5	11.1	4.6	18.5	3.7	56.6
Si/Ca/P	80	-	-	-	15	5	-

Significant variation in the values of the compressive strength, compressive modulus and Weibull modulus can be seen. The bioactive glass composition, chemistry of the binder, porosity, design and the size of the scaffolds are gathered in Table 18. All these factors effect on the mechanical properties and need to be taken into consideration. Additionally, some structural factors or steps in the production may influence on the results, such as surface morphology and sintering temperatures, as already discussed. The brittle structure of the scaffolds that is sensitive to defects, causes great variation in the compressive results. The Weibull modulus, that statistically characterizes the reliability of the strength, was calculated only for two studies. The rest of the studies had a small number of samples as for the Weibull modulus a minimum of 20 samples are required (30 samples are usually preferred) [127]. Additionally, the compressive modulus was not analyzed for most of the studies. This could be due to the great variation in the stress-strain curves, or possibly there was uncertainty of the correct elastic region. An indentation test could be a good alternative to measure stiffness, as it does not depend on the structural design and shape as much as the compression test [20, 28].

Bioactive glass is strong, thus the change in length is small during the compression test and the quality of the device is important. The use of a non-touching optical extensometer could have a great effect on the values of the compressive modulus, but rarely the use of the extensometer is reported. However, Liu et al. reported a compressive modulus as high as 13 GPa, but also measured the change in length from the surface-platen interface [147]. Some difference in the results could have been due to the smaller porosity of the scaffolds and the use of surface grinder that Liu et al. reported. Grinding ensured an even surface of the scaffold and stress distribution during the compression test. This could have enhanced the reliability of the results in the present study but due to the sintering defects, it would not have corrected all the structural challenges. In the literature, the uneven surfaces of ceramic scaffolds have been minimized by grinding or polishing the surface [33, 145, 146].

The dependence of the compressive strength on different structural variations have been studied and porosity seems to have effect to some extend [150-152, 163]. Meille et al. suggested that the pore size effect depends on the degree of the material porosity [19]. Genet et al. studied the relationship between architecture and compressive strength on scaffolds with different strut diameters [151]. The data proposes that the compressive strength depends on the rods' diameter and spacing even if the tested scaffolds had the same porosity. All in all, the studies indicate that the failure mechanism is complicated and needs research. Computational models could enhance the understanding of the failure mechanism. For example, the Finite Element method is one of the potential methods that have been developed, but there are still limitations due to complex structural variations and fracture processes [9, 164]. In the present study, the structure and porosity of the scaffolds were evaluated by μCT. However, this method could not illustrate all the defects in the struts.

In conclusion, great structural defects, such as the unaligned columns and stacked middle part, could be detected. These defects lowered the compressive properties and the reliability of the results. The compressive device had limitations with a strong and brittle material, and with the surface design of the scaffold. The µCT was found not to be precise enough to evidence the small defects that can cause struts failure. However, similar problems with the accuracy of the compressive results have been reported in the literature of 3D-printed ceramic scaffolds.

4.7 Cancellous Bone

The mechanical properties of fourteen cancellous bone samples from pig's femur were compared with literature. The reproducibility was evaluated as the test was conducted exactly according to Karjalainen [126]. Additionally, the inorganic content was analyzed by TGA and structure imaged with µCT. Thus, the structure-property relationships were discussed.

4.7.1 Reproducibility

The exact same compressive device, parameters and methods were used. Figure 55 shows the compressive strength and compressive modulus of the present and previous study and the number of cancellous bone samples can be seen above the columns. More variation between the previous and present study could be seen in the compressive strength compared with the compressive modulus. However, statistically no significant difference in the compressive strength (0.057) or compressive modulus (0.371) was seen.

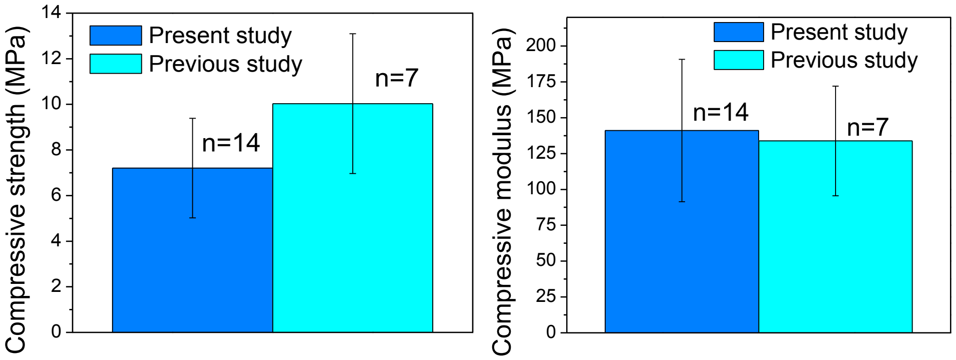

Figure 55. Compressive strength and compressive modulus compared with previous study. The number of tested samples are presented above the columns.

There was some variation between the results even if the sample size, preparation method, testing method and equipment were all almost the same. This was expected due to the challenges of compression testing the cancellous bone. µCT images (Figure 56) illustrates the structure of one bone sample. The structure is anisotropic and non-homogeneous, which is typical of the cancellous bone. The estimated porosity was 73 %. According to

An and Draughn, the porosity of the cancellous bone can vary as much as 30-90 % [9, p. 9].

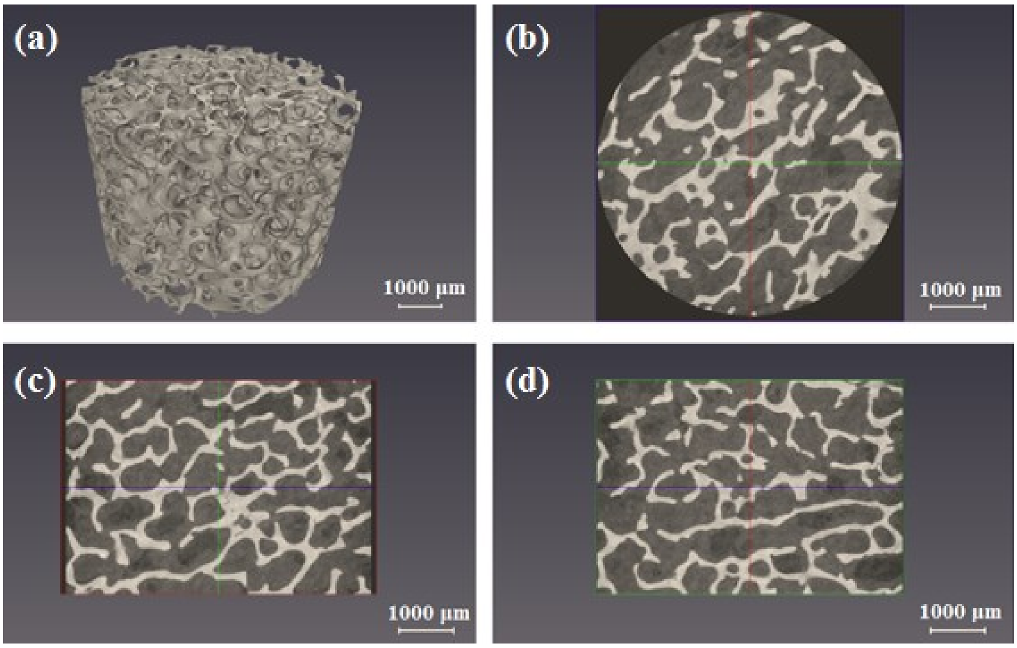

Figure 56. µCT images of a cancellous bone sample. The 3D structure of the scaffold (a), cut surface (b) and the cross-sectional images (c, d) are illustrated.

The microstructural and macrostructural bone properties and their correlation to mechanical properties have been widely studied [165-167]. The cancellous bone has clear variation in architecture that causes variation in mechanical properties. Thus, the comparison of mechanical properties between other studies is complicated if there is no knowledge of the porosity. In addition, the mineral content of the cancellous bone can be used to characterize the mechanical properties [6, 69]. The mean and standard deviation for the inorganic content were 32.1±5.7 % (n=5). Figure 57 represents TGA curve of a cancellous bone sample.

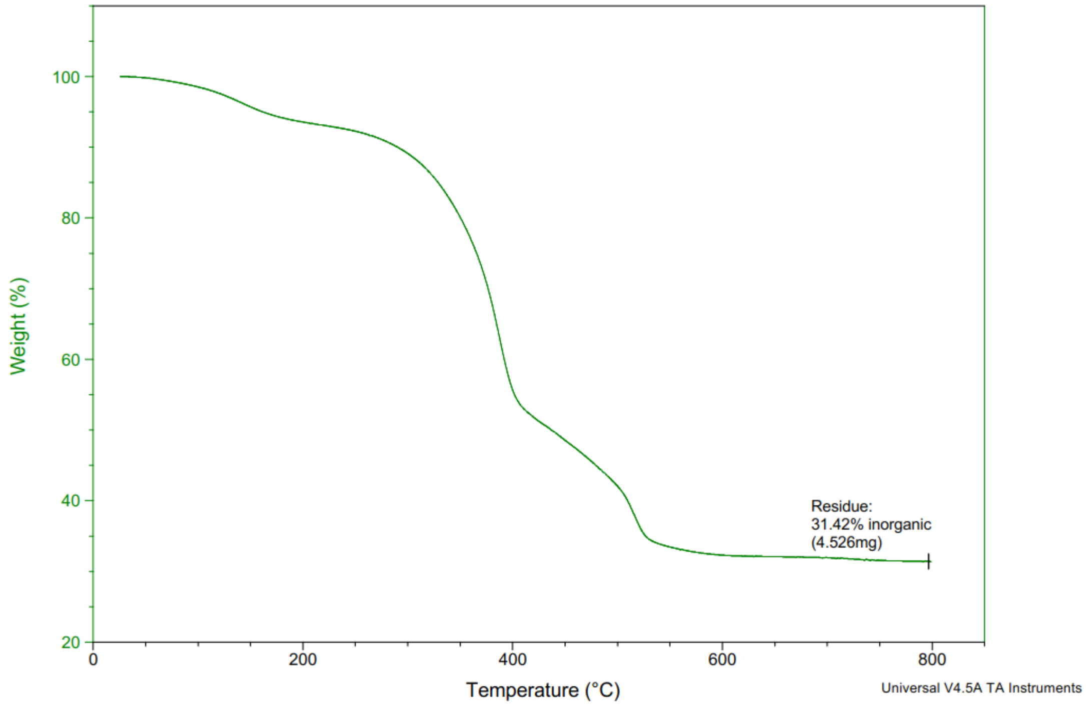

Figure 57. TGA curve of cancellous bone.

Similar results of ceramic content were received from the previous study [126]. Karjalainen reported that the inorganic content of the cancellous bone samples was 33.2±2.6 % (n=8). Both, TGA and the compression test, showed slight variation between the present and the previous study. The increase of the number of test samples or additional tests could have improved the reliability of the exploration. Despite the challenges of compression testing the cancellous bone, the compressive device showed good reproducibility.

4.7.2 Reliability and Limitations

Pig's bone is generally used as an animal model for orthopaedical implants due to its similar biology to human bone [70]. Literature showed some similarities in the compressive properties of human bone compared with the present results of pig's distal femur. Kuhn et al. reported the values of the compressive strength and the compressive modulus of the human distal femur 5.6±3.8 MPa and 298±224 MPa [77]. The large standard deviation in the modulus is typical of cancellous bone as the properties are dependent on the morphological location and direction [168], age [169] and the physiological condition of an individual [9]. No optical extensometer was used in the study and samples were wet at room temperature. Drying was found to increase the bone stiffness [83] and according to Brear et al., mechanical properties were lower at 37°C compared with room temperature [82]. Both factors were the same in the present study and in the study Kuhn et al. reported making the results more comparable. However, there were many limitations when the results were compared together. There was a lack of knowledge on structural factors, such as the bone porosity, the angle of trabecular structure and inorganic content. Before making valid conclusions, the structural differences between the human and the pig should be subtracted from the results. Notable was the differences in the strain rate as bone is viscoelastic and behaves differently depending on the compressive rate [74, 168, 170]. The equipment, compressive direction, sample design and the size were different and the list could go on. Thus, the reliable comparison of studies is questionable and the results are suggestive.

The received results can be compared with other compression test results of pig's femur, which removes the problems with structural differences between species. Lee & Jasiuk reported the conventional compression test results of pig's cancellous bone received from the apical femur [73]. Lee & Jasiuk had three groups of samples; "A", "B", and "C". The group "A" samples were received from fresh bone, group "B" represented bone that was stored in the freezer for one year and group "C" represented bone that was stored for five years in the freezer. They showed that long term freezing affects the bone's structure and mechanical properties. The case of Group "C" was closest to cancellous bone samples tested in this study as the bone had been frozen for several years. The compressive strength and compressive modulus of group "C" compared with the present results showed more similarity than group "A" and "B" (Table 20). Actually, the compressive strength of group "C" showed comparable results to the present study, but the results of the compressive modulus had some difference between the studies.

Table 20. Compressive properties of pig's distal and apical femur. The sample size, mineral content, porosity, compressive strength, compressive modulus and the number of the samples are summarized.

	Size (mm)	**Mineral content (~%)**	**ϕ (%)**	**σ_m (Mpa)**	**E (Mpa)**	**n**
Present	ϕ10x5	32	~73	7.2±2.2	141.1±49.6	14
Lee & Jasiuk 2014 [73]						
Group A	ϕ4x8	50	68.6±3.9	~14-16	~500-600	24
Group B	ϕ4x8	48	65.9±4.9	~12-14	~300-400	23
Group C	ϕ4x8	52	70.6±5.1	~10-12	~300-400	20

The sample size, mineral content and porosity of the tested samples are also gathered in Table 20. Lee & Jasiuk had samples with greater mineral content and slightly denser structure [73]. These properties have found to increase compressive modulus and strength [74]. The size of the samples was different which also effects on the compressive properties. Due to the viscoelasticity of the cancellous bone, the compressive rate should be considered [12, 169]. Lee & Jasiuk used strain at the rate of 0.005 mm/s. In the present study, the samples were compressed at a 1 mm/min rate. An increase in the compressive rate has shown to increase the compressive modulus [12]. For the bone used in the present study, the duration of the freezing period was unknown, which could be one factor effecting the results. However, significant influence on the reliability of comparing the results causes the next two facts. The samples were received from the opposite side of the femur and the compressive angle was about 90˚ different between the studies. The second factor is that the stiffness could be greatly underestimated without the optical extensometer as the samples were cut, but Lee & Jasiuk did not report whether they used the extensometer or not. The optical extensometer has proved to affect about 45 % to the compressive modulus of the cancellous bone [5].

PU foam has been used as a standard material for testing orthopaedical devices. It is said to be a good alternative as it offers consistent material and mimics the mechanical properties of the cancellous bone. In the present study PU foam was compression tested and analyzed using the same method. The compressive modulus and absorbed energy for the cancellous bone were 141.1±49.6 MPa and 134.0±68.9 kJ/m^3, respectively. The densest (320 kg/m^3) PU foam was the closest to these mechanical properties with the compressive modulus 119.9±16.3 MPa and the absorbed energy 71.7±19.5 kJ/m^3. The porosity of the cancellous bone samples was estimated to be similar to PU foam samples.

Under compression, both materials behaved in a similar way. The stress-strain curves are illustrated in Figure 58. Curves show a short toe region, a linear region and a yield region. The two stress-strain curves of the cancellous bone samples in Figure 58 show great variation in behavior, as there probably is variation between the samples. The consistent structure of PU foam showed reproducibility in the stress-strain curves. Hence, PU foam is considered ad a good analog for bone.

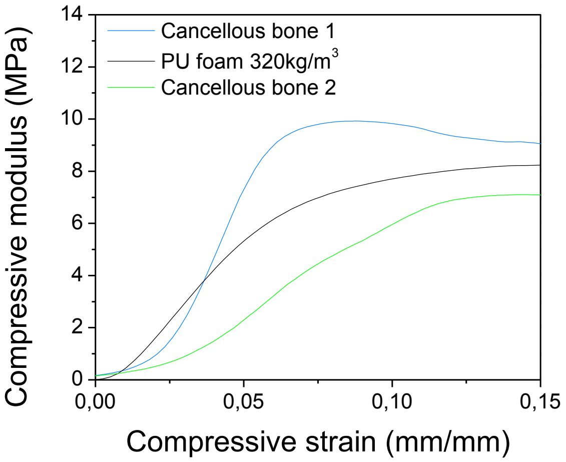

Figure 58. The stress-strain curve of two cancellous bone samples and PU foam with density of 320 kg/m^3.

Overall, there are many considerations when compression testing the cancellous bone in compression. A good planning of the sample size, environment, compressive direction and sample location before preparation is important. If comparison of different studies is desired to conduct, good background of the study is needed. Some variation in the results is always expected. For reliability and comparable analysis, it is important to report the used equipment and methods, such as the use of the optical extensometer. PU foam showed to be a good alternative if consistent compressive properties close to the cancellous bone are desired.

5. CONCLUSION

The objective was to study the limitation and reliability of static uniaxial compression test and the mechanical testing device (Instron Electropuls E 1000). Two reference materials (PET and PU foam), various types of biomaterials (hydrogel scaffolds, a solid polymer rod, knitted polymer scaffolds, bioactive glass scaffolds) and biological tissue (cancellous bone) were compression tested to get better understanding of the performance and limitations of the testing device. In addition, the performance of the compression testing device was compared with other compression testing devices.

The compressive modulus and compressive strength of the reference materials (PET and PU foam) showed that the compression speed, sample size and cell structure have influence on the compression test. The compression test results were compared with the values obtained from the manufacturer. The small diameter of the compressive platen (18 mm) limited the sample size. Hence, we could not use exactly the same compression method as the manufacturer and some differences in the results were expected. The accuracy of the compressive strength was good, but the compressive testing device underestimated the compressive modulus > 34 %. Similar results have been reported in the literature. Inaccuracy was most likely due to surface damage and friction artifacts when measuring the strain from the compressive platen and sample interface. Accuracy could be improved using an optical extensometer, that excludes the surface artifacts by measuring the strain from the center of the specimen without a need of attachment to the specimen.

The adhesive property and viscoelasticity of the hydrogel scaffolds caused limitations in the compression test. The hydrogel scaffold was adhesive toward the compressive platen. Hence, the zero-deformation point was complicated to determine. The effect on the zero-deformation point to the compressive values was evaluated. A significant difference could be seen in the compressive results of three different zero-deformation points ($p<0.05$). The hydrogel scaffolds were produced and compression tested exactly the same way as two previous studies. Only difference was the compressive device. Hence, the performance of these devices could be compared. The stress-strain curves showed less noise to signal ratio and more reproducible dataset for Instron E 1000 compared with the other compression testing device. The reliable comparison of the compressive results between the present and previous studies could not be performed due to noisy stress-strain curves and differences in analysis methodology. Additionally, the hydrogel scaffolds were sensitive to the compressive rate due to viscoelasticity. Hence, comparison between studies was suggestive.

The maximum load Instron E 1000 could deliver is 1 kN. The strong PLA rod samples needed to be compression tested with another compression testing device, for which a 5 kN load cell could be used, to be certain of the measurements at a higher load. Another problem was the non-parallel surfaces of the PLA samples. Uniaxially fixed compressive platen could not align on the tilted sample surface. Hence, the stresses were not distributed evenly on the sample and the results were not reliable. The surface parallelism could be enhanced with polishing or grinding the surfaces, or using a self-aligning platen.

Ten batches of knitted scaffold joint scaffolds were compression tested. Compressive results showed variation between the same sized scaffolds. The variation could be explained with non-homogeneity in the scaffold structure. Various sizes were tested, which showed that a decrease in size increased the compressive modulus and logically lower the compressive strain. Bulging of the joint scaffolds was a problem especially when the diameter of the compressive platen was the same as the diameter of the biggest joint scaffold. Compressive platen could not load the full sample cross-section. Hence, the sample size should not be bigger or equal to the compressive platen.

Bioactive glass (B50) scaffolds with estimated porosity of 52 % was compression tested. Sudden changes in stiffness during the test caused instability of the instrument. Hence, the performance of the device was manually tuned to enable the compression test. The sintering process caused significant changes in the scaffold structure. The structure of the scaffold collapsed from the middle part and the struts packed at the edges which led to distorted columns. The fracture process of B50 glass scaffolds was hard to evaluate and would need special equipment, such as a video extensometer. The structural changes and the brittle property of the scaffold led to the low and scattered compressive results. Low value for Weibull modulus (3.8) showed a high probability of an early failure. Similar values of low Weibull modulus have been reported in the literature and are typical for brittle materials.

The compressive test of the cancellous bone from distal femur of a pig was conducted exactly the same way as in the previous study. Hence, the reproducibility could be evaluated. No significant difference in the results could be seen ($p>0.05$). For the accurate evaluation of the structure-property relationships of the cancellous bone, additional tests are needed. TGA confirmed the similarity of the samples: the inorganic content of the cancellous bone samples used in the present study was 32.1±5.7 % and in the previous study 33.2±2.6 %. Hence, when considering the properties of the cancellous bone, such as anisotropy, viscoelasticity and non-homogenity, Instron E 1000 showed good reproducibility. Additionally, µCT analysis was used to evaluate the porosity of tested cancellous bone (~73 %). Despite the additional tests, the comparison of the compressive results with the literature was complicated. The compressive results may vary due to changes in bone structure (age, gender, diseases, location, freezing, thawing) or changes in compressive methods (compressive direction, compressive rate, equipment, sample size and design, degree of moisture). Seldom all the needed information for reliable comparison is reported.

In conclusion, the testing device showed good reproducibility, and accuracy for the compressive strength. The accuracy of the compressive modulus could be improved with an optical extensometer, self-aligning platen and careful sample preparation. A compression test conducted on a biomaterial is seldom accurate. Different scaffold structures and materials needs special consideration.

6. REFERENCES

[1] S. Bose, A. Bandyopadhyay, Chapter 1 - Introduction to Biomaterials, in: A. Bandyopadhyay, S. Bose (ed.), Characterization of Biomaterials, Academic Press, Oxford, 2013, pp. 1-9.

[2] J.D. Enderle, S.M. Blanchard, J.D. Bronzino, Introduction to biomedical engineering, 2. ed. ed. Elsevier, Acad. Press, UK, 2005, pp. 151-165, 255-393.

[3] R.K. Roeder, Chapter 3 - Mechanical Characterization of Biomaterials, in: A. Bandyopadhyay, S. Bose (ed.), Characterization of Biomaterials, Academic Press, Oxford, 2013, pp. 49-104.

[4] L.A. Pruitt, A.M. Chakravartula, Mechanics of biomaterials: Fundamental principles for implant design, Cambridge Univ. Press, Cambridg, 2011, pp. 3-700.

[5] T.M. Keaveny, R.E. Borchers, L.J. Gibson, W.C. Hayes, Theoretical analysis of the experimental artifact in trabecular bone compressive modulus, Journal of Biomechanics, Vol. 26, Iss. 4-5, 1993, pp. 599-607.

[6] S. Pal, Design of Artificial Human Joints & Organs, 1st ed. Springer, Boston, MA, 2013, pp. 23-73.

[7] J.F. Mano, N.M. Neves, R. Reis, Mechanical Characterization of Biomaterials, in: R.L. Reis, J.S. Román (ed.), Biodegradable Systems in Tissue Engineering and Regenerative Medicine, CRC Press, 2004.

[8] W.D. Callister, D.G. Rethwisch, Materials science and engineering: an introduction, 7th ed ed. John Wiley & Sons, New York, 2007, pp. 3-573.

[9] Y.H. An, R.A. Draughn, Mechanical Testing of Bone and the Bone-Implant Interface, CRC Press, Baton Rouge, 1999, 3-579 p.

[10] Á Oroszlány, P. Nagy, J. Gábor Kovács, Compressive Properties of Commercially Available PVC Foams Intended for Use as Mechanical Models for Human Cancellous Bone, Acta Polytechnica Hungarica, Vol. 12, Iss. 2, 2015, pp. 89-98.

[11] P.S.D. Patel, D.E.T. Shepherd, D.W.L. Hukins, Compressive properties of commercially available polyurethane foams as mechanical models for osteoporotic human cancellous bone, BMC musculoskeletal disorders, Vol. 9, Iss. 1, 2008, pp. 1-7. http://www.ncbi.nlm.nih.gov/pubmed/18844988.

[12] F. Linde, Elastic and viscoelastic properties of trabecular bone by a compression testing approach. Danish medical bulletin, Vol. 41, Iss. 2, 1994, pp. 119-138.

[13] J. Betten, Viscoelastic Materials, 3rd ed., Springer Berlin Heidelberg, Berlin, Heidelberg, 2008, pp. 195-244.

[14] D. Nesic, R. Whiteside, M. Brittberg, D. Wendt, I. Martin, P. Mainil-Varlet, Cartilage tissue engineering for degenerative joint disease, Advanced Drug Delivery Reviews, Vol. 58, Iss. 2, 2006, pp. 300-322. Available (accessed ID: 271323): http://www.sciencedirect.com/science/article/pii/S0169409X06000202.

[15] Charles A. Harper, Handbook of Plastics, Elastomers, and Composites, Fourth Edition, Fourth ed. McGRAW-HILL: New York, Chicago, San Francisco, Lisbon, London, Madrid, Mexico City, Milan, Montreal, New Delhi, San Juan, Seoul, Singapore, Sydney, Toronto, 2002, pp. 8-9.

[16] S. Li, A.G. Patwardhan, F.M.L. Amirouche, R. Havey, K.P. Meade, Limitations of the standard linear solid model of intervertebral discs subject to prolonged loading and low-frequency vibration in axial compression, Journal of Biomechanics, Vol. 28, Iss. 7, 1995, pp. 779-790. Available (accessed ID: 271132271132): http://www.sciencedirect.com/science/article/pii/002192909400140Y.

[17] C.W. Chung, M.L. Buist, A novel nonlinear viscoelastic solid model, Nonlinear Analysis: Real World Applications, Vol. 13, Iss. 3, 2012, pp. 1480-1488.

[18] J.E. Sanders, S.G. Zachariah, Mechanical characterization of biomaterials, Annals of the New York Academy of Sciences, Vol. 831, 1997, pp. 232-243.

[19] S. Meille, M. Lombardi, J. Chevalier, L. Montanaro, Mechanical properties of porous ceramics in compression: On the transition between elastic, brittle, and cellular behavior, Journal of the European Ceramic Society, Vol. 32, Iss. 15, 2012, pp. 3959-3967.

[20] T. Kokubo, Bioceramics and their clinical applications, Woodhead Publ, Cambridge, 2008, pp. 38-43, 78-93.

[21] X. Fan, E.D. Case, I. Gheorghita, M.J. Baumann, Weibull modulus and fracture strength of highly porous hydroxyapatite, Journal of the Mechanical Behavior of Biomedical Materials, Vol. 20, 2013, pp. 283-295. Available (accessed ID: 274145): http://www.sciencedirect.com.libproxy.tut.fi/science/article/pii/S1751616113000477.

[22] J. Chakrabarty, Applied plasticity, Second Edition ed. Springer, 2000, pp. 1-3.

[23] G.E. Dieter, Mechanical Behavior Under Tensile and Compressive Loads, in: M.D. Kuhn H (ed.), ASM Handbook, Volume 8: Mechanical Testing and Evaluation. Vol. 8, ASM International, 2000.

[24] Pipes R. Byron, F. Adams Donald, A. Carlsson Leif, Test Specimen Preparation, Strain and Deformation Measurement Devices, and Testing Machines, Experimental Characterization of Advanced Composite Materials, 4th Edition ed., Taylor & Francis, 2014, pp. 73-86.

[25] ElectroForce Systems Group, ElectroForce 5100 Biodynamic Test Instruments Reference Manual, Bose Corporation, USA, 2006, pp. 1-4.

[26] D. Williams, Chapter 9 - Biocompatibility, in: C.v. Blitterswijk, P. Thomsen, A. Lindahl, J. Hubbell, D.F. Williams, R. Cancedda, J.D.d. Bruijn, J. Sohier (ed.), Tissue Engineering, Academic Press, Burlington, 2008, pp. 255-278.

[27] D.L. Wise, Biomaterials and bioengineering handbook, Dekker, New York, 2000, 144-147, 588-591, pp. 720-721.

[28] P. Clement, S. Meille, J. Chevalier, C. Olagnon, Mechanical characterization of highly porous inorganic solids materials by instrumented micro-indentation, Acta Materialia, Vol. 61, Iss. 18, 2013, pp. 6649-6660.

[29] R. Brown, Handbook of polymer testing: physical methods, CRC press, 1999, pp. 237-238.

[30] Y. Xiao, M. Kawai, H. Hatta, An integrated method for off-axis tension and compression testing of unidirectional composites, Journal of Composite Materials, Vol. 45, Iss. 6, 2011, pp. 657-669.

[31] J. Tsai, C.T. Sun, Constitutive model for high strain rate response of polymeric composites, Composites Science and Technology, Vol. 62, Iss. 10, 2002, pp. 1289-1297.

[32] L.A. Carlsson, D.F. Adams, R.B. Pipes, Experimental characterization of advanced composite materials, Fourth ed. CRC press, 2014, pp. 63–86.

[33] S. Roohani-Esfahani, P. Newman, H. Zreiqat, Design and Fabrication of 3D printed Scaffolds with a Mechanical Strength Comparable to Cortical Bone to Repair Large Bone Defects, Scientific reports, Vol. 6, Iss. 19468, 2016, http://www.ncbi.nlm.nih.gov/pubmed/26782020.

[34] J. Koivisto, O. Koskela, T. Montonen, J.E. Parraga, T. Joki, L. Yl-Outinen, S. Narkilahti, E. Figueiras, J. Hyttinen, M. Kellomki, Texture-property relations of bioamine crosslinked gellan gum hydrogels, IFMBE, Vol. 65, 2017, pp. 189-192.

[35] L. Salonen, Rheological and mechanical properties of hydrogels, master's thesis, Tampere University of Technology, 2014, pp. 1-82, http://dspace.cc.tut.fi/dpub/handle/123456789/22392.

[36] SFS-ISO 17161 "Fine ceramics (advanced ceramics, advanced technical ceramics) - Ceramic composites - Determination of the degree of misalignment in uniaxial mechanical tests", Suomen standardisoimisliitto, Helsinki, 2016.

[37] C.R. Gajjar, M.W. King, Overview of Resorbable Biomaterials, Resorbable Fiber-Forming Polymers for Biotextile Applications, Springer, 2014, pp. 1-5.

[38] N.L. Davison, F. Barrère-de Groot, D.W. Grijpma, Degradation of Biomaterials, Tissue Engineering (Second Edition), Academic Press, Oxford, 2014, pp. 177–215.

[39] W. Cao, L.L. Hench, Bioactive materials, Ceramics International, Vol. 22, Iss. 6, 1996, pp. 493-507.

[40] L.L. Hench, R.J. Splinter, W.C. Allen, T.K. Greenlee, Bonding mechanisms at the interface of ceramic prosthetic materials, Journal of Biomedical Materials Research, Vol. 5, Iss. 6, 1972, pp. 117-141.

[41] L.L. Hench, The story of Bioglass®, Journal of Materials Science: Materials in Medicine, Vol. 17, Iss. 11, 2006, pp. 967-978.

[42] Larry L. Hench, Julia M. Polak, Third-Generation Biomedical Materials, Science, Vol. 295, Iss. 5557, 2002, pp. 1014-1017. http://www.sciencemag.org/content/295/5557/1014.abstract.

[43] B.D. Ratner, A.S. Hoffman, F.J. Schoen, J.E. Lemons, Biomaterials Science: An Introduction to Materials in Medicine, 3rd; 3 ed. Academic Press, US, 2012, pp. 1138-1144.

[44] D.F. Williams, On the mechanisms of biocompatibility, Biomaterials, Vol. 29, Iss. 20, 2008, pp. 2941-2953.

[45] S. Suzuki, Y. Ikada, Bioabsorbable Polymers, 2012th ed., Humana Press, Totowa, NJ, 2012, pp. 19-38.

[46] M. Gomes, H. Azevedo, P. Malafaya, S. Silva, J. Oliveira, G. Silva, R. Sousa, J. Mano, R. Reis, Chapter 6 - Natural Polymers in tissue engineering applications, in: C.v. Blitterswijk, P. Thomsen, A. Lindahl, J. Hubbell, D.F. Williams, R. Cancedda, J.D.d. Bruijn, J. Sohier (ed.), Tissue Engineering, Academic Press, Burlington, 2008, pp. 145-192.

[47] F.J. O'Brien, Biomaterials & scaffolds for tissue engineering, Materials Today, Vol. 14, Iss. 3, 2011, pp. 88-95.

[48] F. Barrère, M. Ni, P. Habibovic, P. Ducheyne, K.d. Groot, Chapter 8 - Degradation of bioceramics, in: C.v. Blitterswijk, P. Thomsen, A. Lindahl, J. Hubbell, D.F. Williams, R. Cancedda, J.D.d. Bruijn, J. Sohier (ed.), Tissue Engineering, Academic Press, Burlington, 2008, pp. 223-254.

[49] M. Huttunen, M. Kellomäki, Strength retention behavior of oriented PLLA, 96L/4D PLA, and 80L/20D,L PLA, Biomatter, Vol. 3, Iss. 4, 2013, e26395.

[50] J.A. Hubbell, Bioactive biomaterials, Current Opinion in Biotechnology, Vol. 10, Iss. 2, 1999, pp. 123-129. http://www.sciencedirect.com/science/article/pii/S0958166999800214.

[51] R.W. Rice, Limitations of pore-stress concentrations on the mechanical properties of porous materials, Journal of Materials Science, Vol. 32, Iss. 17, 1997, pp. 4731-4736.

[52] D. Hutmacher, T. Woodfield, P. Dalton, J. Lewis, Chapter 14 - Scaffold design and fabrication, in: C.v. Blitterswijk, P. Thomsen, A. Lindahl, J. Hubbell, D.F. Williams, R. Cancedda, J.D.d. Bruijn, J. Sohier (ed.), Tissue Engineering, Academic Press, Burlington, 2008, pp. 403-454.

[53] SFS-EN 24506 "Hardmetals. Compression test", Suomen Standardisoimisliitto, Helsinki, 1993, .

[54] S. Donglu, Bioactive Ceramics: Structure Synthesis and Mechanical Properties, Introduction to biomaterials, 1st ed., Tsinghua University Press, Beijing, 2005, pp. 24-26.

[55] J.R. Jones, D.S. Brauer, L. Hupa, D.C. Greenspan, Bioglass and Bioactive Glasses and Their Impact on Healthcare, International Journal of Applied Glass Science, Vol. 7, Iss. 4, 2016, pp. 423-434.

[56] S.v. Gaalen, M. Kruyt, G. Meijer, A. Mistry, A. Mikos, J.v.d. Beucken, J. Jansen, K.d. Groot, R. Cancedda, C. Olivo, M. Yaszemski, W. Dhert, Chapter 19 - Tissue engineering of bone, in: C.v. Blitterswijk, P. Thomsen, A. Lindahl, J. Hubbell, D.F. Williams, R. Cancedda, J.D.d. Bruijn, J. Sohier (ed.), Tissue Engineering, Academic Press, Burlington, 2008, pp. 559-610.

[57] B.V. Slaughter, S.S. Khurshid, O.Z. Fisher, A. Khademhosseini, N.A. Peppas, Hydrogels in regenerative medicine, Advanced materials (Deerfield Beach, Fla.), Vol. 21, Iss. 32-33, 2009, pp. 3307-3329. http://www.ncbi.nlm.nih.gov/pubmed/20882499.

[58] X. Zhang, Y. Yang, J. Yao, Z. Shao, X. Chen, Strong collagen hydrogels by oxidized dextran modification, ACS Sustainable Chemistry & Engineering, Vol. 2, Iss. 5, 2014, pp. 1318-1324.

[59] J.N. Hanson Shepherd, S.T. Parker, R.F. Shepherd, M.U. Gillette, J.A. Lewis, R.G. Nuzzo, 3D Microperiodic Hydrogel Scaffolds for Robust Neuronal Cultures, Advanced Functional Materials, Vol. 21, Iss. 1, 2011, pp. 47-54.

[60] G. Yang, H. Lin, B.B. Rothrauff, S. Yu, R.S. Tuan, Multilayered polycaprolactone/gelatin fiber-hydrogel composite for tendon tissue engineering, Acta Biomaterialia, Vol. 35, 2016, pp. 68-76. http://www.sciencedirect.com/science/article/pii/S1742706116300885.

[61] João T Oliveira, Tírcia C Santos, Luís Martins, Ricardo Picciochi, Alexandra P Marques, António G Castro, Nuno M Neves, João F Mano, Rui L Reis, Gellan Gum Injectable Hydrogels for Cartilage Tissue Engineering Applications: In Vitro Studies and Preliminary In Vivo Evaluation, Tissue Engineering Part A, Vol. 16, Iss. 1, 2010, pp. 343-352. http://www.ncbi.nlm.nih.gov/pubmed/19702512.

[62] G. Sun, X. Zhang, Y. Shen, R. Sebastian, L.E. Dickinson, K. Fox-Talbot, M. Reinblatt, C. Steenbergen, J.W. Harmon, S. Gerecht, Dextran hydrogel scaffolds enhance angiogenic responses and promote complete skin regeneration during burn wound healing, Proceedings of the National Academy of Sciences of the United States of America, Vol. 108, Iss. 52, 2011, pp. 20976-20981.

[63] S. Kalia, Polymeric Hydrogels as Smart Biomaterials, Springer International Publishing, Cham ; s.l, 2016, pp. 1-10.

[64] R. Lanza, R. Langer, J.P. Vacanti, Principles of Tissue Engineering, Fourth; 4; 4th ed. Academic Press, US, 2013, pp. 237-319, 325-489.

[65] M. Ross, W. Pawlina, Histology: a Text and Atlas, with correlated cell and molecular biology, 7th ed. Lippincott Williams & Wilkins, 2015, 194-239 p.

[66] E. Haug, O. Sand, ÖV. Sjaastad, K.C. Toverud, Ihmisen fysiologia, 1.-5. ed. Sanoma Pro Oy, Helsinki, 2012, pp. 113-140, 230-233.

[67] E.N. Marieb, Essentials of human anatomy & physiology, 10.th ed. Pearson Education, 2014, pp. 134-257.

[68] S. Badylak, T. Gilbert, J. Myers-Irvin, Chapter 5 - The extracellular matrix as a biologic scaffold for tissue engineering, in: C.v. Blitterswijk, P. Thomsen, A. Lindahl, J. Hubbell, D.F. Williams, R. Cancedda, J.D.d. Bruijn, J. Sohier (ed.), Tissue Engineering, Academic Press, Burlington, 2008, pp. 121-143.

[69] J.D. Currey, Bones: Structure and Mechanics; 2nd ed. Princeton University Press, Princeton, 2002, pp. 3-176, 247-248.

[70] A.I. Pearce, R.G. Richards, S. Milz, E. Schneider, S.G. Pearce, Animal models for implant biomaterial research in bone: a review, European cells & materials, Vol. 13, 2007, pp. 1-10. http://www.ncbi.nlm.nih.gov/pubmed/17334975.

[71] J. Rho, L. Kuhn-Spearing, P. Zioupos, Mechanical properties and the hierarchical structure of bone, Medical engineering & physics, Vol. 20, Iss. 2, 1998, pp. 92-102.

[72] J.P. Bilezikian, L.G. Raisz, T.J. Martin, Principles of bone biology, Academic Press, 2008, pp. 3-38.

[73] W. Lee, I. Jasiuk, Effects of freeze–thaw and micro-computed tomography irradiation on structure–property relations of porcine trabecular bone, Journal of Biomechanics, Vol. 47, Iss. 6, 2014, pp. 1495-1498.

[74] R.W. Goulet, S.A. Goldstein, M.J. Ciarelli, J.L. Kuhn, M.B. Brown, L.A. Feldkamp, The relationship between the structural and orthogonal compressive properties of trabecular bone, Journal of Biomechanics, Vol. 27, Iss. 4, 1994, pp. 375-389. http://www.sciencedirect.com/science/article/pii/0021929094900140.

[75] M. Martens, R. Van Audekercke, P. Delport, P. De Meester, J.C. Mulier, The mechanical characteristics of cancellous bone at the upper femoral region, Journal of Biomechanics, Vol. 16, Iss. 12, 1983, pp. 971-983. http://www.sciencedirect.com/science/article/pii/0021929083900982.

[76] M.J. Ciarelli, S.A. Goldstein, J.L. Kuhn, D.D. Cody, M.B. Brown, Evaluation of orthogonal mechanical properties and density of human trabecular bone from the major metaphyseal regions with materials testing and computed tomography, Journal of orthopaedic research : official publication of the Orthopaedic Research Society, Vol. 9, Iss. 5, 1991, pp. 674-682. http://www.ncbi.nlm.nih.gov/pubmed/1870031.

[77] J.L. Kuhn, S.A. Goldstein, M.J. Ciarelli, L.S. Matthews, The limitations of canine trabecular bone as a model for human: A biomechanical study, Journal of Biomechanics, Vol. 22, Iss. 2, 1989, pp. 95-107. http://www.sciencedirect.com/science/article/pii/0021929089900328.

[78] D.T. Reilly, A.H. Burstein, V.H. Frankel, The elastic modulus for bone, Journal of Biomechanics, Vol. 7, Iss. 3, 1974, pp. 271-272.

[79] S. Li, E. Demirci, V.V. Silberschmidt, Variability and anisotropy of mechanical behavior of cortical bone in tension and compression, Journal of the mechanical behavior of biomedical materials, Vol. 21, 2013, pp. 109-120. http://www.ncbi.nlm.nih.gov/pubmed/23563047.

[80] K. Tsubota, T. Adachi, Y. Tomita, Functional adaptation of cancellous bone in human proximal femur predicted by trabecular surface remodeling simulation toward uniform stress state, Journal of Biomechanics, Vol. 35, Iss. 12, 2002, pp. 1541-1551.

[81] M. Andrade, C. Sá, A. Marchionni, T. de Bittencourt, M. Sadigursky, Effects of freezing on bone histological morphology, Cell and Tissue Banking, Vol. 9, Iss. 4, 2008, pp. 279-287. http://www.ncbi.nlm.nih.gov/pubmed/18320353.

[82] K. Brear, J.D. Currey, S. Raines, K.J. Smith, Density and temperature effects on some mechanical properties of cancellous bone, Engineering in medicine, Vol. 17, Iss. 4, 1988, pp. 163-167.

[83] J. Rho, G.M. Pharr, Effects of drying on the mechanical properties of bovine femur measured by nanoindentation, Journal of Materials Science: Materials in Medicine, Vol. 10, Iss. 8, 1999, pp. 485-488.

[84] A.R. Poole, T. Kojima, T. Yasuda, F. Mwale, M. Kobayashi, S. Laverty, Composition and structure of articular cartilage: a template for tissue repair, Clinical orthopaedics and related research, Vol. 391, Iss. 391 Suppl, 2001, pp. 26-33. http://www.ncbi.nlm.nih.gov/pubmed/11603710.

[85] M. Brittberg, A. Lindahl, Chapter 18 - Tissue engineering of cartilage, in: C.v. Blitterswijk, P. Thomsen, A. Lindahl, J. Hubbell, D.F. Williams, R. Cancedda, J.D.d. Bruijn, J. Sohier (ed.), Tissue Engineering, Academic Press, Burlington, 2008, pp. 533-557.

[86] R.L. Mauck, J.A. Burdick, Engineering Cartilage Tissue, Tissue Engineering, Form Lab to Clinic, Springer Berlin Heidelberg, Berlin, Heidelberg, 2011, pp. 493-520.

[87] P.R. Moshtagh, B. Pouran, N.M. Korthagen, A.A. Zadpoor, H. Weinans, Guidelines for an optimized indentation protocol for measurement of cartilage stiffness: The effects of spatial variation and indentation parameters, Journal of Biomechanics, Vol. 49, Iss. 14, 2016, pp. 3602-3607.

[88] L.P. Li, W. Herzog, Strain-rate dependence of cartilage stiffness in unconfined compression: the role of fibril reinforcement versus tissue volume change in fluid pressurization, Journal of Biomechanics, Vol. 37, Iss. 3, 2004, pp. 375-382.

[89] S. Bose, M. Roy, A. Bandyopadhyay, Recent advances in bone tissue engineering scaffolds, Trends in biotechnology, Vol. 30, Iss. 10, 2012, pp. 546-554.

[90] H. Cheung, K. Lau, T. Lu, D. Hui, A critical review on polymer-based bio-engineered materials for scaffold development, Composites Part B: Engineering, Vol. 38, Iss. 3, 2007, pp. 291-300. Available (accessed ID: 271637): http://www.sciencedirect.com.libproxy.tut.fi/science/article/pii/S1359836806001235.

[91] J. Massera, Bioactive Glass in Tissue Engineering: Progress and Challenges, Advances in Tissue Engineering and Regenerative Medicine: Open Access, Vol. 1, Iss. 1, 2016, pp. 1-2.

[92] C.R.M. Black, V. Goriainov, D. Gibbs, J. Kanczler, R.S. Tare, R.O.C. Oreffo, Bone Tissue Engineering, Current Molecular Biology Reports, Vol. 1, Iss. 3, 2015, pp. 132-140.

[93] P. Ducheyne, Q. Qiu, Bioactive ceramics: the effect of surface reactivity on bone formation and bone cell function, Biomaterials, Vol. 20, Iss. 23, 1999, pp. 2287-2303. http://www.sciencedirect.com/science/article/pii/S0142961299001817.

[94] V. Karageorgiou, D. Kaplan, Porosity of 3D biomaterial scaffolds and osteogenesis, Biomaterials, Vol. 26, Iss. 27, 2005, pp. 5474-5491.

[95] A.R. Boccaccini, U. Kneser, A. Arkudas, Scaffolds for vascularized bone regeneration: Advances and challenges, Expert Review of Medical Devices, Vol. 9, Iss. 5, 2012, pp. 457-460.

[96] J.R. Jones, New trends in bioactive scaffolds: the importance of nanostructure, Journal of the European Ceramic Society, Vol. 29, Iss. 7, 2009, pp. 1275-1281.

[97] T. Ohji, M. Fukushima, Macro-porous ceramics: processing and properties, International Materials Reviews, Vol. 57, Iss. 2, 2012, pp. 115-131.

[98] J.R. Jones, Reprint of: Review of bioactive glass: From Hench to hybrids, Acta biomaterialia, Vol. 23 Suppl, 2015, pp. S82. http://www.ncbi.nlm.nih.gov/pubmed/26235346.

[99] C. Wu, Y. Zhang, Y. Zhu, T. Friis, Y. Xiao, Structure–property relationships of silk-modified mesoporous bioglass scaffolds, Biomaterials, Vol. 31, Iss. 13, 2010, pp. 3429-3438. Available (accessed ID: 271870): http://www.sciencedirect.com.libproxy.tut.fi/science/article/pii/S0142961210000931.

[100] C. Wu, Y. Ramaswamy, H. Zreiqat, Porous diopside (CaMgSi2O6) scaffold: A promising bioactive material for bone tissue engineering, Acta Biomaterialia, Vol. 6, Iss. 6, 2010, pp. 2237-2245. Available (accessed ID: 273258): http://www.sciencedirect.com/science/article/pii/S1742706109005637.

[101] C. Wu, Y. Luo, G. Cuniberti, Y. Xiao, M. Gelinsky, Three-dimensional printing of hierarchical and tough mesoporous bioactive glass scaffolds with a controllable pore

architecture, excellent mechanical strength and mineralization ability, Acta Biomaterialia, Vol. 7, Iss. 6, 2011, pp. 2644-2650.

[102] P. Miranda, E. Saiz, K. Gryn, A.P. Tomsia, Sintering and robocasting of β-tricalcium phosphate scaffolds for orthopaedic applications, Acta biomaterialia, Vol. 2, Iss. 4, 2006, pp. 457-466.

[103] T. Serra, J.A. Planell, M. Navarro, High-resolution PLA-based composite scaffolds via 3-D printing technology, Acta Biomaterialia, Vol. 9, Iss. 3, 2013, pp. 5521-5530.

[104] J. Zhang, S. Zhao, Y. Zhu, Y. Huang, M. Zhu, C. Tao, C. Zhang, Three-dimensional printing of strontium-containing mesoporous bioactive glass scaffolds for bone regeneration, Acta Biomaterialia, Vol. 10, Iss. 5, 2014, pp. 2269-2281.

[105] A. Zocca, C.M. Gomes, E. Bernardo, R. Müller, J. Günster, P. Colombo, LAS glass–ceramic scaffolds by three-dimensional printing, Journal of the European Ceramic Society, Vol. 33, Iss. 9, 2013, pp. 1525-1533.

[106] N. Bhardwaj, W.T. Sow, D. Devi, K.W. Ng, B.B. Mandal, N. Cho, Silk fibroin-keratin based 3D scaffolds as a dermal substitute for skin tissue engineering, Integrative biology : quantitative biosciences from nano to macro, Vol. 7, Iss. 1, 2014, pp. 53-63. http://www.ncbi.nlm.nih.gov/pubmed/25372050.

[107] V. Ellä, T. Annala, S. Länsman, M. Nurminen, M. Kellomäki, Knitted polylactide 96/4 L/D structures and scaffolds for tissue engineering: Shelf life, in vitro and in vivo studies, Biomatter, Vol. 1, Iss. 1, 2011, pp. 102-113. http://www.tandfonline.com/doi/abs/10.4161/biom.1.1.17447.

[108] Y. Zhu, H. Wu, S. Sun, T. Zhou, J. Wu, Y. Wan, Designed composites for mimicking compressive mechanical properties of articular cartilage matrix, Journal of the mechanical behavior of biomedical materials, Vol. 36, 2014, pp. 32-46. http://www.ncbi.nlm.nih.gov/pubmed/24793172.

[109] J. Guan, J.J. Stankus, W.R. Wagner, Soft Tissue Scaffolds, Wiley Encyclopedia of Biomedical Engineering, John Wiley & Sons, Inc., 2006, pp. 1-16.

[110] S. MacNeil, Progress and opportunities for tissue-engineered skin, Nature, Vol. 445, Iss. 7130, 2007, pp. 874-880. http://dx.doi.org/10.1038/nature05664.

[111] E.R. Kandel, J.H. Schwartz, T.M. Jessell, S.A. Siegelbaum, A.J. Hudspeth, Principles of neural science, 5th ed. McGraw-hill New York, 2000, pp. 5-148.

[112] L. Yla-Outinen, C. Mariani, H. Skottman, R. Suuronen, A. Harlin, S. Narkilahti, Electrospun Poly(L,D-lactide) Scaffolds Support the Growth of Human Embryonic Stem Cell-derived Neuronal Cells, Open Tissue Engineering and Regenerative Medicine Journal, Vol. 3, 2010, pp. 1-9.

[113] A.J. Engler, S. Sen, H.L. Sweeney, D.E. Discher, Matrix Elasticity Directs Stem Cell Lineage Specification, Cell, Vol. 126, Iss. 4, 2006, pp. 677-689. http://www.sciencedirect.com/science/article/pii/S0092867406009615.

[114] M.J. Mahoney, K.S. Anseth, Three-dimensional growth and function of neural tissue in degradable polyethylene glycol hydrogels, Biomaterials, Vol. 27, Iss. 10, 2006, pp. 2265-2274. http://www.sciencedirect.com/science/article/pii/S0142961205010343.

[115] P. Dalton, A. Harvey, M. Oudega, G. Plant, Chapter 20 - Tissue engineering of the nervous system, in: C.v. Blitterswijk, P. Thomsen, A. Lindahl, J. Hubbell, D.F. Williams, R. Cancedda, J.D.d. Bruijn, J. Sohier (ed.), Tissue Engineering, Academic Press, Burlington, 2008, pp. 611-647.

[116] J. He, X. Wang, M. Spector, F. Cui, Scaffolds for central nervous system tissue engineering, Frontiers of Materials Science, Vol. 6, Iss. 1, 2012, pp. 1-25.

[117] AIREX® T92 Safety data sheet, 2017, http://www.airexbaltekbanova.com/airex-t92-pet-foam.html.

[118] Asm International Handbook Committee, Engineering Tables: Polymeric Materials, ASM Desk Editions: Engineered Materials Handbook, ASM International, 1995, pp. 92-99.

[119] International temperature scale of 1990, ITS-90, HMSO, London, 1990, pp. 277-288.

[120] Sawbone Printed Catalog, https://www.sawbones.com/about/printed-catalog/.

[121] M. Fabert, N. Ojha, E. Erasmus, M. Hannula, M. Hokka, J. Hyttinen, J. Rocherullé, I. Sigalas, J. Massera, Crystallization and sintering of borosilicate bioactive glasses for application in tissue engineering, Vol. 5, Iss. 23, 2017, pp. 4514-4525.

[122] Z.C. Chen, K. Ikeda, T. Murakami, T. Takeda, Effect of particle packing on extrusion behavior of pastes, Journal of Materials Science, Vol. 35, Iss. 21, 2000, pp. 5301-5307.

[123] ISO 15814 "Implants for Surgery - Copolymers and Blends Based on Polylactide - In Vitro Degradation Testing", Switzerland, 1999.

[124] SFS-EN ISO 844 "Rigid cellular plastics - Determination of compression properties", Suomen Standardisoimisliitto, Helsinki, 2014.

[125] SFS-ISO 604 "Plastics - Determination of compressive properties", Suomen Standardisoimisliitto, Helsinki, 2003.

[126] S. Karjalainen, Static and dynamic mechanical behavior of biomaterials in dry and simulated physiological conditions, master's thesis, Tampere University of Technology, 2016, pp. 1-93,

https://dspace.cc.tut.fi/dpub/bitstream/handle/123456789/24456/karjalainen.pdf?sequence=1&isAllowed=y.

[127] SFS-EN 843-5 "Advanced technical ceramics - Mechanical properties of monolithic ceramics at room temperature - Part 5: Statistical analysis", Suomen Standardisoimisliitto, 2007.

[128] N. Gupta, Kishore, E. Woldesenbet, S. Sankaran, Studies on compressive failure features in syntactic foam material, Journal of Materials Science, Vol. 36, Iss. 18, 2001, pp. 4485-4491.

[129] J. Korpela, A. Kokkari, H. Korhonen, M. Malin, T. Nrhi, J. Seppl, Biodegradable and bioactive porous scaffold structures prepared using fused deposition modeling, Journal of Biomedical Materials Research Part B: Applied Biomaterials, Vol. 101, Iss. 4, 2013, pp. 610-619.

[130] J. Case, Lord Chilver Of Cranfield, C.T.F. Ross, Chapter 1: Tension and compression: direct stresses, Strength of Materials and Structures, 4th; 4 ed., Butterworth Heinemann, GB, 1999.

[131] W. Ju, L. Jifeng, L. Lei, Research on Static Compression Test of Polyurethane Foam/Honeycomb Paperboard Composite Material, Open Materials Science Journal, Vol. 9, 2015, pp. 64-70.

[132] L. Li, P. Xue, Y. Chen, H.S.U. Butt, Insight into cell size effects on quasi-static and dynamic compressive properties of 3D foams, Materials Science and Engineering: A, Vol. 636, 2015, pp. 60-69. Available (accessed ID: 271387): http://www.sciencedirect.com/science/article/pii/S0921509315002944.

[133] C. Chen, N.A. Fleck, Size effects in the constrained deformation of metallic foams, Journal of the Mechanics and Physics of Solids, Vol. 50, Iss. 5, 2002, pp. 955-977.

[134] E.W. Andrews, G. Gioux, P. Onck, L.J. Gibson, Size effects in ductile cellular solids. Part II: experimental results, International Journal of Mechanical Sciences, Vol. 43, Iss. 3, 2001, pp. 701-713.

[135] M.C. Saha, H. Mahfuz, U.K. Chakravarty, M. Uddin, M.E. Kabir, S. Jeelani, Effect of density, microstructure, and strain rate on compression behavior of polymeric foams, Materials Science and Engineering: A, Vol. 406, Iss. 1, 2005, pp. 328-336. Available (accessed ID: 271387): http://www.sciencedirect.com.libproxy.tut.fi/science/article/pii/S0921509305006830.

[136] W.H. King, Rubber and related products: new methods for testing and analyzing; a symposium, American Society for Testing and Materials, Philadelphia, 1974, pp. 155-158.

[137] K.L. Calvert, K.P. Trumble, T.J. Webster, L.A. Kirkpatrick, Characterization of commercial rigid polyurethane foams used as bone analogs for implant testing, Journal of Materials Science: Materials in Medicine, Vol. 21, Iss. 5, 2010, pp. 1453-1461.

[138] A.-. Harte, N.A. Fleck, M.F. Ashby, Fatigue failure of an open cell and a closed cell aluminium alloy foam, Acta Materialia, Vol. 47, Iss. 8, 1999, pp. 2511-2524. Available (accessed ID: 271635): http://www.sciencedirect.com.libproxy.tut.fi/science/article/pii/S135964549900097X.

[139] A. Johnson, T. Keller, Mechanical properties of open-cell foam synthetic thoracic vertebrae, Journal of Materials Science: Materials in Medicine, Vol. 19, Iss. 3, 2008, pp. 1317-1323. http://www.ncbi.nlm.nih.gov/pubmed/17882383.

[140] M. Xanthos, R. Dhavalikar, V. Tan, S.K. Dey, U. Yilmazer, Properties and applications of sandwich panels based on PET foams, Journal of Reinforced Plastics and Composites, Vol. 20, Iss. 9, 2001, pp. 786-793.

[141] J.T. Oliveira, L. Martins, R. Picciochi, P.B. Malafaya, R.A. Sousa, N.M. Neves, J.F. Mano, R.L. Reis, Gellan gum: a new biomaterial for cartilage tissue engineering applications, Journal of biomedical materials research. Part A, Vol. 93, Iss. 3, 2010, pp. NA. http://www.ncbi.nlm.nih.gov/pubmed/19658177.

[142] G. Sworn, S. Kasapis, Effect of conformation and molecular weight of co-solute on the mechanical properties of gellan gum gels, Food Hydrocolloids, Vol. 12, Iss. 3, 1998, pp. 283-290. http://www.sciencedirect.com/science/article/pii/S0268005X98000162.

[143] D.F. Coutinho, S.V. Sant, H. Shin, J.T. Oliveira, M.E. Gomes, N.M. Neves, A. Khademhosseini, R.L. Reis, Modified Gellan Gum hydrogels with tunable physical and mechanical properties, Biomaterials, Vol. 31, Iss. 29, 2010, pp. 7494-7502. http://www.sciencedirect.com/science/article/pii/S0142961210007982.

[144] R.M. Felfel, I. Ahmed, A.J. Parsons, G.S. Walker, C.D. Rudd, In vitro degradation, flexural, compressive and shear properties of fully bioresorbable composite rods, Journal of the Mechanical Behavior of Biomedical Materials, Vol. 4, Iss. 7, 2011, pp. 1462-1472. Available (accessed ID: 274145): http://www.sciencedirect.com/science/article/pii/S1751616111001184.

[145] A.M. Deliormanlı, M.N. Rahaman, Direct-write assembly of silicate and borate bioactive glass scaffolds for bone repair, Journal of the European Ceramic Society, Vol. 32, Iss. 14, 2012, pp. 3637-3646.

[146] S. Eqtesadi, A. Motealleh, P. Miranda, A. Pajares, A. Lemos, J.M.F. Ferreira, Robocasting of 45S5 bioactive glass scaffolds for bone tissue engineering, Journal of the European Ceramic Society, Vol. 34, Iss. 1, 2014, pp. 107-118.

[147] X. Liu, M.N. Rahaman, G.E. Hilmas, B.S. Bal, Mechanical properties of bioactive glass (13-93) scaffolds fabricated by robotic deposition for structural bone repair, Acta Biomaterialia, Vol. 9, Iss. 6, 2013, pp. 7025-7034.

[148] M. Mutanen, Studies of Bio-Reconstructive Finger Joint Prosthesis, Tampere University of Technology, 2004, pp. 79-88.

[149] T. Kulmala, Biokorvautuvan sorminivelimplantin tuotannollisen valmistuksen kehittäminen, Tampere University of Tcchnology, 2002, pp. 86-91.

[150] J. Franco, P. Hunger, M.E. Launey, A.P. Tomsia, E. Saiz, Direct write assembly of calcium phosphate scaffolds using a water-based hydrogel, Acta biomaterialia, Vol. 6, Iss. 1, 2010, pp. 218-228.

[151] M. Genet, M. Houmard, S. Eslava, E. Saiz, A.P. Tomsia, A two-scale Weibull approach to the failure of porous ceramic structures made by robocasting: Possibilities and limits, Journal of the European Ceramic Society, Vol. 33, Iss. 4, 2013, pp. 679-688.

[152] Q. Fu, E. Saiz, A.P. Tomsia, Direct ink writing of highly porous and strong glass scaffolds for load-bearing bone defects repair and regeneration, Acta Biomaterialia, Vol. 7, Iss. 10, 2011, pp. 3547-3554.

[153] S. Eqtesadi, A. Motealleh, A. Pajares, F. Guiberteau, P. Miranda, Improving mechanical properties of 13–93 bioactive glass robocast scaffold by poly (lactic acid) and poly (ε-caprolactone) melt infiltration, Journal of Non-Crystalline Solids, Vol. 432, Part A, 2016, pp. 111-119.

[154] K.S. Suslick, Sonochemistry, Science, Vol. 247, Iss. 4949, 1990, pp. 1439-1445.

[155] J. Massera, M. Mayran, J. Rocherullé, L. Hupa, Crystallization behavior of phosphate glasses and its impact on the glasses' bioactivity, Journal of Materials Science, Vol. 50, Iss. 8, 2015, pp. 3091-3102.

[156] J. Massera, S. Fagerlund, L. Hupa, M. Hupa, L. Pinckney, Crystallization Mechanism of the Bioactive Glasses, 45S5 and S53P4, Journal of the American Ceramic Society, Vol. 95, Iss. 2, 2012, pp. 607-613.

[157] Christopher E. Hinton, Structure testing machine, Patent US 5511431 A, US 08/310,871.

[158] F. Berto, L. Marsavina, M.R. Ayatollahi, S.V. Panin, K.I. Tserpes, Brittle or Quasi-Brittle Fracture of Engineering Materials 2016, Advances in Materials Science and Engineering, Vol. 2016, 2016, pp. 1-2. http://search.proquest.com/docview/1833896004.

[159] E. Feilden, E.G. Blanca, F. Giuliani, E. Saiz, L. Vandeperre, Robocasting of structural ceramic parts with hydrogel inks, Journal of the European Ceramic Society, Vol. 36, Iss. 10, 2016, pp. 2525-2533. http://www.sciencedirect.com/science/article/pii/S0955221916301054.

[160] P. Miranda, A. Pajares, E. Saiz, A.P. Tomsia, F. Guiberteau, Mechanical properties of calcium phosphate scaffolds fabricated by robocasting, Journal of Biomedical Materials Research Part A, Vol. 85A, Iss. 1, 2008, pp. 218-227. http://onlinelibrary.wiley.com/doi/10.1002/jbm.a.31587/abstract.

[161] C.B. Carter, M.G. Norton, Ceramic Materials: Science and Engineering, Springer New York, New York, NY, 2007, pp. 289-303.

[162] L. Ruiz-Cantu, A. Gleadall, C. Faris, J. Segal, K. Shakesheff, J. Yang, Characterisation of the surface structure of 3D printed scaffolds for cell infiltration and surgical suturing, Biofabrication, Vol. 8, Iss. 1, 2016, pp. 015016. http://www.ncbi.nlm.nih.gov/pubmed/26930179.

[163] S. Barui, S. Chatterjee, S. Mandal, A. Kumar, B. Basu, Microstructure and compression properties of 3D powder printed Ti-6Al-4V scaffolds with designed porosity: Experimental and computational analysis, Materials Science and Engineering: C, Vol. 70, 2017, pp. 812-823.

[164] A. Nazarian, D. von Stechow, D. Zurakowski, R. Müller, B. Snyder, Bone Volume Fraction Explains the Variation in Strength and Stiffness of Cancellous Bone Affected by Metastatic Cancer and Osteoporosis, Calcified Tissue International, Vol. 83, Iss. 6, 2008, pp. 368-379. http://www.ncbi.nlm.nih.gov/pubmed/18946628.

[165] S. Majumdar, M. Kothari, P. Augat, D.C. Newitt, T.M. Link, J.C. Lin, T. Lang, Y. Lu, H.K. Genant, High-Resolution Magnetic Resonance Imaging: Three-Dimensional Trabecular Bone Architecture and Biomechanical Properties, Bone, Vol. 22, Iss. 5, 1998, pp. 445-454.

[166] M. Ding, C.C. Danielsen, I. Hvid, S. Overgaard, Three-dimensional microarchitecture of adolescent cancellous bone, Bone, Vol. 51, Iss. 5, 2012, pp. 953-960. Available (accessed ID: 271131): http://www.sciencedirect.com.libproxy.tut.fi/science/article/pii/S8756328212010022.

[167] C. Öhman, M. Baleani, E. Perilli, E. Dall'Ara, S. Tassani, F. Baruffaldi, M. Viceconti, Mechanical testing of cancellous bone from the femoral head: Experimental errors due to off-axis measurements, Journal of Biomechanics, Vol. 40, Iss. 11, 2007, pp. 2426-2433.

[168] M. Ding, M. Dalstra, C.C. Danielsen, J. Kabel, I. Hvid, F. Linde, Age variations in the properties of human tibial trabecular bone, The Journal of bone and joint surgery. British volume, Vol. 79, Iss. 6, 1997, pp. 995-1002. http://www.ncbi.nlm.nih.gov/pubmed/9393920.

[169] F. Linde, P. Nørgaard, I. Hvid, A. Odgaard, K. Søballe, Mechanical properties of trabecular bone. Dependency on strain rate, Journal of Biomechanics, Vol. 24, Iss. 9, 1991, pp. 803-809. http://www.sciencedirect.com/science/article/pii/0021929091903057.

APPENDIX 1: DATA RECEIVED FROM AIREX® AND SAWBONES®

Table 21. The compressive values of PET and PU foams received from their Technical data sheet provided by Airex® and Sawbones®.

Airex®	**Density (kg/m^3)**	**Compressive Strength (MPa)**	**Compressive Modulus (MPa)**
T92.100	100 (range 95-110)	1.75 (min1.4)	90 (min 65)
T92.130	135 (range 127-143)	2.4 (min 2.1)	140 (min 110)
T92.200	210 (range 200-220)	3.8 (min 3.2)	180 (min 150)
Sawbones®	**Density (g/cc)**	**Compressive Strength (MPa)**	**Compressive Modulus (MPa)**
#1522-23	0.08	0.60	16
#1522-01	0.16	2.2	58
#1522-03	0.32	8.4	210

APPENDIX 2: RESULTS OF PET FOAM SAMPLES

Table 22.Gathered information of density, used glue, compressive rate, sample size, compression strength at 10% strain, compressive modulus and absorbed energy until yield. % errors represent the % difference between compressive results received from Airex®.

Preparation	Density (kg/m^3)	Size (mm)	σ_{10} (MPa)	Error in σ_{10}	E (MPa)	Error in E	U_y (kJ/m^3)
Welding line, Instron E 1000							
Punched	210±10	Φ10x5	4.6±0.4	+21 %	82.9±10.6	-54 %	39.1±8.8
Hand-carved	210±10	Φ10.2±0.2 x5	4.9±0.4	+28 %	80.6±5.4	-55 %	37.3±5.0
Punched+epoxy	210±10	Φ10x5.2±0.1	4.8±0.2	+26 %	118.1±9.7	-34 %	44.3±12.5
Punched	210±10	Φ10x5	5.0±0.5	+31 %	86.9±11.8	-52 %	42.4±12.9
Punched	210±10	Φ10x5	4.3±0.6	+12 %	77.8±11.1	-57 %	33.1±9.0
Punched	210±10	Φ6x5	4.9±0.9	+30 %	89.2 ±15.4	-50 %	48.5±12.3
Punched	210±10	Φ14x5	3.7±0.2	+1.5 %	61.6±3.0	-66 %	41.0±5.5
Punched	135±8	Φ 10x5	3.3±0.3	+39 %	46.0±3.3	-67 %	39.9±7.1
Punched	100±10	Φ 10x5	2.1±0.1	+21 %	31.3±1.7	-65 %	24.7±3.3
Without welding line, Instron E 1000							
Punched	210±10	Φ10x5	2.4±0.5	-36 %	37.8±6.5	-79 %	15.5±2.3
Punched +silicone	210±10	Φ10x5	2.0±0.5	-47 %	39.9±5.4	-78 %	26.0±4.4
Punched	210±10	Φ10x5	2.1±0.3	-44 %	29.6±0.4.8	-84 %	19.8±5.3
Punched	210±10	Φ10x5	2.1±0.3	-44 %	29.1±4.6	-84 %	15.2±5.4
Punched	210±10	Φ14x5	0.5±0.2	-86 %	8.2±0.9	-95 %	5.3±2.1
Punched	135±8	Φ 10x5	1.6±0.4	-33 %	22.2±6.2	-84 %	15.3±5.2
Punched	100±10	Φ 10x5	1.2±0.1	-31 %	18.2±2.6	-80 %	8.8±3.6
Welding line, Instron 4411							
Punched	210±10	Φ 10x5	4.1±0.1	+9 %	52.4±3.5	-71 %	71.6±9.2
Punched+epoxy	210±10	Φ 10x 5.5±0.2	4.3±0.6	+12 %	71.0±10.7	-61 %	92.8±17.6

APPENDIX 3: RESULTS OF JOINT SCAFFOLDS

Table 23.Results of measured diameter (ϕ), intial length (l_0), strain at 80N, 220 N and 440 N and compressive modulus for tested joint scaffolds.

	ϕ (mm)	**l_0 (mm)**	**ε_{80N} (%)**	**ε_{220N} (%)**	**ε_{440N} (%)**	**E (MPa)**
Bionx, PLA 96/4						
S34	8.2±0.3	3.6±0.1	25.1±11.1	38.5±10.0	48.4±8.0	10.9±7.7
S37	8.7±0.5	3.8±0.2	30.5±8.6	47.2±6.6	56.0±5.0	6.3±3.4
S40	8.6±0.4	3.8±0.2	49.7±3.0	60.6±2.0	67.4±2.0	3.4±1.3
F22	14.3±0.4	4.3±0.1	26.9±2.9	40.3±3.6	48.5±3.4	2.6±0.8
Linvatec PLA 96/4						
S54	12.0±0.2	4.2±0.1	41.5±3.8	54.2±3.3	62.0±3.0	1.2±0.5
S54	13.9±0.2	4.6±0.2	33.4±3.3	46.1±3.0	54.0±2.6	3.4±0.8
S49/E68	13.9±0.2	4.4±0.1	24.4±2.5	37.7±2.7	46.6±2.6	1.9±0.6
S38	16.0±0.3	4.4±0.1	21.7±3.0	34.9±3.1	44.2±3.0	3.1±0.8
S38	18.0±0.2	4.7±0.1	27.6±1.9	40.8±1.4	49.7±1.6	2.0±0.9
Tampere University of Technology PLA 96/4 + PEG 5 %						
-	14.0±0.3	4.4±0.1	57.4±2.3	69.7±2.2	75.4±2.1	0.5±0.1